Molecular working memory enables cells to navigate through changing complex environments

vorgelegt von
Abhishek Das
geb. in Kolkata, India

zur Erlangung des akademischen Grades
Doktor der Naturwissenschaften
-Dr.-rer.-Nat.
genehmigte Dissertation

technische universität
dortmund

von der Fakultät Chemische und Chemische Biology
der Technischen Universität Dortmund
Deutschland

Dortmund 2022

Gutachter:
Priv. Doz. Dr. Aneta Koseska
Prof. Dr. Philippe Bastiaens

The work presented in this dissertation was performed in the group of PD Dr. Aneta Koseska at the Department of Systemic Cell Biology, Max Planck Institute of Molecular Physiology, Dortmund, Germany and at Cellular Computations and Learning, Max Planck Institute for Neurobiology of Behaviour - CAESAR, Bonn, Germany. Abhishek Das was affiliated to the International Max Planck Research School for Living Matter, Dortmund, Germany.

The work described in this thesis partly has been included in the following publication: Akhilesh P. Nandan*, Abhishek Das*, Robert Lott, Aneta Koseska. Cells use molecular working memory to navigate in changing chemoattractant fields. bioRxiv, 2021. (DOI: 10.1101/2021.11.11.468222) (*-equal contribution)

Abstract

In order to migrate within the complex environments of tissues and in organisms, cells rely on sensing local chemical cues that are noisy, disrupted or change both in space and time. The mechanism of how cells can maintain prolonged directional migration when signals are irregular or conflicting, while being able to quickly re-adapt the directional migration to novel sensory cues however has remained unknown. It has been predicted that organization at criticality gives rise to a transient memory that is maintained in the receptor's activity via a slow-escaping remnant, a dynamical "ghost" of the attractor of polarized signaling state. Quantifying the dynamics of Epidermal Growth Factor Receptor (EGFR) phosphorylation in live cells, as well as single-cell migration assays in microfluidic devices, we provide experimental proof that the memory in cell polarization results from dynamical trapping in a "ghost" state. We demonstrate that this memory serves as a basis to integrate changing signals, but also to transform the extracellular information for guidance of memory-directed migration. The results therefore indicate that navigation in a complex environment is an emergent feature of receptor networks organized at criticality. Generally, the molecular working memory described here resembles the properties of working memory in neuronal networks, as it enables information of previous signals to be temporally maintained while retaining responsiveness to upcoming signals.

Zusammenfassung

Um sich in der komplexen Umgebung von Geweben und anderen Organismen fortbewegen zu können, sind Zellen auf die Wahrnehmung lokaler chemischer Signale angewiesen, die verrauscht, unterbrochen, oder räumlich und zeitlich veränderlich sind. Ein Mechanismus mit dem Zellen bei unregelmäßigen oder widersprüchlichen Signalen eine verlängerte, gerichtete Fortbewegung beibehalten können, gleichzeitig aber in der Lage sind, die Fortbewegung schnell an neue sensorische Signale anzupassen, ist derzeit noch unbekannt. Es wurde vorhergesagt, dass die Organisation bei der Kritikalität zu einer transienten Erinnerung eines polarisierten Signalzustandes der Aktivität eines Rezeptors führt, die über einen langsam verschwindenden Rest, einen dynamischen „Geist“, des Attraktors erhalten wird. Durch die Quantifizierung der Dynamik der Phosphorylierung des epidermalen Wachstumsfaktor-Rezeptors (EGFR) in lebenden Zellen sowie durch Einzelzell-Migrationsuntersuchungen in mikrofluidischen Geräten erbringen wir den experimentellen Nachweis, dass das Gedächtnis in der Zellpolarisation aus dem dynamischen Einfangen in einem "Geister“ Zustand resultiert. Wir demonstrieren, dass dieses Gedächtnis als Basis für die Integration von veränderlichen Signalen dient, aber auch die Transformation extrazellulärer Signale zur Lenkung der von der Gedächtnis-diktierten Fortbewegung erlaubt. Die Ergebnisse deuten darauf hin, dass die Navigation in einer komplexen Umgebung ein Merkmal ist, das aufgrund der Organisation des Rezeptor Netzwerkes bei der Kritikalität entsteht. In den Grundzügen ähnelt das hier beschriebene molekulare Arbeitsgedächtnis den Eigenschaften eines Arbeitsgedächtnisses in neuronalen Netzwerken insofern, dass es die temporäre Erhaltung vorheriger Signale ermöglicht, gleichzeitig aber die Reaktionsfähigkeit zu neuen Signalen erhält.

Dedicated to science beyond borders....

Acknowledgements

I started this wonderful journey of a Ph.D. almost three and a half years ago on 1st August 2018 and now have the chance to look upon the journey with satisfaction and gratitude. I was fortunate to have shared my time and space with some fantastic people who made this journey enjoyable and unforgettable. Coming from a scientific discipline of physics, this journey of the Ph.D. reiterated my belief that science doesn't need to be restricted and confined by specific fields or barriers but should be inclusive of all opinions. There were tough and challenging moments, some imposed by the current world climate of the COVID-19 pandemic. But all of them shaped me into the person I am today.

My foremost thanks go to my supervisor, Aneta Koseska. I am fortunate to have had a talented and caring mentor like you, who supported me and pushed me to achieve my best possible self. I hope I can embed some of your curiosity for innovative scientific ideas and attention to detail along as well. A big thanks go to Philippe Bastiaens and Dept. II from MPI Dortmund for the strong support, the discussions, and the unique interdisciplinary multicultural experience that shaped my scientific expertise. Philippe's willingness to provide me with the opportunity to conduct experiments in his department during pandemic times is something I will always be thankful for. I am happy to have initially joined this great department at a crucial point in my life. I want to give a massive thanks to Angel, who had incredible patience with me and taught me most of the techniques utilized in this thesis. I will never forget the good times of scoring in a football match against you.

My following appreciation is for my colleagues and friends Akhilesh, and Robert without whom none of this work would have been possible. The numerous discussions, data analysis sessions, late-night imaging schedules showed the teamwork and commitment involved in this project. I have gained a great deal of knowledge working with you.

To Manish, Maitreyi, Sarah, Kitso, thanks for putting up with my goofing around in the office and for the impropmtu break sessions. I enjoyed interacting with every one of you, within the lab and outside of it. Thanks to Farid, Dhruv, Hans, Mike, Manuel, Konstantin, Bruno, Lena, and the whole of department II (who I may have missed by name) for being fun, kind, and supportive friends.

Thank you to all of the people that made the lab function smoothly - Astrid, Tanja (MPI Dortmund), Caroline, Bettina (MPI-CAESAR Bonn); thanks for the management; Sven, Michael, Kirsten, Manu, Lisaweta, Michelle, Jutta, Hendrike, the rest, and Antje (MPI-CAESAR Bonn) thanks for all the help.

Thank you, Lucia, Christa, and the IMPRS faculty members and students; being part of the school was an honor and a thoroughly enjoyable experience.

Thanks to all the other people that made Max Planck Institute for Molecular Physiology, Dortmund and Max Planck Institute for Neurobiology of Behaviour - CAESAR, Bonn such great places to conduct scientific research and learn.

I want to say my special thanks to my parents, Ajay Das and Tulu Das. Nothing would have been possible for me without their constant support, perseverance, and sacrifices. Thanks for being the best sister anyone can ask for my sister Indrani. Thanks to Swami Purnatmananda Maharaj for his blessings and care.

My final thank you goes to Kavya, who has always been a great and encouraging partner throughout this Ph.D. journey. Thank you for all the love and support, especially during stressful times; it means the world to me.

Table of Contents

List of Figures

List of Tables

Acronyms

^oC degree Celsius 37

ATP adenosine triphosphate 9

cAMP cyclic adenosine monophosphate 3

CCP clathrin-coated pits 14

CCV clathrin-coated vesicle 14

CME clathrin-mediated endocytosis 14

DMEM Dulbecco's Eagle's medium 34

DPBS Dulbecco's phosphate-buffered saline 36

ECD extracellular domain 8

ECM extracellular matrix 3

EGF epidermal growth factor 3

EGFR epidermal growth factor receptor xi

ErbB erythroblastic leukemia viral oncogene homologue 7

Erk Extracellular Regulated Kinase 17

FCS Fetal Calf Serum 34

FNN False Nearest Neighbourhood 28

Grb2 growth factor receptor-bound protein 2 8

GTP guanosine-5'-triphosphate 4

h hour 35

HER human epidermal growth factor receptor 7

IM imaging media 36

kPa kilo Pascal 39

M molar 39

MAP microtubule-associated protein 5

MAPK mitogen-activated kinase module 3

MDCK Madin-Darby Canine Kidney cells 8

MEBM Mammary Epithelial Basal Medium 35

ml millilitre 39

mOU modified Ornstein-Uhlenbeck 43

MT microtubules 4

MTOC microtubule organizing center 4

ng nanogram 39

nm nanometre 37

NOX nicotinamide adenine dinucleotide phosphate oxidase 13

PAK1 P21 (RAC1) activated kinase 1 5

PI3K phosphoinositide 3-kinase 2

PLC phospholipase C 2

PM plasma membrane 4

PTB phosphotyrosine-binding domains 9

PTP phosphotyrosine phosphatases 11

pY phosphorylation of tyrosine residues 9

Rab Ras-associated binding 14

Rac1 Ras-related C3 botulinum toxin substrate 1 5

ROS reactive oxygen species 12

SH2 Src homology 2 domains 9

Shc SHC(Src homology 2 domain containing) transforming protein 1 8

Src Proto-oncogene tyrosine-protein kinase Src 8

1 Introduction

1.1 Information processing of single cells in dynamic environments

In the human body, cells are exposed to diverse changing environments within tissues and organs, including time-varying stimuli and spatial-temporal gradients of soluble proteins, biochemical interactions of cells with other neighboring cells and mechanical interactions with the environment [1, 2, 3]. They continuously sense these changes in the surroundings and interpret them to perform relevant functions like cell growth, proliferation, apoptosis, cell migration among others (Figure 1.1). Eukaryotic cells can thus be defined as far-from-equilibrium membrane-bound units containing fundamental molecules, which constantly exchange information in the form of matter and energy with their surroundings to sustain the physiological needs of the global system, which is the organism [4, 5].

1.1.1 Migratory behavior of cells

Directed cell migration is an essential physiological process in human biology and plays a crucial role in developmental processes, directed immune responses, as well as wound healing processes [6, 7]. The migration process is a product of several complex integrated processes that are highly regulated by cellular mechanisms [8]. For example, migration of neutrophils, which are the most abundant leukocytes in the blood, to a site of a bacterial infection or tissue damage is regulated through the release of cytokines, proteases, and other cytoplasmic proteins. Directed neutrophil movements are mediated by chemoattractant signaling when chemokines like CXCL1, CXCL8, and others are recognized by G protein-coupled receptors (GPCRs) and other receptors that induce polarization and activation of specific signaling molecules, like phosphoinositide 3-kinase

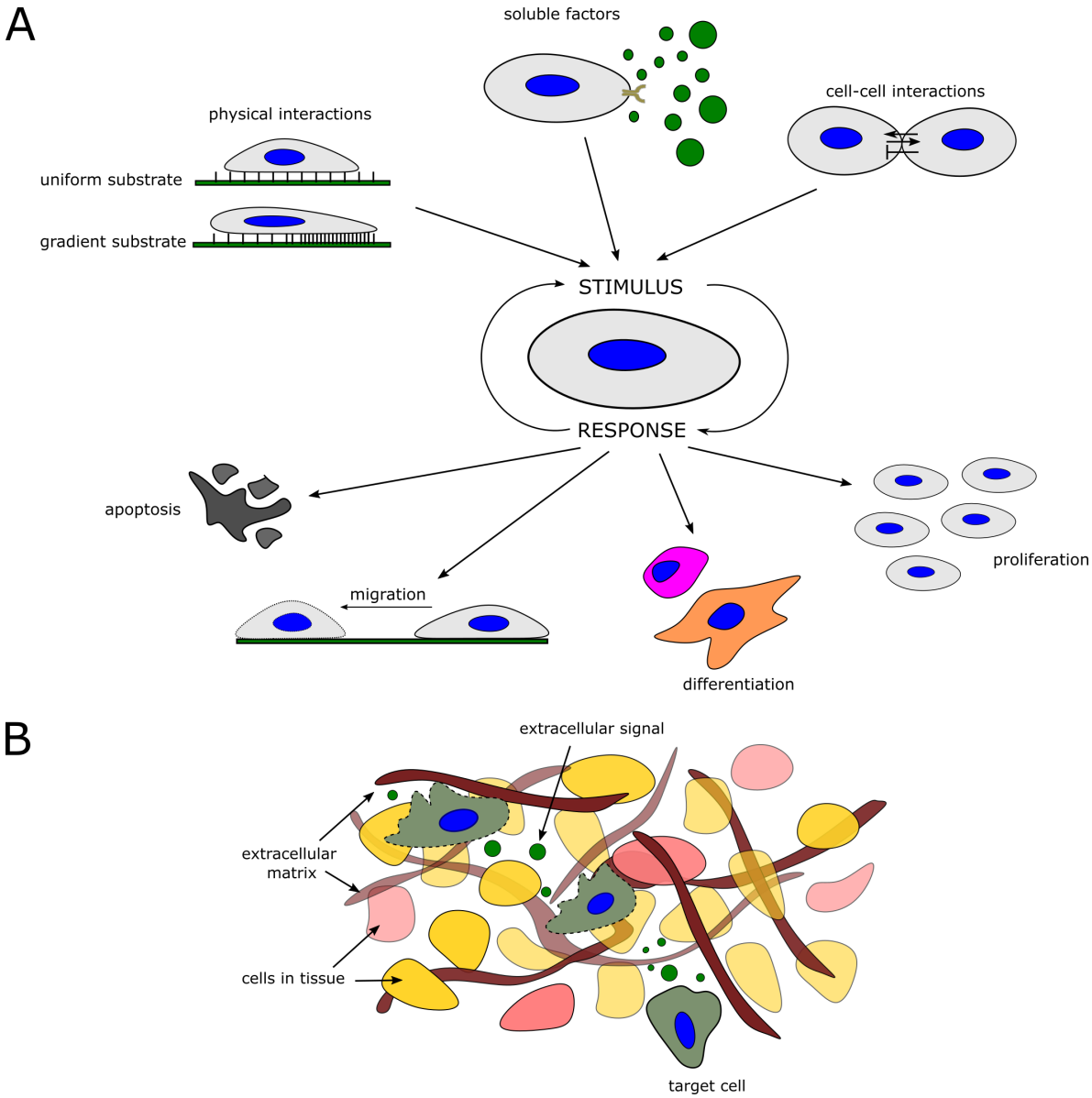

Figure 1.1: Multiple responses by cells - (A) Varying cellular response upon different external stimuli. Stimuli and response can be seen as a coupled phenomena where the cell acts as a processing reservoir. (B) Migration of cell within a complex tissue environment mediated by spatially and temporally changing growth factor concentrations and interactions between other cells and extracellular matrix.

(PI3K), phospholipase C (PLC) and members of the Rho GTPase family, such as Rac [9, 10]. Bacteria-induced neutrophil migration is another physiological example of cell migration studied extensively in the past decades (Figure 1.2 A). Bacterial residues are recognized by either the pathogen recognition receptors (PRRs) or opsonic receptors on neutrophils that activate phagocytosis [11]. During early developmental processes like embryogenesis, primordial germ cells (PGCs) or precursor cells migrate from their site of specification through epithelial sheets to the target location of the formation of different organs [12, 13]. It is an active mode of directed migration characterized by protrusions towards the destination and cell shape changes. In -in vivo experiments with zebrafish embryos, PGC migration is induced by the sensing of the chemokine Cxcl12a

by Cxcr4b receptors [14, 15, 16]. Migration also occurs in the adults in pathological states during cancer metastasis. Increased levels of low molecular weight hyaluronic acid (LMW-HA), its receptor CD44, and hyaluronan synthase (HAS2) are reported in tumor microenvironments, including breast, oral and ovarian cancers [17, 18]. HA is a glycosaminoglycan that plays a role in extracellular matrix (ECM) remodeling and regulates cancer cell migration via receptor signaling in a context-dependent manner. One of the targets of CD44 engagement by HA is the activation of RhoGTPase signaling [19]. Clinical studies have shown that decreasing LMW-HA production inhibited breast cancer cell migration and invasion [20].

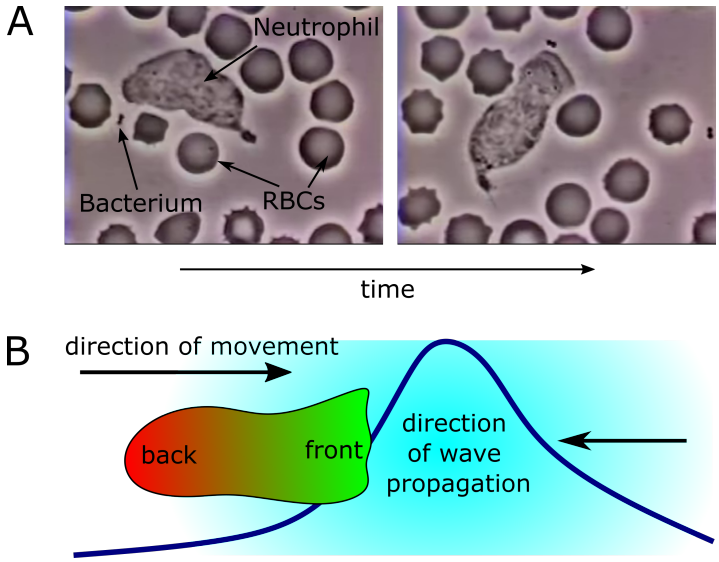

Figure 1.2: Examples of cell migration in nature - (A) Crawling behavior of human polymorphonuclear leukocyte (neutrophil) on a blood film, among field of red blood cells, chasing *Staphylococcus aureus* microorganisms. Images from a 16-mm movie made in the 1950s by the late David Rogers at Vanderbilt University; (B) Directional motility of *Dictyostelium discoideum* during cAMP wave propagation. Reproduced from [21]

During wound healing processes, fibroblasts like NIH3T3 cells migrate towards the wound site and play a crucial role in tissue repair [22]. Fibroblasts possess cell surface receptors (epidermal growth factor receptors (EGFR), platelet-derived growth factor receptors (PDGFR), etc.) which bind with their corresponding ligands like epidermal growth factor (EGF), platelet-derived growth factor (PDGF). Receptors regulate downstream signaling of PI3K and the downstream kinase Akt, the mitogen-activated kinase module (MAPK network) including Ras/Raf/Mek/Erk 1/2 and others. The activation of the PI3K-Rac-RhoGTP network is an important signaling target of EGFR by which it can engage the cytoskeletal network of a cell [23, 24].

Even isolated single-celled organisms can perform directed migratory behavior in changing environments. In a nutrient-deficient environment, social amoeba *Dictyostelium discoideum* has been shown to migrate to form aggregates by sensing periodic waves of a gradient of cAMP. Although the traveling waves of cAMP change the directionality of the chemoattractant over the length of a single cell, *Dictyostelium* showed polarization

('front' in green and 'back' in red) and persisted motion in the direction of the gradient from the source, thus exhibiting cellular memory (Figure 1.2 B) [25, 21].

Downstream signal integration via the biochemical networks inside the cell is a crucial step in deciphering cellular motility. Along with signal transduction, subsequent coordination and reorganization of cell cytoskeleton and cell adhesion effectors collectively maintains the mobile phase of cells [26, 27]. Understanding how cells process environmental information to respond optimally and adapt to spatial and temporal changes is one of the principal goals in cell signaling biology.

1.1.2 Molecular processes underlying cellular migration

Eukaryotic cells have evolved several regulatory mechanisms for sensing, storing, and processing extracellular information to undertake efficient cell migration. Over the years, classical studies in molecular biology and proteomic analysis have helped in uncovering and characterizing proteins and intracellular protein-protein interactions involved in dynamic cellular responses to external cues [28]. Cells are enclosed by a plasma membrane (PM), a 2-dimensional bilayer barrier composed of different lipids and proteins, maintaining the physical integrity of the cell. Directed chemotactic behavior relies on generating polarized signaling activity of multiple proteins at the cell's PM that is translated to an elongated cell shape and subsequent persistent migration in the direction of the signal [29, 30, 31]. The signaling networks localized near the PM regulate the microfilament dynamics i.e., the cytoskeleton via regulator molecules [26, 29].

In eukaryotes, cell morphology and motility are mainly controlled by such dynamic cytoskeletal networks composed of actin filaments, intermediate filaments, and microtubules which operate at different time and length scales [32, 33]. Actin filaments with a diameter of about 7 nm consist of repeating subunits of actin monomers to produce filaments that form cross-linked networks. Networks of actin filaments are found beneath the cell cortex, which is the meshwork of membrane-associated proteins that supports and strengthens PM. The microtubules (MTs) are the main thicker and stronger filaments to generate, support, and maintain the global shape of the cells. They are composed of α- and β- tubulin subunits forming protofilaments which wind up together forming hollow cylinders ($\sim 25nm$ diameter). MTs undergo a process of dynamic instability of polymerization (mediated by Guanosine-5'-triphosphate (GTP)) and depolymerization by which they can either grow slowly ("rescue") or shrink rapidly ("catastrophe"). The microtubule organizing centers (MTOC) globally organize the MTs forming MT-asters with MTs radiating from the center to the peripheral regions of the cell. The dynamical MT network is crucial for plasticity in cell shape formation depending on external cues and cell shape stabilization [34, 35].

Extracellular morphogen gradients, including growth factors and chemoattractants, direct the reorganization of the cytoskeleton by inducing localized signaling reactions. These reactions generate cytoplasmic activity of the microtubule-associated proteins (MAPs). The interactions with the MAPs regulate MT dynamics, e.g., stabilizing, destabilizing, or bundling MTs [36]. One example of such signal transduction of external cues into cytoskeletal reorganization is the Rho-GTPases signaling consisting of the Rac1-PAK1-stathmin MT-regulator network (Figure 1.3) [37, 38, 39]. In the absence of growth factors, the kinase PAK1 remains in the cytosol, where the high activity of phosphatases maintains low steady-state phosphorylation levels of MT-regulator stathmin, which sequesters tubulin, thereby constraining MT growth. Upon localized external signals and morphogen-induced activation of Rac1, recruitment and activation of kinase effectors like PAK1 occurs on the PM through the principle of dimensionality reduction [40]. PAK1 phosphorylates the MT-regulator stathmin, which diminishes its tubulin sequestration capability. Hence the availability of free tubulin for MT growth increases. The concentration of the kinase activity and the cytosolic MAPs towards the morphogen exposed areas leads to gradients of activity within the cell. Such local spatial gradients enable actomyosin cytoskeletal reorganization direction in the morphogen direction by local modulation of MAP activity [41]. Thus, a recursive interdependence between cytoskeleton-induced deformation and signaling activity at the membrane underlies the process of cell polarization and subsequent directed migration [26].

In human neutrophils, directed stimulation with the chemoattractant tripeptide fMet-Leu-Phe (fMLP) induces cell polarization creating a front-back asymmetry of the migrating cells [11, 42]. It is characterized by actively polymerizing F-actin at the polarized front with contracting acto-myosin complexes at the rear end [43]. In response to fMLP, neutrophils secrete a secondary chemoattractant leukotriene B4 (LTB4) [44]. LTB4 plays a significant role in sensitizing neutrophils to fMLP by facilitating polarization in the direction of the cue. Knockout and co-injection experiments have reiterated the role of LTB4 paracrine signals in relaying the information of gradient of fMLP to sites far away from the wounded tissue [45]. Similarly, microfluidic experiments with HeLa cells have shown polarization during chemotaxis under external gradients of rapamycin which is translated into intracellular gradients of Rac1 activation [29]. These cells were able to sense a reversal of rapamycin gradient and repolarize in the direction of the gradient leading to a reversal of migration [46]. Cell polarization plays a crucial role in maintaining apicobasal polarity of epithelial cells [47] with the help of polarity proteins, including the Par complex, which consists of Par proteins and atypical protein kinase C (aPKC) and the Scrib complex [48, 49]. As such aberrant cell polarization leads to a progression of abnormal tumor growth and tumor cell migration. Overexpressed Scrib has been shown to contribute to the progression of hepatocellular carcinoma in humans [50]. Typically found on the membrane of epithelial cells, Scrib complexes are mislocalized in the cytosol of tumor cells [49].

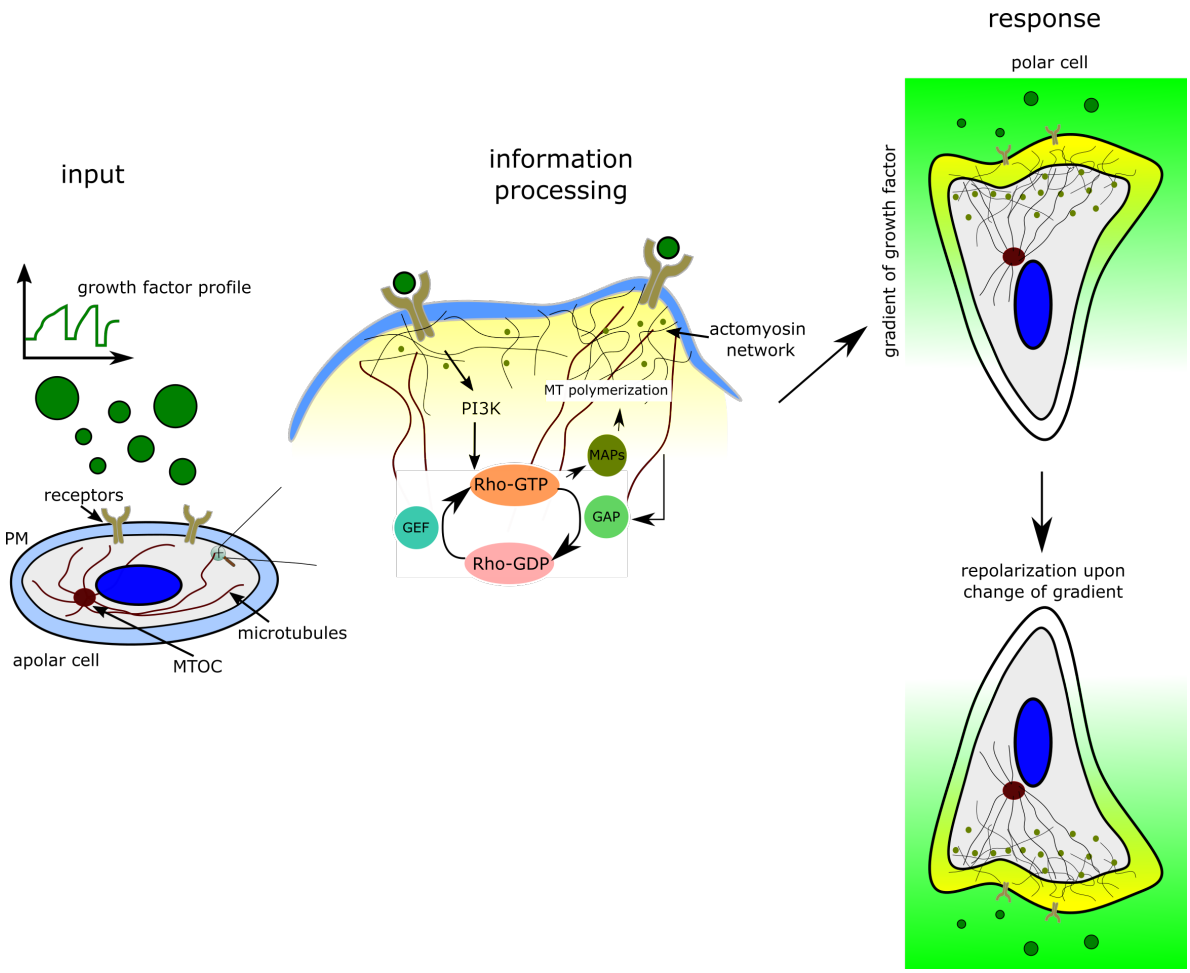

Figure 1.3: Information processing via network topology - Scheme of receptor induced cell polarization as a symmetry breaking event leading to cytoskeletal changes, interdependence of signaling and cell shape results in migration.

Thus, cells store and process the stream of information from the non-stationary environment wherein a chemokine signal induces polarization of the cells and directs migration. Upon change in direction of chemokine signal cells require to retain the ability to sense continuously and repolarize accordingly. Directed chemotaxis of neutrophils has been shown for less than 5% difference in fMLP across the front and back of the cell [45]. The cellular sensing systems, therefore, not only infers the direction of the chemoattractant gradient but must also sense very shallow gradients, amplify and translate these gradients in the activation of the corresponding biochemical networks to achieve robust polarization in the direction of the signal [29].

1.2 Cell surface receptors as sensing entitites – Epidermal Growth Factor Receptor (EGFR)

Cell surface receptors convert extracellular signals into intracellular signaling events [51]. Receptor tyrosine kinases (RTKs) are among the most well-known families of

transmembrane protein receptors that recognize growth factors and act as enzymes upon activation by respective ligands (Figure 1.4) [52, 53]. Cellular responses like cell motility, cell growth, and differentiation are triggered by the activation of RTKs generally via receptor-specific ligands [54]. These ligands induce receptor dimerization or oligomerization and propagate the signal downstream in the cell cytoplasm by interacting with other proteins [55, 56]. The 58 known RTKs in humans are subdivided into 20 different classes based on structural similarities [53]. The ErbB/HER family of proteins form the RTK Class I, which are structurally similar to the epidermal growth factor receptor (EGFR). The ErbB family consists of 4 subgroups: Her1 (EGFR, ErbB1), Her2 (Neu, ErbB2), Her3 (ErbB3), and Her4 (ErbB4).

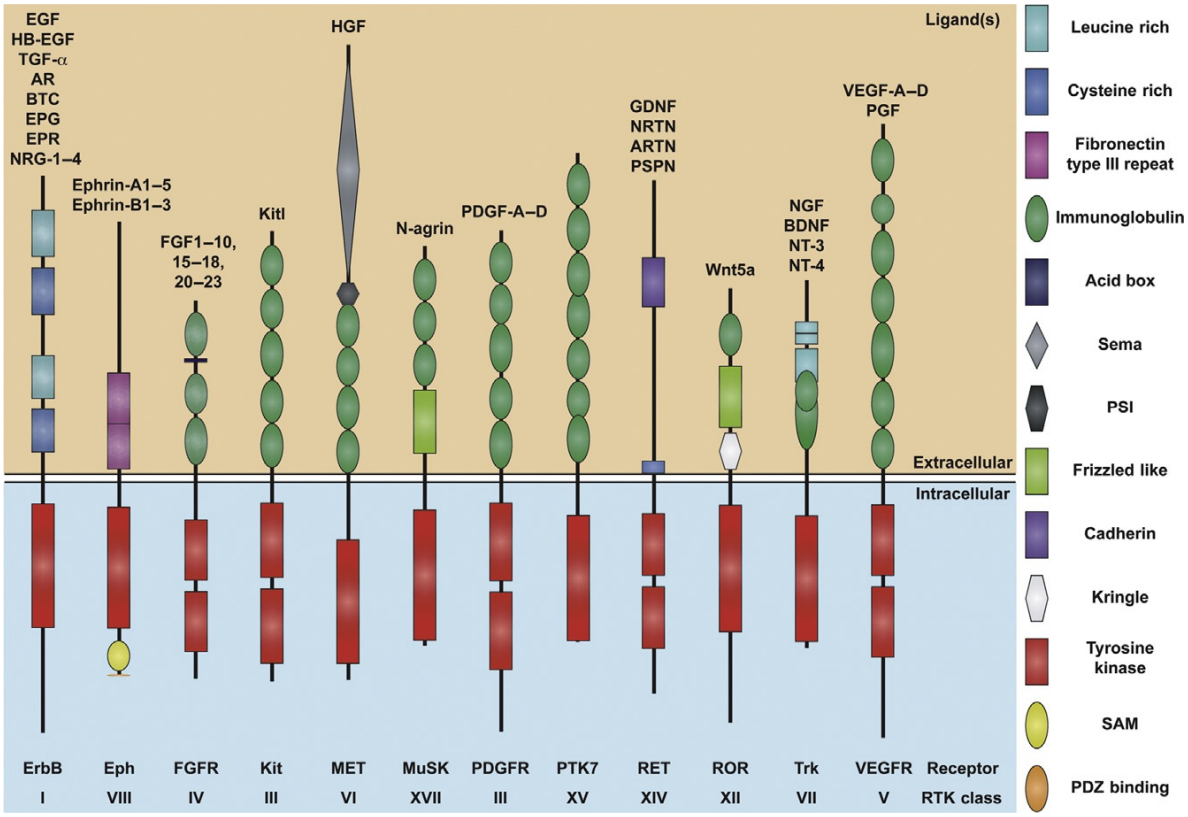

Figure 1.4: Family of receptor tyrosine kinases known in humans - The schematic representation shows some of the subfamilies of RTKs with their known extracellular ligands. Reprinted from [57]

EGFR (ErbB1) was among the first RTKs to be discovered. The role of EGFR initiated signaling is crucial in the regulation of cellular migration, growth, survival, proliferation, and tumor progression. Extensive analysis of EGFR specific ligands has revealed seven types of ligands that activate a diverse range of biological responses through EGFR signaling downstream (Figure 1.4). These are epidermal growth factor (EGF), transforming growth factor-alpha (TGF-α), betacellulin (BTC), heparin-binding EGF-like growth factor (HB-EGF), amphiregulin (ARG), epiregulin (EPR), and epigen (EGN) [58, 59]. Although EGFR or ErbB1 is bound and activated by all seven ligands leading to different functional cellular behavior, ErbB4 is only bound by the ligands

EREG, HB-EGF, and BTC as well as neuregulins (e.g., heregulins). ErbB2 does not bind with any known EGFR ligand [60]. One of the first growth factors shown to bind with EGFR was the Epidermal growth factor (EGF) which activates the intracellular tyrosine kinase activity [61]. EGF binds to EGFRs with a high affinity with dissociation constant (K_D) reported to be 1.77×10^{-7} M [62, 63].

Phosphorylated tyrosine residues of EGFR and its substrates act as binding sites for effector proteins that initiate intracellular signaling, such as Grb2, PI3K, Shc, Src and PLCγ [64]. Hence, it is important for maintaining tissue homeostasis and during developmental processes [65, 66]. Receptor-induced EGFR signaling has been revealed to promote cell migration in osteoblasts and osteocytes during bone formation [67] as well as collective cell migration of various epithelial and endothelial cell types including MDCK cells [68, 69]. Regulation of cell migration via the EGFR signaling pathway has been shown in oral squamous cell carcinoma cells [70]. Dysregulation of EGFR signaling is a known mechanism in cancer progression in non-small cell lung cancer (NSCLC) [71]. Overexpression of EGFR is also an independent predictor of poor prognosis in inflammatory breast cancer (IBC) [72]. Therapeutically EGFR has been studied extensively as a target protein against different forms of cancer.

1.2.1 Structure and activation of EGFR

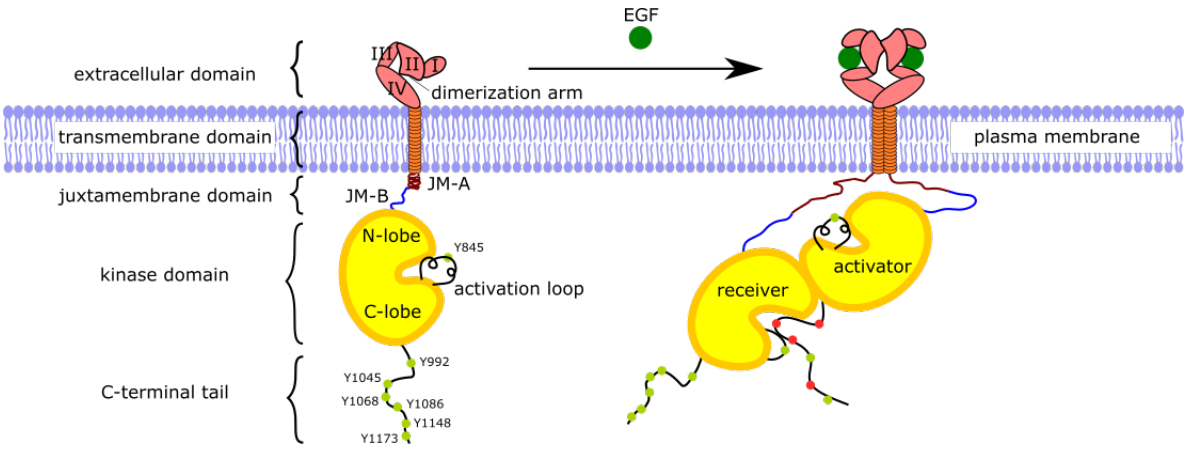

Figure 1.5: Structural organisation of EGFR and EGFR activity - EGFR consists of mainly 5 domains noted here (Left) Unphosphorylated tyrosine residues denoted by green circles. (Right) EGF-induced assymetric dimer formation leads to one receptor being "activator" which allosterically changes the activation loop of another receptor, the "receiver". Receiver can then trans-phosphorylate the tyrosine residues of the activator.

Monomeric EGFR comprises five major domains: extracellular domain, a transmembrane domain, juxtamembrane domain, a kinase domain, and a C-terminal domain (Figure 1.5 Left). The extracellular domain (ECD) comprises four parts: I, II, III, and IV. I and III make up the recognition pocket for EGF binding, while II and IV maintain a tethered conformation in the absence of EGF by interacting with each other [73]. The kinase domain is made up of 2 lobes: C-lobe and N-lobe. The trans-phosphorylation

process depends on the role of these two lobes. Crystal studies have revealed that the N lobe contains five β sheets (β1- β5), one α helix (αC-helix), and the C lobe consists of multiple α helices and an activation loop [74]. A short hinge connects the two lobes where the catalytically active site is present [75]. Multiple interactions stabilize the inactive conformation of EGFR to avoid spurious activation in the absence of any ligand. Functional and NMR studies indicate that the polybasic motifs of the juxtamembrane and the kinase domain interact with the negatively charged plasma membrane holding the inactive conformation in place [76]. The C-terminal tail also interacts with the tyrosine kinase domain and the threshold for EGFR activation is increased by the local disorder in the αC-helix of the N-terminal [77].

1.2.1.1 EGF-induced activation of EGFR

EGF binding to the ECD results in conformational rearrangement of the receptor protein on the extracellular membrane, thus releasing II, which acts as a "dimerization arm" which induces association with the same arm of other receptors (Figure 1.5 Right) [73, 78]. Such extracellular transformations also result in conformational changes in the intracellular region via the transmembrane domain and the release of the juxtamembrane segments from the plasma membrane. It allows the kinase domains to interact asymmetrically forming an EGFR dimer [79]. The C-lobe of one receptor acts as an activator, while the N-lobe of the other receptor, binding to the first one, acts as the receiver of activity. This is the asymmetric dimer model, where the allosteric activation mechanism rearranges the position of the activation loop and initiates the open conformation of the receiver receptor's kinase domain (Figure 1.5 Right) [79]. EGF-induced conformational changes in the αC-helix and the activation loop of the EGFR kinase domain stabilize the active kinase conformation in the asymmetric dimer. The coordination of the α- and β phosphate group of a substrate adenosine triphosphate (ATP) molecule and subsequent phosphate transfer is coordinated by the active conformation of the αC-helix which contains a catalytically important salt bridge [80]. The activation loop frees the catalytic cleft upon the active conformation of the kinase domain, and the C-terminal tail separates from the dimerization interface. These processes lead to the transphosphorylation of the tyrosine residues (pY) like Y992, Y1045, Y1068, Y1086, Y1148, and Y1173 located on the C-terminal tail of the "activator" receptor [64, 79]. Hydrophobic interactions between protein residues in the C lobe of the 'activator' receptor and the N lobe of the 'receiver' receptor also stabilize the asymmetric dimer [81].

Subsequent recruitment of adaptor proteins that contain Src homology 2 domains (SH2s to pY992, 1068, 1086, 1114) or phosphotyrosine-binding domains (PTBs to pY992, 1068, 1173, 1148) then couple activated receptor dimers to diverse signaling pathways in the cytoplasm [64], such as the Ras-mitogen-activated protein kinase (MAPK), phosphoinositide-3-kinase (PI3K), protein kinase B (Akt), and phospholipase C-gamma

(PLC-γ) pathways [82]. The activation of the PI3K-Rac-RhoGTP network is an essential signaling target of EGFR by which it can engage the cytoskeletal network of a cell [24]. E3 ubiquitin ligase c-Cbl also binds to pY1045 of EGFR either directly or via an adaptor protein Grb2 to pY1068 and pY1086 and attaches a ubiquitin group at the kinase domain of EGFR, which marks the protein for degradation [83]. Receptor ubiquitination is a direct readout for ligand-bound EGFR [84].

1.2.1.2 Autocatalytic activation of EGFR

Overexpression of EGFR has been shown to lead to ligand-independent spurious activation of EGFR signaling in multiple cancerous tumors [85]. Despite the auto-inhibitory mechanisms, such activation can happen when the thermal conformational fluctuations enable a group of EGFRs to attain active conformation, thus releasing the activation loop [86]. To unravel their mechanism, the phosphorylation of the Y845 tyrosine residue (pY845) within the activation loop of the kinase domain has been studied using multiple FRET-based conformational EGFR indicators (CONEGI) [87]. pY845 stabilizes the active open conformation of the receptor. Thus pY845, kinase active EGFR monomers can further propagate receptor phosphorylation to other monomers, resulting in an autocatalytic EGFR activation that can lead to laterally propagated phosphorylation [88, 86, 84]. Y845 has been reported to be phosphorylated by Src, which in turn is activated by phosphorylated EGFR [84, 89, 90] indicating that an autocatalytic loop can also be realized indirectly. In this respect, it has been demonstrated that the two kinases in an asymmetric dimer cannot access each other's activation loops. Therefore, they require the recruitment of a kinase such as Src on pY1086 [77]. This is consistent with the findings that phosphorylation on signaling tyrosines precedes phosphorylation on Y845 [91]. Phosphorylation of the distal segments of the tail (Y999–Y1186) also enhances pY845 [77].

This autocatalytic amplification can also be triggered by EGF-bound allosterically activated EGFR dimers [92, 84]. For physiological, subsaturating EGF concentrations (below or in the range of the nanomolar EGF dissociation constant), most EGFR dimers are occupied by a single EGF, but can still exhibit transphosphorylation activity [93]. Negative cooperativity or decrease in the rate of subsequent binding for a second EGF molecule [94, 95], emerges from an altered asymmetrical dimer interface in the ECD [96]. This phenomena suggests that EGF-EGFR dimers with 1:2 stoichiometry are even shorter-lived intermediates [97]. That transient dimers can give rise to catalytic amplification of phosphorylation [40, 92] is further supported by the fact that low-affinity ligands such as EPR and EGN act as partial agonists of dimerization (due to a weakened dimerization interface) but are full agonists of receptor phosphorylation [98]. On the population level, the catalytic amplification of the phosphorylation is spatially restricted by the diffusion of the ligand-bound receptors [40].

Under normal physiological conditions, cells exhibit basal EGFR activation therefore fundamental constraints to autocatalysis and lateral propagation exist. Diffusional barriers limit the free diffusion of EGFR to nanoscopic membrane domains (50–300 nm wide) that are delimited by actin-based membrane skeleton fences [99, 100]. This acts as a layer of constraint against uncontrolled phosphorylation amplification and aberrant signaling. The crossing of signaling proteins through these fences thus becomes the rate-limiting factor in lateral information transfer by reaction-diffusion mechanisms such as autocatalysis [101, 40, 102]. Equipartitioning among the domains results in few receptors per domain at physiological EGFR expression levels of $\sim 5 \times 10^4$ receptors per cell. This homogeneous distribution also limits EGFR reactivity [103, 104].

1.2.2 Dephosphorylating properties of PTPs

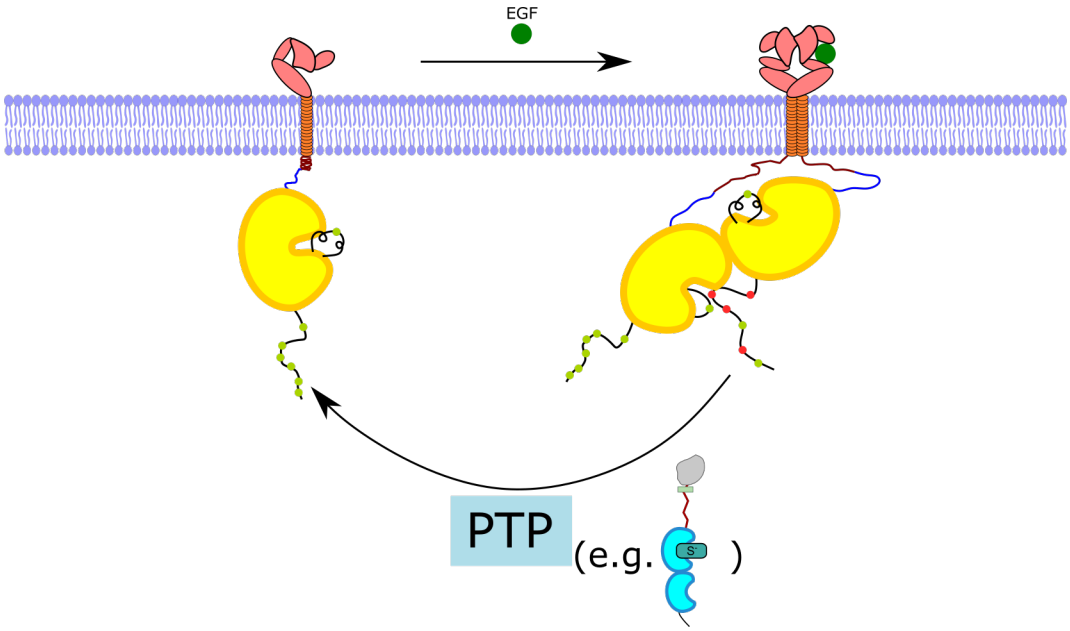

Figure 1.6: Dephosphorylation by PTPs - PTPs dephosphorylate phosphorylated tyrosine (red to green dots) on EGFRs at the plasma membrane

The kinase activity of the EGFR is influenced by the dephosphorylation of the autocatalytic and signaling tyrosine residues (Figure 1.6) [86]. A family of phosphotyrosine phosphatases (PTPs) carries out the dephosphorylation of phosphorylated tyrosine residues of EGFR. They are divided into 38 classical phosphotyrosine-specific PTPs and 61 dual-specificity phosphatases (DSPs) [105]. The 38 known classical PTPs in the human genome can be further categorized according to their localization motifs.

A common two-step catalytic mechanism is used by PTPs based on a nucleophilic cysteine with a low pKa within the PTP domain [106]. Initially, the phosphorous atom in the phosphotyrosine residue of the bound substrate is attacked by cysteine. The catalytic aspartate donates a proton to the oxygen, leaving a substrate group upon cleavage of the ester bond. Thus, it reverts to the non-phosphorylated state. Secondly,

water molecule hydrolyses the cysteine-phosphate intermediate, thus resulting in the restored enzyme and inorganic phosphate.

The role of PTPs has been well studied in suppressing tumor growth related to abnormal RTK signaling e.g., PTPN1 role in human disease [107]. Several solid tumors have reported reduced expression of transmembrane receptor-like PTPs (RPTPs) like PTPRG, PTPRJ, PTPRD, and PTPRK [108]. Continuous and rapid cycles of phosphorylation and dephosphorylation events regulate cell signaling [109]. RPTPs are located on the PM and contain extracellular domains with ligand recognizing features. They generally act on the RTKs localized near it while the cytosolic PTPs have specific sequences with which they can interact with their substrates, e.g., the SH2 domains of PTPN6 (SHP1) and PTPN11 (SHP2) [105]. Localization sequences present on some cytoplasmic PTPs target them to specific compartments to interact locally with their substrate partner. PTPN1 (PTP1B) and PTPN2 (TCPTP) are ER-bound PTPs, and they interact with RTKs on the cytoplasmic face of the contact sides with the RTK rich vesicles [110, 111]. The high catalytic activities of PTPs (∼two orders of magnitude higher than EGFR) manages to suppress both spontaneous and low dose of ligand-induced EGFR phosphorylation [84, 112].

1.2.2.1 Redox regulation of PTPs via EGFRs

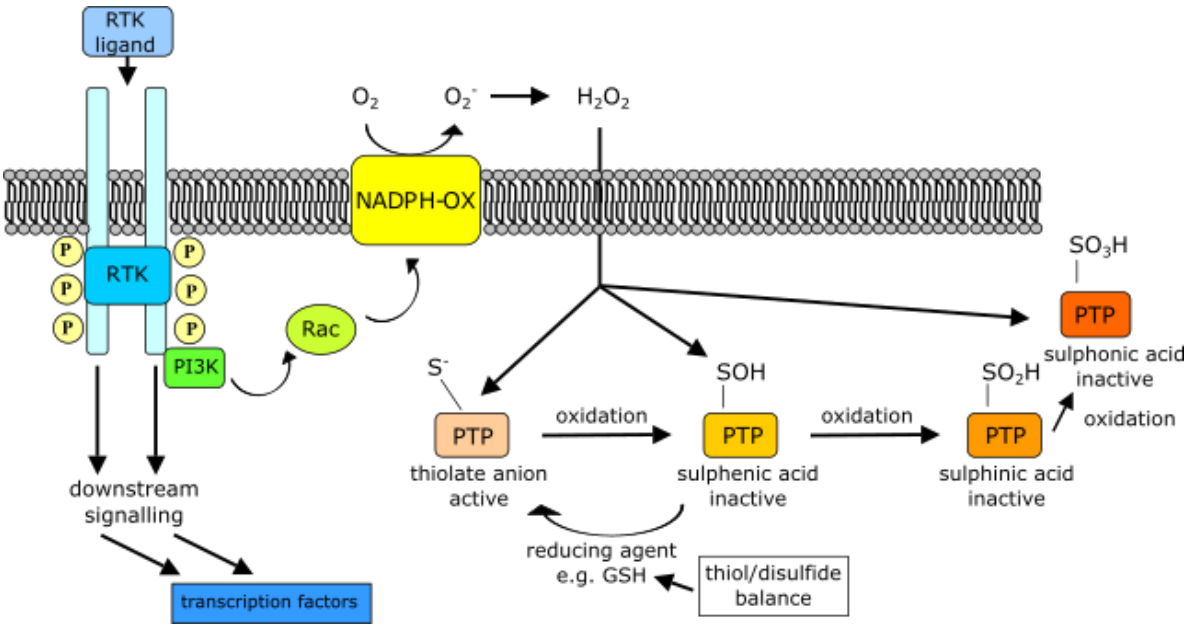

Figure 1.7: Redox regulation of PTPs - EGFR induced PI3K activation leads to NOX complex formation at PM mediated by Rac and PIP3. Extracelullar superoxide or H_2O_2 diffuses through PM and oxidises PTPs rendering it inactive. Reprinted from [113]

However, if high PTP activity is present at the membrane, no signal propagation via EGFR phosphorylation would be possible. An intrinsic regulatory mechanism governs PTP activity. Due to the low pKa of the active cysteine, the PTPs are sensitive to oxidation by reactive oxygen species (ROS), e.g., superoxide anion (O_2-) or hydrogen

peroxide (H_2O_2) [114]. Along with EGFR phosphorylation, the EGF stimulation also promotes the recruitment and activation of reactive oxygen species (ROS) producing enzyme systems like the NADPH oxidase (NOX) complex to the plasma membrane. PM-localised NOX2 complex produces H_2O_2 which is transported into the cells via diffusion or aquaporins [86]. Activation and formation of NOX complexes are enhanced by PI3K-induced PI(3,4,5)P3 formation and Rac1 activation [115, 116]. The ROS is spatially constrained only to the plasma membrane due to their short half-life time. This local ROS production forms an intracellular gradient in the cytoplasm and transiently inhibits the catalytic activity of the PTPs, namely the RPTPs. The ROS targets the thiol group (Cys-SH) in the cysteine residues of PTPs and oxidizes it to sulfenic acid (Cys-SOH). This reaction renders the PTPs catalytically inactive. Phosphorylated EGFRs can activate PI3K, thereby inducing H_2O_2 production near the plasma membrane and thus exhibiting redox regulation of PTPs on the membrane (Figure 1.7) [86]. The cysteine can be reverted to an active state via secondary redox reaction mediated by reducing agents [113]. These agents prevent irreversible overoxidation, which can occur due to oxidative stress.

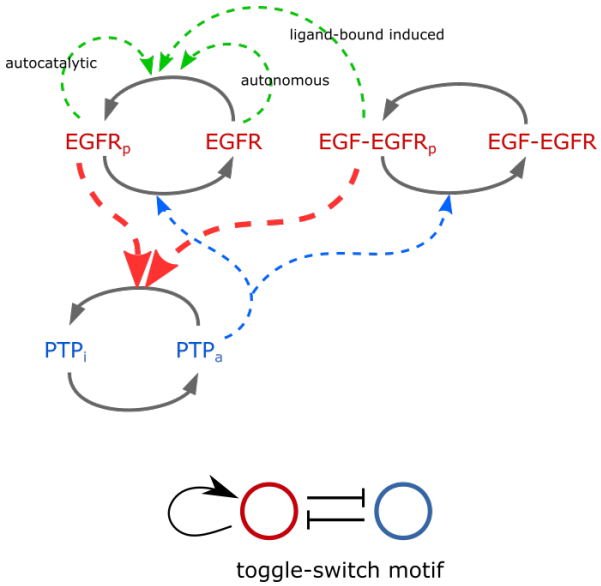

Figure 1.8: Diagrammatic representation of EGFR-PTP activity regulation - (A) Schematic representation showing the regulation and state transitions between different forms of EGFR and PTP. Transitions between phosphorylated (p) and unphosphorylated states of unliganded EGFR (EGFR) and ligandbound EGFR (EGF-EGFR) are shown. Green dashed arrows show affect of autocatalytic, ligandbound induced and autonomous activation of unliganded EGFR phosphorylation. Red dashed arrows indicate redox regulation of EGFRs on PTPs while blue dashed arrows indicate dephosphorylation regulation of PTPs on EGFRs. (B) Toggle-switch motif of EGFR-PTP system. Adapted from [86, 101].

Thus, at the plasma membrane, EGFR activation and PTP inhibition are coupled processes exemplifying a double-negative feedback loop, which, together with the autocatalytic kinase activity, establishes a bistable reaction network (Figure 1.8 top)

[86, 101]. PTP dephosphorylate activated EGFRs and establish negative feedback. The autocatalytic activation of EGFR creates a one-component positive feedback motif while the EGFR induced H_2O_2 production negatively regulates the interacting PTP, effectively establishing a double-negative feedback motif. This 'toggle-switch '-like motif (Figure 1.8 below) creates a bistable regime in the system, where upon threshold EGF stimulation, a switch from low to high EGFR phosphorylation can occur and signal propagation takes place [92, 40, 86, 101].

1.2.3 Regulation of spatial and temporal distibution of EGFR via vesicular recycling

Upon EGF stimulated phosphorylation of EGFRs on the membrane and signal initiation, EGFRs undergo internalization and vesicular trafficking through the cell cytoplasm [53, 84]. Phosphorylated EGFRs are engulfed into clathrin-coated pits (CCPs) (Figure 1.9). This process is mediated by phosphatidylinositol-2-bisphosphate (PIP2), effector Grb2, and clathrin adaptor AP-2 [118, 119]. After nucleation and attaining a threshold curvature, CCPs pinch off the PM into clathrin-coated vesicles (CCVs) containing the EGFR molecules, which are internalized via the classical clathrin-mediated endocytosis (CME) mechanism [120]. However, clathrin-independent endocytosis (CIE) of EGFRs has also been reported when cells are stimulated with high doses of EGF due to saturation of CME [121]. The formation and fusion of vesicles are controlled by small Rab GTPases, the critical players in vesicular trafficking [122, 123]. Rab proteins can interchange between a GDP-bound 'off' state and a GTP-bound 'on' state, regulated by guanine nucleotide exchange factors (GEFs) and GTPase-activating proteins (GAPs). GDP dissociation inhibitors (GDI) displacement factors (GDFs) confer specificity to Rab membrane association by recognizing Rab-GDI complexes.

Following internalization, EGFR loaded endocytic vesicles are transported to perinuclear regions inside the cell via motor proteins and microtubules [124, 34]. Afterward, they fuse into Rab5-positive early endosomes (EE), where proteins are initially sorted and redistributed towards different cellular compartments [125, 126]. The EE sorts the recycling proteins and the proteins marked for the degradative pathway, which contains the ubiquitinated EGFR. c-Cbl binds EGFR either directly at phosphorylated Y1045 via its tyrosine binding domain or indirectly through Grb2, which binds EGFR at phosphorylated Y1068 and Y1086 via its SH2 domain [127, 128, 129]. EGFR is either targeted to Rab7-positive late endosomes (LEs), dephosphorylated in pericentriolar areas with high PTP1B activity [130], or recycled back to the PM via the Rab4-positive fast recycling endosome (RE) or the Rab11-positive pericentriolar slow RE [83, 131, 132]. Multivesicular bodies (MVBs) are formed by the invagination of the endosomal membranes mediated by the recruitment of the ESCRT complex [133]. The ubiquitinated EGFRs are sorted into the MVBs and subsequently committed

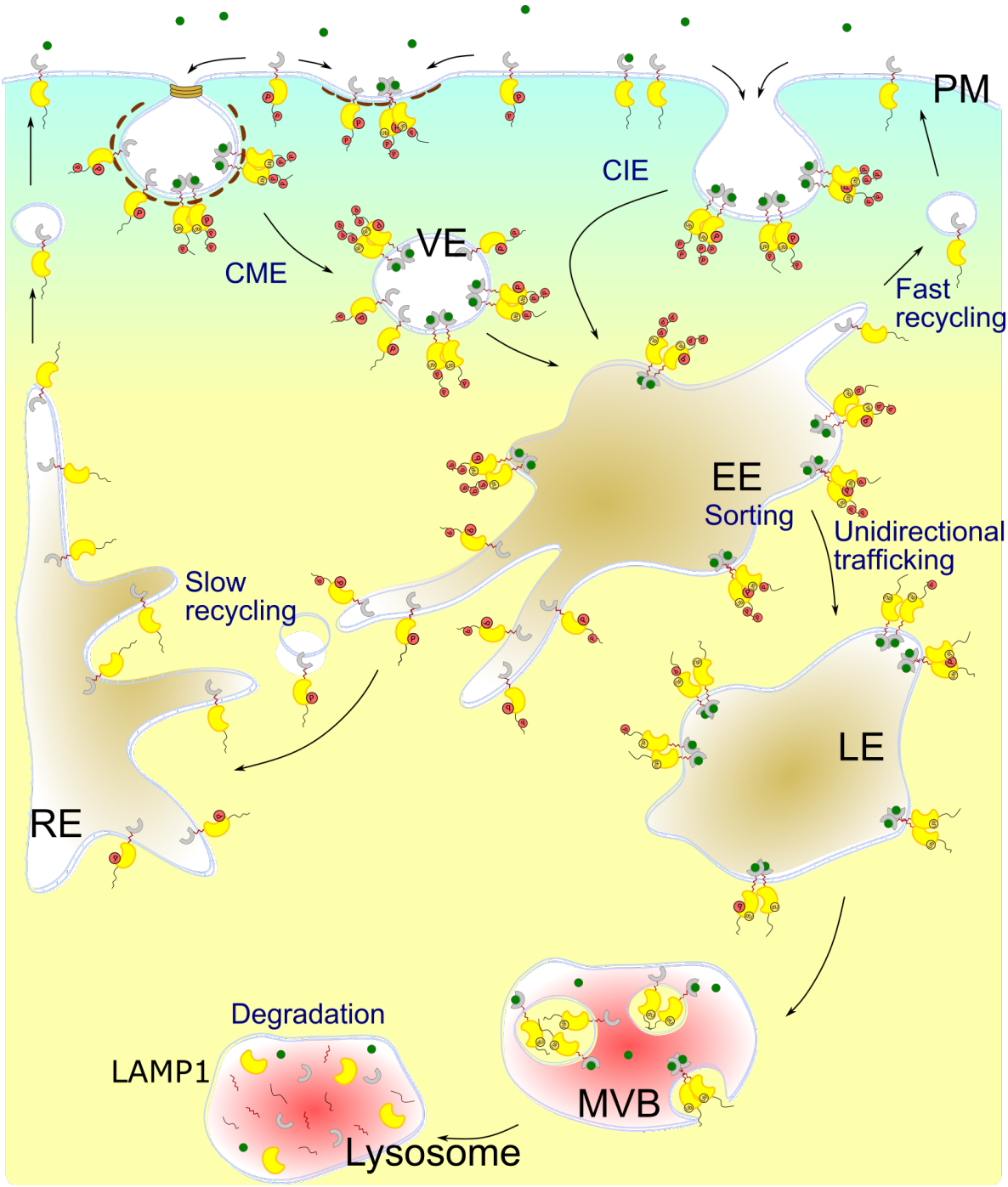

Figure 1.9: Vesicular trafficking of EGFR - Schematic diagram of CME or CIE mediated internalisation of phosphorylated EGFRs from the PM. Vesicular trafficking initates from EEs where receptor sorting takes place. Ubiquinated ligandbound receptors are unidirectionally transported towards lysosomal degradation while unliganded EGFRs are recycled to the PM either via RE-mediated or fast-recycling route. Adapted from [117]

to LAMP1-positive lysosomes for degradation purposes. The vesicular trafficking of EGFR is summarized in the Figure 1.9. Besides these mechanisms, EGF-induced macropinocytosis at the plasma membrane caused by the dynamic ruffling can also internalize the bound receptors.

1.2.3.1 EGF dose dependent EGFR trafficking dynamics

At low physiological doses of EGF (0.4 -20 ng/ml) [134], receptor internalization occurs via CME, and hence the sorting in EE depends on the state of the receptor, whether ligand-bound or ligand-independent. In the absence of EGF, unliganded EGFR monomers recycle through the RE in the perinuclear regions. PTP1B suppresses the spontaneous activation of EGFR by dephosphorylating Y845 on constitutively recycling receptors [130, 84]. However, ligand-induced ubiquitination of EGFR acts as a sorting cue for receptor fate and undertakes unidirectional trafficking towards lysosomal degradation. In contrast, under saturating doses of EGF stimulation, receptor internalization occurs via CIE [121]. At saturating EGF concentrations, a high steady-state amount of ligand-bound, ubiquitinated dimers are generated, which are marked for degradation. Due to the spatial regulation of the phosphorylated EGFR via the vesicular dynamics, EGFR can signal from different levels: both at PM and the endosomes. Akt activation has been shown to occur via the PI(3,4,5)P3-enriched membrane domains present at the PM, but the MAPK module activation has been reported to take place from the endosomal compartments [126, 135]. Thus EGFR signaling dynamics depends on the extracellular concentration of EGF, and is thereby context-dependent [136, 137].

1.2.4 Context-dependent EGFR signaling enables cell migration

Depending on the extracellular concentration of EGF, the vesicular trafficking of EGFR determines the sensing capacity of a cell [84]. As described earlier, at high saturating doses, the ligand-bound dimeric EGFRs are unidirectionally trafficked from the PM to the lysosome for degradation, while at low concentrations majority of the monomeric EGFRs are recycled back on the PM. The recycled dephosphorylated receptors are available to bind new EGF and thus enable sensing of growth factors over time. EGF binds with EGFR with a high affinity, and the dissociation rate of EGF is around 0.5-0.05 per min [138, 139]. Thus, ligand-bound EGFR cannot sense further signal but promotes autocatalytic phosphorylation of recycled EGFRs [40].

During wound healing processes, for efficient wound closure, cells operate in a complex, continuously changing environment with low physiological doses of multiple growth factors. High levels of autonomous EGFR phosphorylation have been shown to promote the phosphorylation of Akt. Phosphorylated Akt promotes vesicular recycling of EGFR generating positive feedback due to the autocatalytic nature of EGFR phosphorylation. An Akt-dependent EGFR recycling on the PM is promoted, which maintains further sensitivity to EGF and maintains a migratory mode of the cell by keeping an adequate number of receptors at the PM (Figure 1.10) [137, 140]. However, differential modulation of EGFR trafficking by the stimulation of different ligands like heregulin (HRG) indicates distinct activation of the downstream Erk signaling from

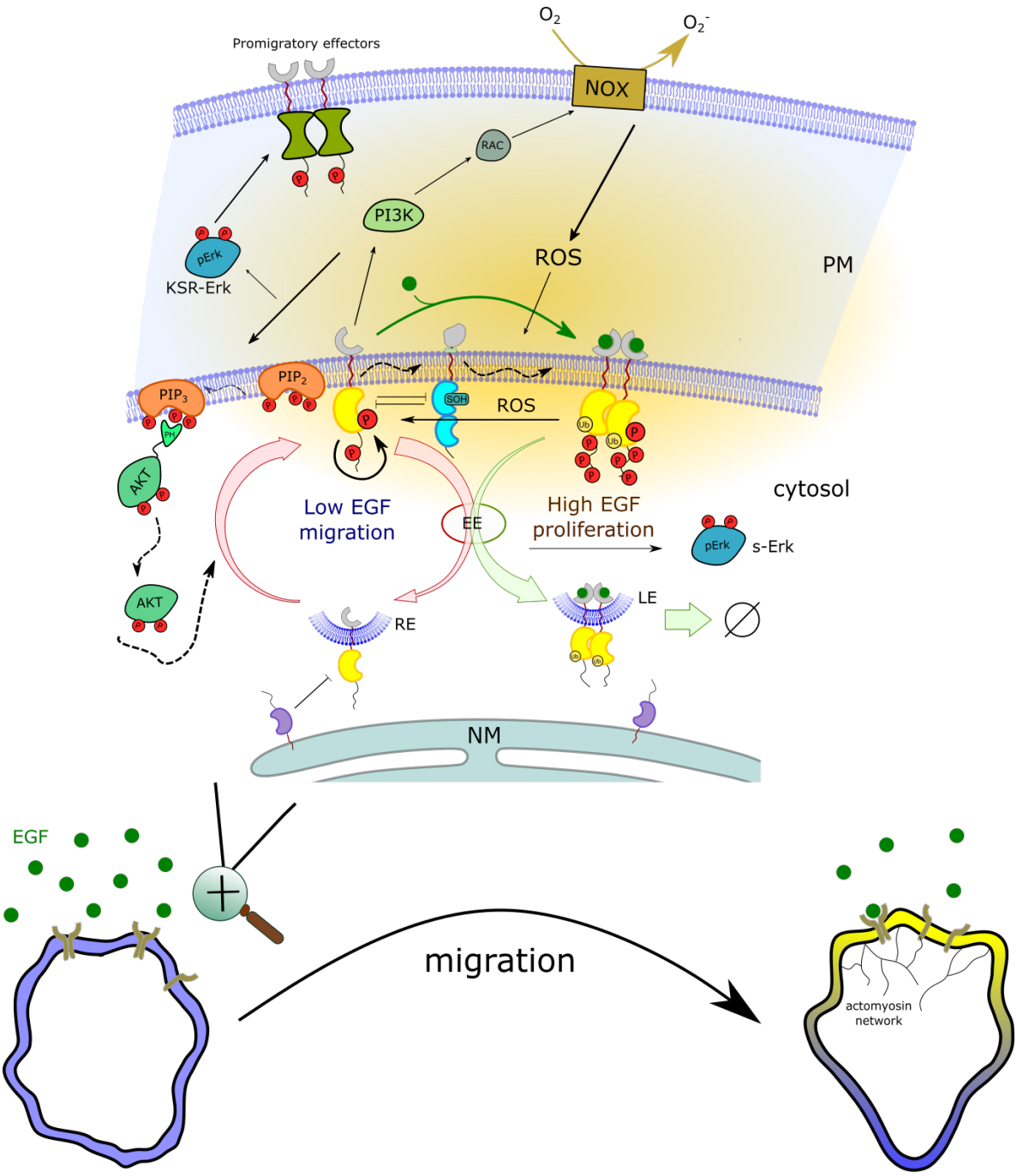

Figure 1.10: EGFR signaling in cell motility - EGF-dependent downstream EGFR signalling results in cell migration. Low physiological concentration of EGF stimulation promotes EGFR-Akt-dependent EGFR monomer recycling and autocatalytic phosphorylation amplification of monomers is sustained by ligandbound EGFR dimers. High level of activated, phosphorylated EGFR at the PM activates the PI3K-mediated singalling molecules (Akt, Rac) which produce ROS by NOX complex. This promotes the migratory state of cells. Adapted from [136].

multiple subcellular compartments (PM and endosomes) [141]. In contrast to EGF, HRG stimulation leads ErbB2/3 receptors to remain on the PM and generate a persistent, localized Kinase Suppressor of Ras - Erk (KSR-Erk) response from the PM [136]. Internalized EGFR on EGF stimulation, on the other hand, activates sustained Erk (s-Erk) signaling from the endosomal membranes. The Erk-dependent phosphorylation

of various effector molecules was observed to be involved in regulating cellular motility in response to HRG stimulation. Thus, the spatial and temporal regulation of receptor kinase activity enables the cell to generate different pools of active Erk with distinct functionalities - transcriptional activity in the nucleus and local morphogenetic function at the PM. Membrane proximal KSR-Erk activity leads to pro-migratory phosphorylation of EphA2 on serine 897 (S897) [136]. Phospho-S897-EphA2 has been reported previously to localize to the leading edge of migrating cells, promoting the assembly of actin cytoskeleton and extension of lamellipodia [141]. Hence the PM localized receptor tyrosine kinase activity provides a mechanism to promote cell shape change and cell motility in a spatially controlled manner (Figure 1.10).

1.2.5 EGFR interaction network enables sensing of time-varying signals

It has been shown that key EGFR-PTP network motifs regulate the EGFR phosphorylation response [86]. Through combined and coordinated action of vesicular dynamics, EGFR reaction kinetics, and the EGFR-PTP interactions regulating the EGFR phosphorylation dynamics enables cellular sensing of time-varying growth factors [84, 92, 40]. Using an EGFR phosphorylation response to EGF dose as a dynamical signature of the underlying EGFR-PTP feedback motif along with genetic perturbations, key causal links between EGFR-PTP pairs has been established. Based on a combination of enzymatic biochemical assays and cell array fluorescence lifetime imaging microscopy (CA-FLIM) screening of 55 PTPs with quantifiable genetic perturbations, three major PTPs which dephosphorylate EGFR both temporally and spatially were identified: the PM localized PTPRG, PTPRJ, and the ER-associated PTPN2 (Figure 1.11 A). The activity of PTPRG is regarded as the central regulator of the EGFR responsiveness to EGF stimulation over PTPRJ since knock-down of PTPRJ, unlike PTPRG, showed no significant effect on increasing the phosphorylated EGFR. Hence, a double-negative EGFR-PTPRG feedback (toggle switch) and negative regulation of EGFR phosphorylation by PTPRJ on the PM were revealed. The vesicular recycling of EGFR also established spatial negative feedback regulation by PTPN2. Upon EGF stimulation, PTPN2 was shown to determine signal duration by dephosphorylating liganded EGFR during the vesicular trafficking, while PTPRG/RJ played a role in determining the sensitivity of EGFR phosphorylation by dephosphorylating recycling ligandless EGFR. The trafficking thereby unifies these pairwise EGFR-PTP interactions into a core receptor network that is distributed in space. The resulting dynamical behavior of this network governs cell sensing and responsiveness to EGF stimulation (Figure 1.11 B) [92].

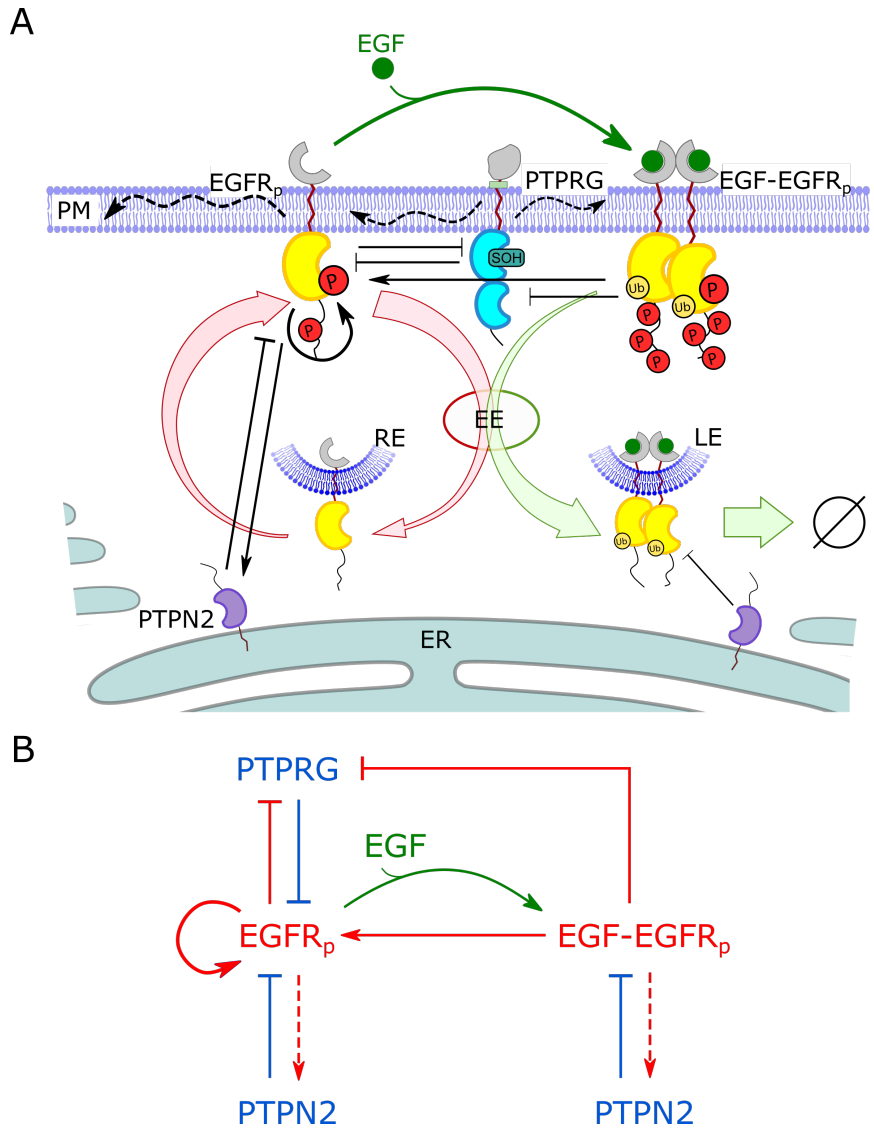

Figure 1.11: Spatially distributed interdependence of PTPs on EGFR - (A) Representative scheme of the EGFR-PTP interaction network established through EGFR trafficking dynamics. EGFR interacts with PTPRG at the PM and PTPN2 in the cytoplasm. Causal links: solid black lines; curved arrow lines: diffusion. (B) Causal diagram of EGFR-PTP network. Red/blue lines: causal interactions; green arrow: ligand binding. Modified from [92]

1.3 Dynamical features of EGFR-PTP network motif

To further study EGFR response dynamics which is determined by the activity regulation between EGFR and a given PTP, the network can be mathematically represented through a system of ordinary differential equations (ODEs) which show the evolution of the combination of variables: $EGFR_p$ – the amount of phosphorylated receptors and PTP_a – the amount of active PTPs. These two variables can be assumed as time-dependent variables which follow the law of mass action wherein kinetics is given by the network motif itself. The coevolution of the two variables then informs one about the dynamical

system. The state-space or the phase space is a multidimensional space enclosing all of the possible combinations of system states that $[EGFR_p, PTP_a]$ can occupy. Time invariant states occupied by such systems are known as stable steady states or attractors, which describe the stable configurations of the system. A trajectory through phase space is equivalent to a trajectory in time which represents the response of a system.

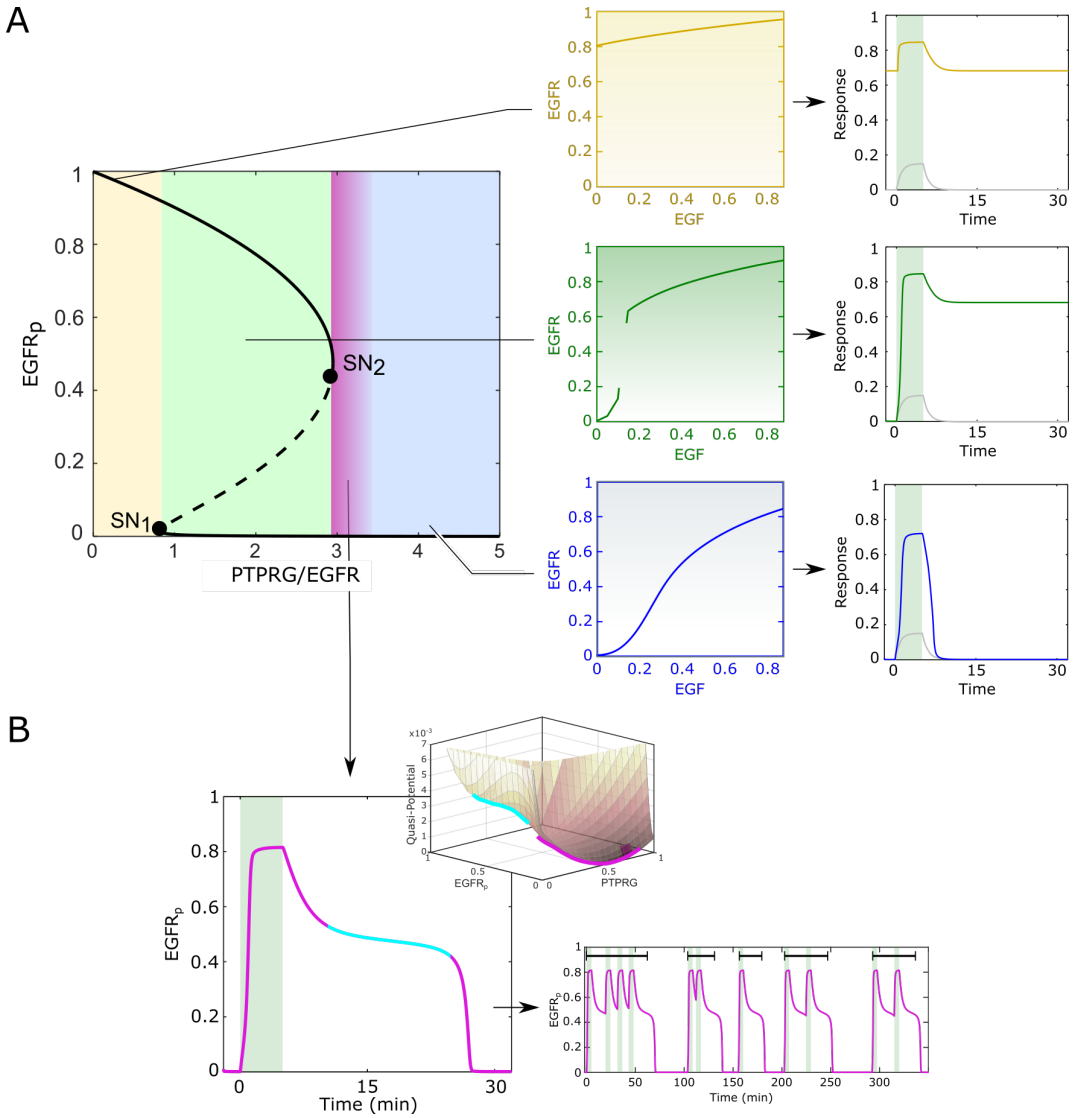

Figure 1.12: Dynamical features of EGFR-PTP system - (A) (Left) Bifurcation diagram of the EGFR-PTPRG toggle switch, depicting phosphorylated $EGFR$ ($EGFR_p$) response with respect to $PTPRG/EGFR$, in the absence of EGF. Shading: yellow/blue—monostable region, magenta—vicinity of the saddle-node (SN) bifurcation point and green—bistable region. Solid/dashed lines—stable/unstable steady states. (Right) Temporal response of the system upon stimulation with pulse of suprathreshold concentration of EGF (B) (Left) For positioning at the critical transition between monostability and bistability, the temporal response and the quasi-potential landscape demonstrate the existence of a "ghost" attractor. Green shaded area: Stimulation with suprathreshold EGF, cyan colour: existence of "ghost" attractor. (Right) Exemplary temporal EGFR phosphorylation profiles for different EGF pulse trains realizations for critical organization. Black line segments: disjoint intervals of EGFR phosphorylation. Green shaded area: growth factor pulse duration. Reprinted from [142]

Based on the identified network topology (Figure 1.11 B), the EGFR phosphorylation depends on two parameters: the fraction of ligand-bound EGFR (EGF-EGFR %) and the concentration of PTPRG relative to that of EGFR on the PM (PTPRG/EGFR). An investigation of the dynamical properties of the motif using bifurcation analysis has reported three possible dynamical modes of operation, which have been verified experimentally: a bistable regime bordering two monostable regimes characterized by basal and continuously high EGFR phosphorylation (Figure 1.12) [86]. These dynamical states are an intrinsic property of the network topology that is centered around the EGFR–PTPRG toggle-switch motif with autocatalytic EGFR activation [101].

As described in the bifurcation scheme in Figure 1.12 A, at low membrane EGFR concentrations or high PTPRG/EGFR ratio, a monostable regime of basal EGFR phosphorylation is attained (Figure 1.12 A right bottom). In this regime, EGFR phosphorylation gradually increases with growth factor receptor occupancy. Upon pulsatile thresholded EGF stimulation, switch-like activation occurs, and the system jumps to a high EGFR phosphorylation state but reverses to the basal state upon EGF removal without any signal integration. For a given range of PTPRG/EGFR on the PM, the system operates in the bistable regime where phosphorylation state of EGFR, i.e., the steady-state solution, depends on the initial phosphorylation level, i.e., history-dependent [142] (Figure 1.12 A right middle). When starting from the basal EGFR phosphorylation state, upon pulsatile thresholded EGF stimulation, switch-like activation occurs, and the system jumps to the high EGFR phosphorylation state. On removal of stimulus, even though PTPRG's activity suppresses the autocatalysis of EGFR and dominates in the bistable regime, the high phosphorylation level is maintained upon reverting to the initial bistability as it remains stable. Thus autocatalysis alone is sufficient to maintain the monomeric unliganded receptors phosphorylated even after EGF removal. Hence although the EGFR phosphorylation response is rapid and robust in the bistable regime, the system's responsiveness to time-varying cues is limited. However, for high EGFR concentrations relative to PTPRG, the system operates in the monostable regime of continuously high EGFR phosphorylation (Figure 1.12 A right top). In this case, the autocatalytic EGFR phosphorylation amplification always leads to PTPRG inhibition via H_2O_2 production, regardless of EGF stimulus. Weak and dampened phosphorylation response to pulsed EGF stimulation reiterated the inability of the system to sense growth factor signals. The temporal evolution of the average EGFR phosphorylation state has been estimated from microscopic experiments showcasing all the dynamical regimes manifested depending upon relative PTPRG/EGFR expression on the PM [92].

1.3.1 Role of metastable dynamics in sensing time-varying EGF signals

Rapid amplification of EGFR phosphorylation under pulses of low dosage of EGF and the ability to reset to basal EGFR phosphorylation when EGF is removed are necessary prerequisites for sensing time-varying EGF signals. An in-depth analysis displayed both these features arises from the critical organization of the system between the mono- and bistable regimes of operation demarcated by a saddle-node (SN) bifurcation point. When the system is organized close to this SN bifurcation point, prolonged EGFR phosphorylation after growth factor removal was revealed in simulations, generating a transient memory of the previous EGF signal (Figure 1.12 B) [142]. Such a transient memory arises due to the emergence of a metastable state which enables the duration of EGFR phosphorylation to depend on previous stimulus history, effectively displaying signal-integration capabilities. It does not hinder further responsiveness of the system to upcoming pulses of EGF.

The metastability is a feature of the dynamical properties at the critical organization. At the vicinity of the SN bifurcation, only one stable steady state is available for the system to occupy - basal EGFR phosphorylation level, which is estimated by the intersection of nullclines in phase space [142]. This can be depicted by a basal state residing in a narrow valley of a quasi-potential landscape. The quasi-potential landscapes [143, 144] depict energy-like levels associated with the steady states in the phase space. The phase space trajectories flow downhill the landscapes towards the valleys defined by the stable steady states. Upon EGF pulse, the steady state of high EGFR phosphorylation becomes stable for bistable organization and the system changes its steady state. Upon EGF removal, when the system transits back from the bistable to the monostable region, the incoming trajectories get trapped in a quasi-potential landscape with a very shallow slope (Figure 1.12 B) [142]. Thus the SN "ghost" serves as a unique dynamical mechanism of transient temporal memory, enabling EGFR phosphorylation to be maintained at high levels for a transient period after EGF removal [142]. However, using systematic multi-pulse EGF experiments it has been demonstrated that, lowering of EGFR's steady-state concentration occurs upon each EGF pulse due to ubiquitination-dependent removal of EGF-bound receptors from the PM [92]. This results in shifting the system toward the monostable regime, wherein it loses the ability to robustly sense and responds to upcoming growth factor signals. Hence dose and duration of EGF stimuli play a crucial role in limiting the EGFR-PTP sensing system.

1.3.2 Symmetry breaking polarization features of the EGFR-PTP network

During embryogenesis or tissue homeostasis, surface receptors like EGFR play a significant role in sensing novel and time-varying complex signals and polarizing towards the directional cue while maintaining responsiveness to previous stimuli [145]. Real-time cellular navigation in nonstationary environments, e.g., chemoattractant gradient fields likely rely on a dynamical mechanism that enables efficient navigation which can be achieved when the polarized phosphorylation dynamics of receptors is transiently stable. Directed cellular migration upon a gradient of growth factor stimulation requires a reliable mechanism for EGF-induced transition from a non-polarized symmetric state to an asymmetric polarized receptor signaling state and subsequently polarized cell shape, with defined 'front' and 'back', towards the EGF signal (Figure 1.13 A). In another study in the group (See Dissertation by Akhilesh P. Nandan) [146], it has been proposed that a symmetry breaking can be achieved via specific dynamical transitions, namely, pitchforck bifurcations (PBs). The PB characterizes a transition from a homogeneous unpolarized state to an inhomogeneous polarized steady state in receptor phosphorylation[147, 143]. The inhomogeneous steady state (IHSS) is a single attractor defined as a combination of the front and back EGFR phosphorylation states of a cell. Furthermore, it has been theoretically demonstrated that the PB must be subcritical to achieve polarization features such as amplification of the signal and because the symmetry broken states are stabilized via SN. Thus organization at criticality - in the vicinity of a SN_{PB} through which a subcritical PB is stabilized (magenta shaded area in Figure 1.13 B), the dynamical characteristics of both bifurcations, signal integration through dynamic transient memory and cell polarization, will be uniquely manifested to render a minimal mechanism for responsiveness in changing environments.

To test this hypothesis, the dynamics of the experimentally identified spatially-distributed EGFR sensing network has been described using mass-action kinetics and formalised mathematically in the following one-dimensional system of partial differential equations (PDEs):

$$\begin{aligned}
\frac{\partial[E_p]}{\partial t} &= f_1([E_p],[E-E_p],[RG_a],[N2_a],[EGF_t]) + D_{E_p}\frac{\partial^2[E_p]}{\partial x^2} \\
\frac{\partial[E-E_p]}{\partial t} &= f_2([E_p],[E-E_p],[EGF_t]) + D_{E-E_p}\frac{\partial^2[E-E_p]}{\partial x^2} \\
\frac{\partial[RG_a]}{\partial t} &= f_3([E_p],[E-E_p],[RG_a]) + D_{RG_a}\frac{\partial^2[RG_a]}{\partial x^2} \\
\frac{\partial[N2_a]}{\partial t} &= f_4([E_p],[E-E_p],[N2_a])
\end{aligned} \tag{1.1}$$

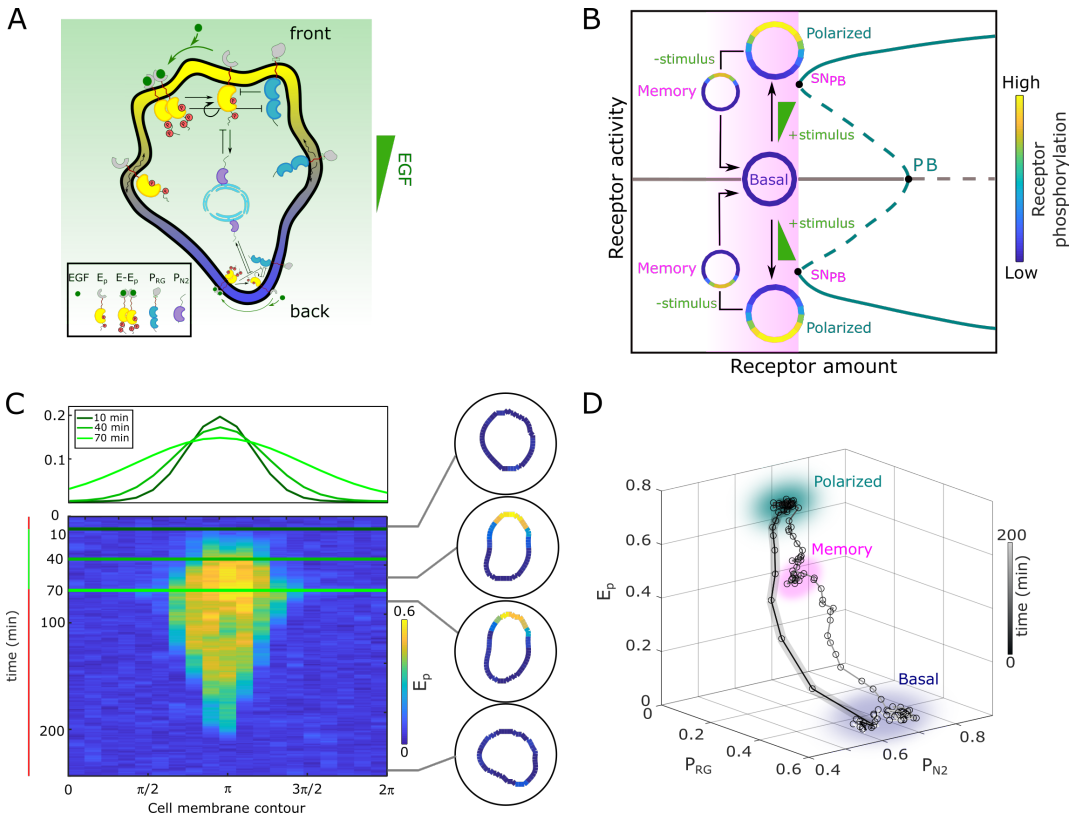

Figure 1.13: Symmetry breaking description of EGFR-PTP system - (A) Scheme of the EGFR-PTP interaction network. Ligandless EGFR (E_p) interacts with PTPRG (P_{RG}) and PTPN2 (P_{N2}). Liganded EGFR ($E-E_p$) promotes autocatalysis of E_p. Causal links: solid black lines; curved arrow lines: diffusion. (B) Dynamical mechanism: critical organization before sub-critical pitchfork bifurcation (PB, magenta shaded area). Stable/unstable steady states (solid/dashed lines): basal (homogeneous) and polarized (inhomogeneous) receptor activity; stimulus induced transitions between states: arrow lines. SN_{PB}: saddle-node bifurcation through which PB is stabilized. (C) Top: (*In silico*) evolution of spatial EGF distribution. Bottom: Kymograph of $EGFR_p$ for organization at criticality from reaction-diffusion simulations of the network in A. Corresponding exemplary cell shapes with color coded $EGFR_p$, obtained with a viscoelastic model. Green/red lines: stimulus presence/absence. (D) State-space trajectory of the system with denoted trapping state-space areas (colored arbitrarily). Thick/thin line: signal presence/absence.

with

$f_1 = ([E_t] - [E_p] - [E - E_p]) \cdot (\alpha_1 \cdot ([E_t] - [E_p] - [E - E_p]) + \alpha_2 \cdot [E_p] + \alpha_3 \cdot [E - E_p]) - \gamma_1 \cdot [RG_a] \cdot [E_p] - \gamma_2 \cdot [N2_a] \cdot [E_p] - k_{on} \cdot ([EGF_t] - [E - E_p]) \cdot [E_p]^2 + 1/2 \cdot k_{off} \cdot [EE_p]$;

$f_2 = k_{on} \cdot ([EGF_t] - [E - E_p]) \cdot ([E_p]^2 + ([E_t] - [E_p] - [E - E_p])^2) - k_{off} \cdot [E - E_p]$;

$f_3 = k_1 \cdot ([RG_t] - [RG_a]) - k_2 \cdot [RG_a] - \beta_1 \cdot [RG_a] \cdot ([E_p] + [E - E_p])$; and

$f_4 = \epsilon \cdot (k_1 \cdot ([N2_t] - [N2_a]) - k_2 \cdot [N2_a] + \beta_2 \cdot ([E_p] + [E - E_p]) \cdot ([N2_t] - [N2_a]))$.

The reaction terms are described in [92]. $[E - E_p]$ is the phosphorylated ligand-bound dimeric EGFR, $[E_p]$ - ligandless phosphorylated EGFR, $[E_t]$ - total amount of EGFR, $[RG_a], [RG_t]$ and $[N2_a], [N2_t]$ - the active and total amount of the membrane localized PTPRG and the ER-bound PTPN2, respectively. Both, the receptor and the deactivating enzymes have active and inactive states, and the model equations describe their state

transition rates. Therefore, mass is conserved in the system and the total protein concentrations of the three species ($[E_t]$, $[RG_t]$ and $[N2_t]$) are constant parameters.

Autonomous, autocatalytic and ligand-bound-induced activation of ligandless EGFR ensue from bimolecular interactions with distinct rate constants α_{1-3}, respectively. Other parameters are as follows: k_1/k_2 — activation/inactivation rate constants of the phosphatases, β_1/β_2 - receptor-induced regulation rate constants of $PTPRG/PTPN2$, γ_1/γ_2 - specific reactivity of the enzymes ($PTPRG/PTPN2$) towards the receptor. The EGFR-PTPN2 negative feedback is on a time scale (ϵ) approximately two orders of magnitude slower than the phosphorylation-dephosphorylation reaction, as estimated from the $\sim 4min$ recycling time of $EGFR_p$ [92]. This enables, when necessary, to consider a quasi-steady state approximation for the dynamics of PTPN2 for simplicity:

$$[N2_a]_{qss} = [N2_t] \cdot \frac{(k_1 + \beta_2 \cdot ([E_p] + [E - E_p]))}{k_1 + k_2 + \beta_2 \cdot ([E_p] + [E - E_p])} \tag{1.2}$$

$[EGF_t]$ denotes the total ligand concentration. Assuming that at low, physiologically relevant EGF doses, the ligand will be depleted from the solution due to binding to EGFR [148], ligand-binding unbinding was explicitly modeled (k_{on}, k_{off}) in Eqs.1.1.

The diffusion terms model the lateral diffusion of the EGFR and PTPRG molecules on the plasma membrane, whereas PTPN2 is ER-bound and does not diffuse. Single particle tracking studies have demonstrated that EGFR molecules on the plasma membrane occupy three distinct mobility states, free, confined and immobile, with the occupations of the free and immobile states decreasing and increasing significantly after EGF stimulation (2 min after EGF stimulation, corresponding with the time-scale of EGF binding) [102]. In the reaction-diffusion (RD) simulations therefore for simplicity, it has been assumed that $D_{E-E_p} \approx 0$, whereas diffusion constants of same order are assumed for the ligandless EGFR and PTPRG ($D_{E_p} \sim D_{RG_a}$).

A weakly nonlinear analysis [149] for the system of PDEs revealed that the EGFR signalling dynamics undergoes a symmetry-breaking transition through the PB. Polarized EGFR signaling will effectively lead to reorganization of the cortical actomyosin cytoskeleton by regulating members of the Rho GTPase family, thereby inducing signal-dependent cell shape changes and subsequent migration [150, 151]. To incorporate the mechanical regulation of cell shape, the cell was modelled as a viscoelastic cortex surrounding a viscous core [152], where EGFR signaling dynamics affects cell shape changes through the protrusion/retraction stress and the viscoelastic nature of the cell membrane.

To observe polarization of receptor phosphorylation in simulated cells, $EGFR$ phosphorylation on the PM in single cells was plotted using kymographs which report the phosphorylated receptor amount around the cell contour over time. Simulations of the cell system in the absence of threshold EGF stimulus exhibited basal EGFR

phosphorylation uniformly distributed along the cell's plasma membrane rendering a symmetrical cell shape. When dynamic gradient stimulation was applied to the cells in the simulation, it resulted in rapid polarization of EGFR phosphorylation towards the EGF source generating a cell shape with a clear front and back (Figure 1.13 C). The polarized signaling state was maintained for a transient period after removing the gradient, corresponding to manifestation of memory of the localization of the previously encountered signal (Figure 1.14 A). The prolonged polarized state does not result from remnant ligand-bound receptors on the plasma membrane, as they exponentially decline after signal removal. The phase space trajectory shows that the temporal memory in EGFR phosphorylation polarization is established due to transient trapping of the signaling state trajectory in state-space, indicating that the system is maintained away from steady states (Figure 1.13 D). The memory in polarized signalling (Figure 1.14 A) was also reflected on the level of the cell morphology, as shown by the difference of normalized cell protrusion area in the front and the back of the cell over time (Figure 1.14 B).

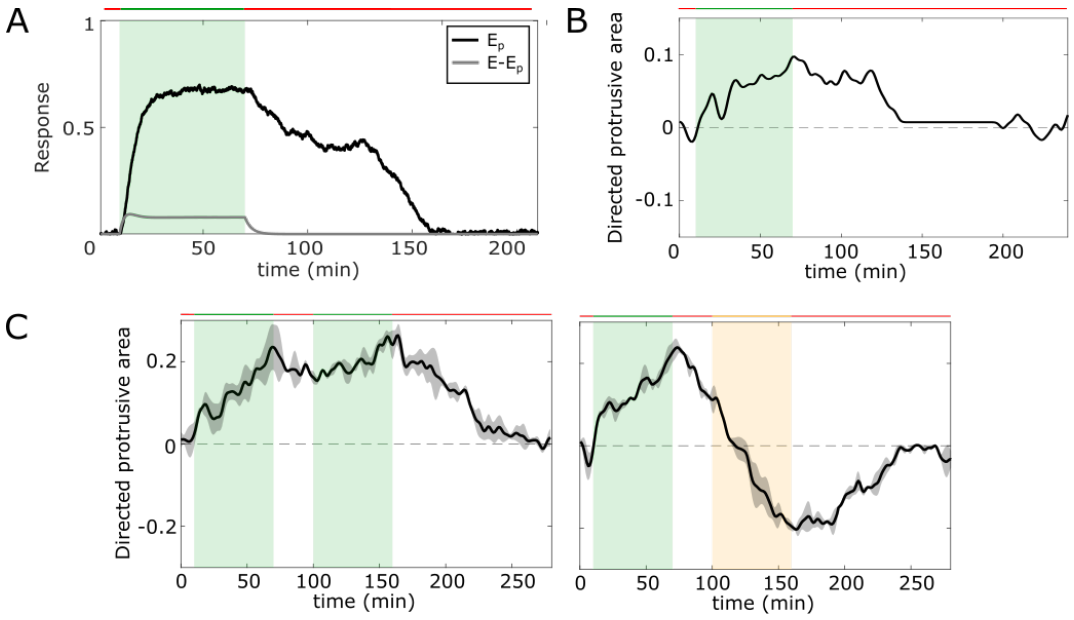

Figure 1.14: Evidence of memory in EGFR activity - (A) Temporal profiles E_p (black) and $E - E_p$ (grey). Green shaded area: EGF gradient presence. (B) Quantification of in silico cell morphological changes from the cell in Figure 1.13 C. (C) Left: Same as in B, only when stimulated with two consecutive dynamic gradients from same direction. Second gradient (yellow) within the memory phase of the first. Right: the second has opposite localization. Mean+/-s.d. from n=3. Green(yellow)/red lines: stimulus presence/absence

The cell polarity is sustained even when the EGF signal is briefly disrupted (Figure 1.14 C left), and the cell can reverse the direction of polarization when the signal direction is inverted (Figure 1.14 C right). Thus, it has been shown via simulations that the trapping in the dynamically metastable memory state does not hinder sensing and adapting to subsequent signals. This suggests that organization at criticality, in a vicinity of a SN_{PB}, is a unique mechanism for processing changing signals. However,

experimental validation of the theory of symmetry breaking and cellular information processing needs to be tested systematically.

1.4 Methods of identification of metastable states from experimental data

A metastable state can be defined as a topological domain in a system's state space with relatively large dwell time and slow evolution, which is separated from another stable state through a fast transient regime. Thus metastability is prone to be manifested when a system has multiple and well-distinguished time scales [153, 142]. H.A. Kramer was the first to study metastability occurring in stochastic systems in 1940. The concept was initially used to study the time evolution of chemical reactions corresponding to a double-well potential with added diffusion in the system [154].

Metastability arises in the EGFR-PTP system near the critical organization of the system due to the trapping in the "ghost" attractor. The dynamical features of metastability are different from slow relaxation kinetics [142]. It reflects in the polarization of EGFR phosphorylation where high EGFR phosphorylation is maintained transiently for a significant time after removing the EGF stimulus. Hence, it is possible to systematically validate the presence of metastable states from the EGFR phosphorylation's temporal data.

One of the essential concepts of time-series analysis is the identification of structures that correspond to dynamical features of the underlying system, i.e., the different dynamical states and the transitions between those states. A time series is generally a result of applying an unknown measurement function to the states of the dynamical states. This function is a projection of the space containing all the states of the dynamical system, or state space, into a subspace of lower dimensions. Reconstruction of the state space of the underlying dynamical system enables one to identify the different dynamical states in a time series.

A commonly used method of reconstructing state space from a time series is the time delay-embedding mapping based on Taken's theorem [155, 156]. Taken's theorem essentially states that one can obtain a structure that is topologically equivalent to the attractor of the analyzed univariate time series of a system by means of a time delay embedding. Such mapping depends on essentially two embedding parameters: the time delay (τ) and the embedding dimension (m). Suppose there is a time series denoted by $x(t_i)$, $i = 1, ..N$ which is to be embedded into a m-dimensional state space by the delay vectors (Figure 1.15 A). In the state space (Figure 1.15 B), a point along the trajectory of the system can be given as a vector:

$$\mathbf{Y}(t_i) = [x(t_i), x(t_i + \tau), .., x(t_i + (m-1)\tau)] \tag{1.3}$$

where $i = 1$ to $N-(m-1)\tau$, τ is the embedding delay, m - is a dimension of reconstructed space (embedding dimension). m is given by the expression $m = 2D + 1$. D is the dimension of the original attractor.

The optimal delay time (τ) can be estimated using the autocorrelation function on the analyzed time-series data. (τ) is typically chosen as the value at which the autocorrelation lowers to a fraction of its initial value [157]. When the dimension of the system under observation is unknown, one way to estimate the appropriate embedding dimension (m) is the False Nearest Neighbourhood (FNN) algorithm [158]. The method utilizes how the neighbors of a point along a trajectory in state space change with increasing dimension. Ideally, the points which remain close in the embedding space will remain close during forward iterations. If a point has a close neighbor violating such a condition, it is a false nearest neighbor. Optimal m is estimated for a fraction of points where FNN converges to 0.

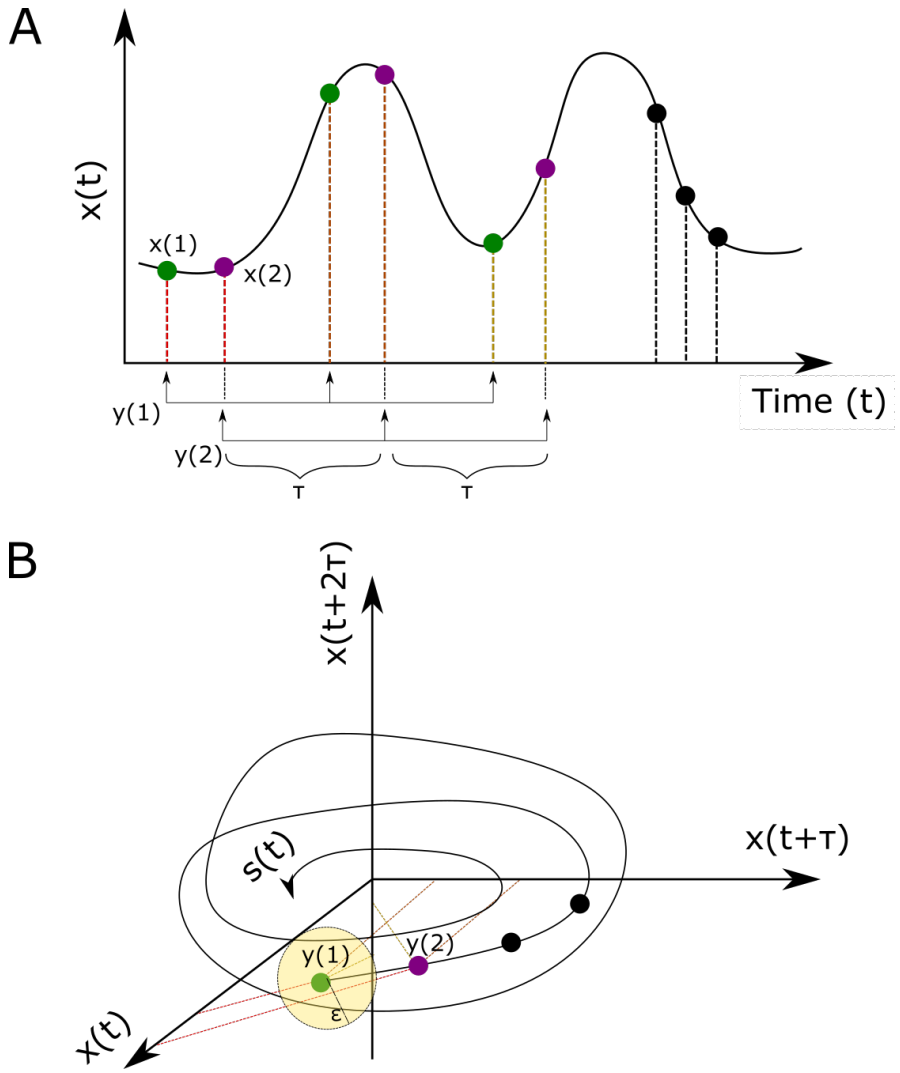

Figure 1.15: Theory of attractor reconstruction - (A) Example time series of a continuous function $x(t)$ with discrete measured points given x. Projection of x on m^{th} dimension after a chosen delay τ given by y(t). (B) Reconstructed phase space from time series in A given by s(t) with denoted points given by y(t). ϵ shows the radius of a ball within which the number of nearest neighbours are chosen.

1.5 Characterization of cell migration

With the advance of modern microscopic advancements, one has been able to track the movements of single cells, amoeba, and unicellular organisms over long durations. Similarly, it has been possible also to characterize the nature and movement of these cells in detail using physical principles. Tracking immune cells like leukocytes in tissues towards polarised cytokines generates noisy, biased directional cell tracks [159]. Upon low doses of EGF stimulation over a prolonged duration, epithelial cells undergo migratory behavior [160]. Hence the activation of the EGFR-PTP system with EGF stimulation provides a setup to identify and characterize the nature of migratory cell modes. Stochastic models from physics are generally used to model cell movements.

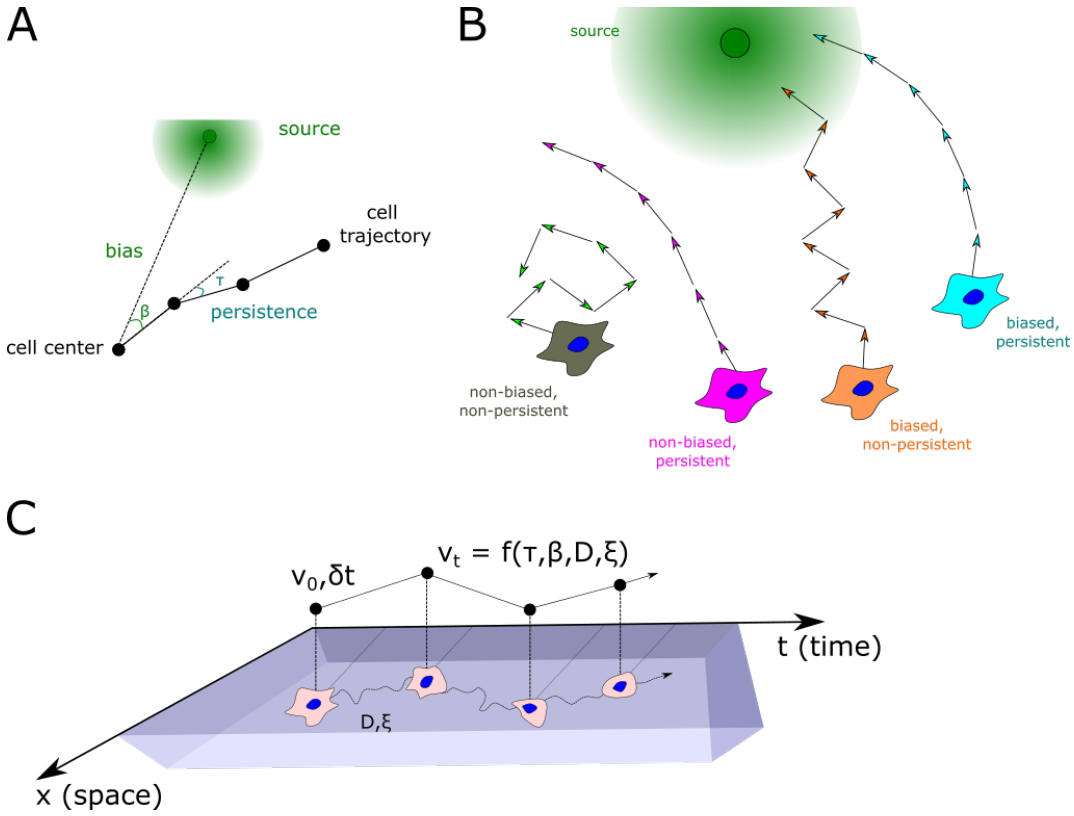

Figure 1.16: Characterization of migratory modes - (A) Bias and persistence in terms of cell migration - Relative bias angla denoted by β, persistence angle denoted by τ, diffusing point source given by green dot black dots mark cell center over time; (B) Different modes of migratory behaviour; (C) Ornstein-Uhlenbeck model of cell migration using velocity vector ν as a function of measurable parameters. D represents diffusion and ξ represents noise.

Previous studies have shown quantitative metrics of cell migration estimated from the cell tracks, e.g., diffusion rate, cell velocity, persistence, directionality, and mean-square deviation [161]. Persistence is defined as the capacity of the cell or an object to maintain a direction of motion regardless of the changes in the environment (Figure 1.16 A). The persistence time characterizes the average time between significant changes in the direction of a cell's translocation [162]. Similarly, directionality can be defined as the

bias of the cell or object towards a particular location which a growth factor or cytokine can provide. Conventionally a random walk-like behavior due to Brownian motion can describe a random cell movement with no directionality and only diffusion propelled. Such walks have been described using simple Langevin dynamics by modeling the velocity of the cell as a function of the intrinsic properties of the cell for e.g., diffusion [163]. However, cell migration is a complex global phenomenon that needs to be characterized by directed motion and direction changes upon signal changes.

Possible cases of cell migration (Figure 1.16 B) which may arise and needs to be taken into account while characterizing the migratory behaviour are: (i) a completely random walk with no persistence or directionality towards any source, (ii) a persistent motion but with no directionality towards any source, (iii) a motion without persistence but with directionality towards a source, (iv) a persistent and directional movement towards a particular source. Often a mix of these three types is observed in real systems.

The Ornstein-Uhlenbeck (OU) process has long been considered a popular model to characterize such complex migratory motion of single cells or organisms [161]. The OU process is a Gaussian, Markov process and was originally was used as a model for the velocity of a Brownian object under external forces (Figure 1.16 C). The process can be defined by the Langevin equation for the velocity vector ν:

$$\frac{d\nu(t)}{dt} = -\frac{1}{\tau} \cdot \nu(t) + \frac{\sqrt{2D}}{\tau} \cdot (\xi(t) + b) \tag{1.4}$$

where $\xi(t)$ represents a white noise component, D is a diffusion coefficient characteristic of a Brownian motion, τ is the persistence time and b is the bias of the cell movement. The bias can be incorporated into such models as the direction of the external stimuli. The diffusion and the persistence time parameters can be extracted from the migratory tracks of the cells with the help of mean-square displacement (MSD) and the velocity auto-correlation function (VACF) [164]. The behaviour of the MSD and VACF has been shown to fit the following equations:

$$< x^2(t) >= 2n \cdot D \cdot \tau \cdot (e^{-\frac{t}{\tau}} + \frac{t}{\tau} - 1) \tag{1.5}$$

$$< v(t)v(0) >= \frac{nD}{\tau} \cdot e^{-\frac{t}{\tau}} \tag{1.6}$$

where Eqn. 1.5 is popularly known as the Furth formula and n is the space dimension. Both Eqns. 1.5 and 1.6 describe the behaviour of average number of cells [164].

1.6 Fluorescence microscopy as a tool for observing receptor activity

While classical molecular biology methods and proteomic analysis provide knowledge of the protein interactions, dynamics of signaling in single cells can be obscured in the population behavior of cells. Fluorescence microscopy is an important tool for studying dynamical processes in single living cells allowing for time-lapse imaging of fluorescent-tagged proteins inside cells. It provides an insight into the dynamics of signaling networks.

Fluorescence microscopy utilizes the photo-physical properties of fluorescent molecules. When proteins are excited by a light source with high frequency, the molecule's electrons absorb photons from the light source and jump to the excited state, as shown in the Jablonski diagram (Figure 1.17 A) [165]. It is a very fast process. A fluorescent molecule, tagged to the protein, emits photons from its electrons when they relax from an excited state (S_1 or S_2) to the ground state (S_0). Initially, due to the non-radiative process, the excited electron loses energy and falls to the sublevels of the first excited state (S_1). As the electron falls to the ground state S_0, fluorescent emission takes place. The energy of the emitted photon due to fluorescence corresponds to the energy difference of the transition levels (Figure 1.17 A). Therefore, it is crucial to identify the appropriate fluorescent proteins and reporters while designing the experiments. For optimized imaging purposes, it is necessary to avoid spectral overlap, which may lead to photo-activation or bleed-through from one channel to another.

For observing and quantifying receptor phosphorylation in live single cells, mainly two fluorescent reporters are used on the EGFR (mCitrine) and the PTB domain (mCherry) and ratiometric imaging is performed. Ratiometric imaging uses the ratio of the intensity of emission of one fluorophore over the emission of the other fluorophore to quantify the activity of the protein of interest (Figure 1.17 B) [166]. Shifting of intensities due to protein interactions lead to change in intensity ratio.

To image the interactions of these proteins over long durations, multichannel time-lapse confocal microscopy is used (Figure 1.17 C). Confocal laser scanning system can provide high spatial data which has a point illumination system with a pinhole to focus the light on the optimal plane of the cell. A detector is used to gather the emitted fluorescent signal which has a pinhole to eliminate unwanted out-of-plane light signals. Following the conclusion of imaging, single cell spatial and temporal data can be used for image segmentation as well as cell tracking purposes. These results elucidate information about the signalling systems.

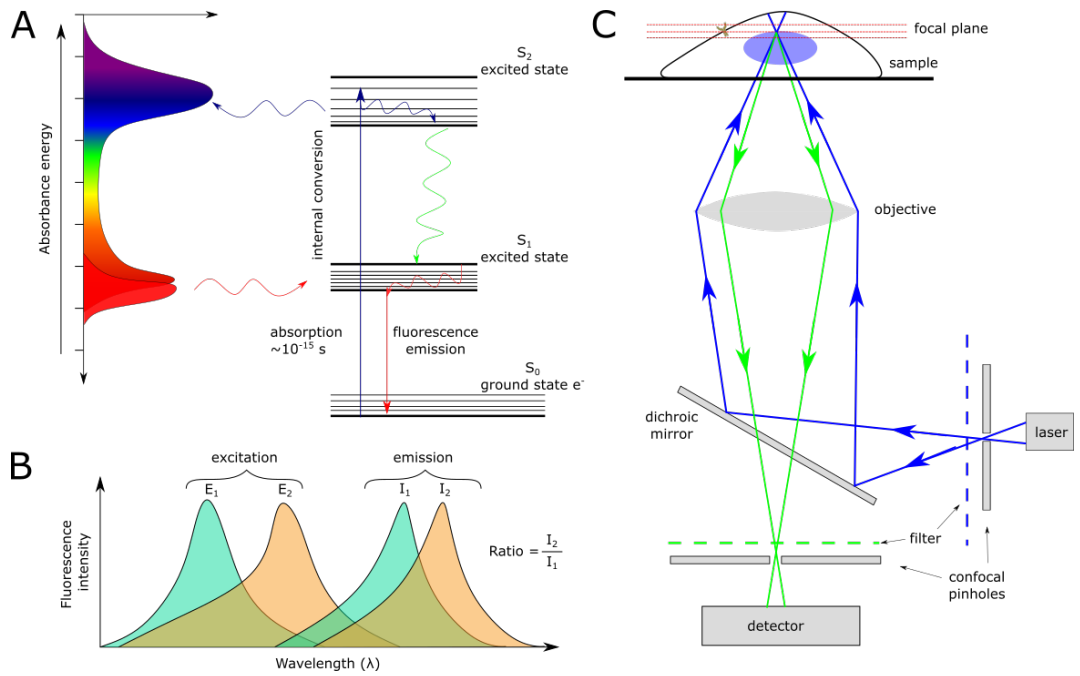

Figure 1.17: Confocal microscopy and ratiometric imaging - (A) Jablonski diagram showing the excitation of an e^- to a higher energy state (blue), internal conversion via vibrational relaxation to the lowest S_1 sub-level (green wavy lines) and fluorescent emission (red); (B) Ratiometric imaging principle - Absorption and emission spectrum of two fluorophores; (C) Schematic of how a confocal microscope works.

1.7 Research objectives

Information processing of varying external gradients of growth factors requires maintenance of stability in the cellular responses along with simultaneously perceiving new changes in the surroundings. Such stability in responses requires cellular memory with respect to the signals the cell has previously sensed, but this should not hinder the adaptability of the cell to changes in its environment. Thus, for cells to operate and process information in a changing environment they must have the following features: (i) polarization in the direction from which graded EGF signal is generated, (ii) robust and rapid maintenance of the polarized state of EGFR phosphorylation longer than the signal duration along with (iii) the ability to integrate multiple new EGF signals from different spatial locations. Based on a formal description of a mechanism for information sensing and processing, it is necessary to experimentally identify how the above features are realized at the level of signaling networks.

I have set out to do this by probing the well-established spatially distributed EGFR-PTP network in epithelial cells and demonstrated that a dynamic transient memory is maintained in prolonged EGFR phosphorylation via a dynamical "ghost" of the attractor of polarized signalling. This memory helps the cells in maintaining directional motility as well as integrate novel signals in the environment. Hence I conclusively argue that cells implement real-time computations without stable-states to navigate in changing chemoattractant fields.

2

Materials and Methods

2.1 Materials

2.1.1 Reagents and Instruments

Consumables, reagents, chemicals, and instruments were purchased from the following suppliers, unless otherwise stated: Thermo Fisher Scientific, PAN Biotech, Lonza, Bio-Rad, Carl Roth, Eppendorf, GE Healthcare, Invitrogen, Merck, Millipore, New England Biolabs, Qiagen and Sigma-Aldrich. De-ionized sterile water, sterile solutions, and sterile flasks were usually used for experiments.

2.1.2 Software and Resources

This thesis work was prepared using the Microsoft Windows 10 and 11 operating system installed on a Lenovo V15 laptop and written in LaTex using Overleaf. Standard software used for data analysis or visualization and data/text preparation include Python 3.8 (Anaconda), MATLAB (Mathworks), GraphPad Prism 7 (GraphPad Software), ImageJ (National Institutes of Health), Inkscape (Open Source Software), Leica Application Suite v3.3.0 (Leica Camera), Mendeley (Mendeley Ltd.), Microsoft Office Professional Plus 2016 (Microsoft corp.), PlotsOfData (https://huygens.science.uva.nl/PlotsOfData/), Lasergene Molecular Biology (DNASTAR), xCellence (Olympus Microscope Systems) and Millipore Microfluidic system software.

2.2 Methods

2.2.1 Mammalian cell culture

MCF7 cells (sex: female, ECACC, Cat. No. 86012803) were grown at 37°C and 5% CO_2 in Dulbecco's Eagle's medium (DMEM) (PAN-Biotech, Germany), supplemented with 10% inactivated Fetal Calf Serum (FCS) (Sigma-Aldrich), 100 ng/ml L-Glutamine, 0.5 mg/ml non-essential amino acids, 100 µg/ml penicillin and 100 µg/ml streptomycin (PAN-Biotech, Germany). MCF10A cells (sex: female, ATCC-CRL 10317) were grown at 37°C and 5% CO2 in Mammary Epithelial Cell Growth Basal medium (MEBM) (Lonza Pharma and Biotech), supplemented with 5% Horse Serum (HS) (Invitrogen), 20 ng/ml EGF (Sigma-Aldrich), 0.5 mg/ml hydroscortisone (Sigma-Aldrich), 100 ng/ml cholera toxin (Sigma-Aldrich), 10 µg/ml insulin (Sigma-Aldrich), 100 µg/ml penicillin and 100 µg/ml streptomycin. Serum starvation was performed by culturing the cells in the DMEM supplemented with 0.5% HS, 0.5 mg/ml hydrocortisone, 100 ng/ml cholera toxin, 100 µg/ml penicillin and 100 µg/ml streptomycin. Both the MCF7 and MCF10A cells were authenticated by Short Tandem Repeat (STR) analysis and did not contain DNA sequences from mouse, rat and hamster (Leibniz-Insitut DSMZ). Cells were regularly tested for mycoplasma contamination using MycoAlert Mycoplasma detection kit.

2.2.2 Seeding

The cells were grown in culture until 80% confluence, after which they were detached and seeded in new tissue culture flasks or Lab-Tek plates. The growth media was discarded, cells were washed once with DPBS (PAN Biotech) and 100 µl Accutase (Sigma-Aldrich) was added for detachment. After 10-15 min incubation at 37°C, fresh growth media, containing 10% FCS (for MCF7 cells) or 5% HS (for MCF10A cells), was added to the cells and the cell density and viability was measured using a cell counter (Vi-CELL XR Cell Viability Analyzer System). Finally, the cells were seeded with the desired concentration in new tissue culture flasks or plates for experiments.

2.5x10^5 MCF7 cells were seeded per well in a 6-well Lab-Tek chamber (Nunc) for the pulsed EGF (5 min-EGF), double-pulse (5+5 min EGF) and gradient EGF (1 h) live cell experiments. For these experiments, following the transient DNA transfection of the required plasmids, the cells were transferred to the CellASIC ONIX microfluidic switching plate (M04S-03, Millipore) or to the CellASIC ONIX microfluidic gradient plate (M04-G02, Millipore) in complete growth media for at least 5 h prior to serum starvation. The cells were incubated with 100 µl Accutase for ∼10-15 min for gentler detachment, after which they were spun down and concentrated to 10 million cells/ml, as per the instruction's manual. Finally, the cells were loaded and perfused using the CellASIC ONIX Microfluidic Platform (Millipore).

$2x10^5$ MCF7 cells and $1.5x10^5$ MCF10A cell were seeded per well in extracellular matrix coated 6-well Lab-Teks (Nunc) for the single cell migration experiments. For migration experiments with gradient EGF stimulation, both MCF7 and MCF10A cells were washed with DPBS and detached with Accutase and spun down to concentrate to 2 million cells/ml before being loaded in the M04-G02 microfluidic plates according to the manufacturer's instructions.

2.2.3 Transfection

Transient transfection was performed 24 h after seeding with a total of 1 µg (6-well dishes) of cDNA using FUGENE6 (Roche Diagnostics) transfection reagent. For the receptor activity measurement experiments, expression plasmids were used of $EGFR^{mCitrine}$, $PTB^{mCherry}$ and $cCbl^{BFP}$ in the ratio of 4:3:4 by mass. All plasmids were generously provided by Prof. P. I. H. Bastiaens, Max Planck Institute for Molecular Physiology, Dortmund, Germany. Cells were incubated for 7-8 h to allow the expression of the transfection proteins prior to serum starvation.

2.2.4 EGF stimulation

In-house fluorescently mono-labelled EGF^{647} was used in the experiment to observe its association with EGFR. The His-CBD-Intein-(Cys)-hEGF-(Cys) plasmid [[167]] was kindly provided by Prof. Luc Brunsveld, University of Technology, Eindhoven. Human EGF was purified from E. coli BL21 (DE3) and N-terminally labelled with Alexa647-maleimide as described previously [reference] and stored in PBS at 20°C in Prof Prof. P. I. H. Bastiaens lab. Following transfection or seeding on the previous day, the cells were serum starved with supplemented DMEM with 0.5% FCS (for MCF7 cells) or MEBM supplemented with 0.5% HS (for MCF10A cells) for at least 6 h before EGF stimulation.

For the single pulse experiments, the MCF7 cells were seeded and starved in a CellASIC ONIX microfluidic switching plate (M04S-03, Millipore). An EGF pulse washout program consisting of a 5 min pulse of EGF^{647} (20 ng/mL) followed by continual perfusion with serum-free media for 65 min was delivered using the CellASIC ONIX Microfluidic Platform (Millipore). For double pulse experiments this step was performed per pulse, with an interval period of washout for 10 min.

For EGFR phosphorylation polarization experiments, 1 h gradient stimulation was performed using a maximal concentration of 10 ng/ml EGF^{647} which was passed through a perfusion channel in the M04-G02 plates using the CellASIC ONIX Microfluidic Platform (Millipore) and washed away subsequently for 3 h using serum-free media.

For the uniform stimulation migration experiment, incremental doses of EGF^{647} diluted in serum-free medium (0, 2.5 ng/ml, 5 ng/ml, 10 ng/ml 15 ng/ml, 20 ng/ml

and 100 ng/ml) were administered in separate wells of 6-well Lab-Tek plate and imaged subsequently.

For the single gradient and multiple gradient migration experiments, gradient stimulation was performed using a maximal concentration of 30 ng/ml EGF^{647} and washed away following stimulation using either serum-free media or EGFR inhibitor solution.

2.2.5 EGFR activity inhibition

For a subset of the polarization and migration experiments EGFR phosphorylation activity was inhibited using an ATP analog EGFR inhibitor Lapatinib (Lap) (Cayman Chemical, Ann Arbor, MI), that inhibits the EGFR signal processes by binding to the ATP-binding pocket of the receptor protein kinase domain. Lapatinib was solubilized in DMSO (Thermo Fisher Scientific) to a stock concentration of 5 mM and stored at -20°C. The cells were treated with 1 µM or 3 µM of Lap following gradient stimulation of EGF^{647} for 1 h and 5 h respectively.

2.2.6 Reagents

Serum-free imaging media was prepared using DMEM without Phexedwith 25 mM HEPES. For gradient quantification, 2.5 µM Fluorescein (Sigma Aldrich) was prepared by diluting in serum-free imaging media (IM). For nuclear staining, 20 mM Hoechst 33342 (Thermo Fisher Scientific) was diluted with DPBS to 2 µM working concentration which was added to cells 30 min before imaging.

2.2.7 Confocal and wide-field microscopy

Confocal images were recorded using a Leica TCS SP8i confocal microscope (Leica Microsystems) with an environment-controlled chamber (Life Imaging Services) maintained at 37°C and HC PL APO 63x/1.2 N.A / motCORR CS2 water objective (Leica Microsystems) or a HC PL FLUOTAR 10x/0.3 N.A. dry objective (Leica Microsystems). mCitrine, mCherry and Alexa647 were excited with a 470-670 nm pulsed white light laser (Kit WLL2, NKT Photonics) at 514 nm, 561 nm and 633 nm, respectively. BFP and Hoechst 33342 (Thermo Fisher Scientific) were excited with a 405 nm diode laser. The detection of fluorescence emission was restricted with an Acousto-Optical Beam Splitter (AOBS): BFP (425-448 nm), Hoechst 33342 (425-500 nm), mCitrine (525-551 nm), mCherry (580-620 nm) and Alexa647 (655-720 nm). Transmission images were recorded at a 150-200% gain. To suppress laser reflection, Notch filter 488/561/633 was used whenever applicable. When using the dry objective for migration experiments, the pinhole was set to 3.14 airy units and 12-bit images of 512x512 pixels were acquired in frame sequential mode with 1x frame averaging. When using the water objective for

polarization experiments, the pinhole was fixed (1.7 airy units) for all channels. The Leica Application Suite X (LAS X) software was used.

Wide field images were acquired using an Olympus IX81 inverted microscope (Olympus Life Science) equipped with a MT20 illumination system and a temperature-controlled CO_2 incubation chamber at 37^oC and 5% CO_2. Fluorescence and transmission images were collected via a 10x/0.16 NA air objective and an Orca CCD camera (Hamamatsu Photonics). Hoechst 33342 fluorescence emission was detected between 420-460 nm via DAPI filter, mCitrine fluorescence emission between 495-540 nm via YFP filter and Alexa647 fluorescence emission between 705-745 nm via Cy5 filter. The xCellence (Olympus) software was used.

2.2.8 Simulation of pulsatile EGF in EGFR-PTP system

Suprathreshold EGF pulses was simulated to estimate the responsiveness of phosphorylated EGFR and ligand-bound EGFR in critical organization of the subcritical pitchfork bifurcation regime. The dynamics of the experimentally identified spatially-distributed EGFR sensing network can be described using the following system of ordinary differential equations:

$$\begin{aligned}
\frac{d[EGFR_p]}{dt} &= f_1([EGFR_p],[EGF-EGFR_p],[PTPRG_a],[PTPN2_a],[EGF_t]) \\
\frac{d[EGF-EGFR_p]}{dt} &= f_2([EGFR_p],[EGF-EGFR_p],[EGF_t]) \\
\frac{d[PTPRG_a]}{dt} &= f_3([EGFR_p],[EGF-EGFR_p],[PTPRG_a]) \\
\frac{d[PTPN2_a]}{dt} &= f_4([EGFR_p],[EGF-EGFR_p],[PTPN2_a])
\end{aligned} \tag{2.1}$$

The reaction terms are described in [92]. f_{1-4} are elaborately explained in Results section 3.1. The parameter and variable values chosen for Equation 3.1 are written in the below Table 2.1.

2.2.9 Pressure protocol for pulse experiments

The CellAsic Onix Microfluidic Platform (EMD Millipore) was used for $EGFR^{mCitrine}$ phosphorylation experiments under pulse stimulations. The M04-S03 microfluidic standard plates were primed for usage by flowing cell culture media through the cell chamber for 5 min according to manufacturer's instructions. For $EGFR^{mCitrine}$ phosphorylation experiments upon single pulse of EGF stimulation, stimulation was

$EGFR_t$	EGF_t	$PTPRG_t$	$PTPN2_t$
0.8	0.05	1.27321	0.5
k_1	k_2	k_3	k_4
0.01	0.5	0.22	2.25
β_1	β_2	γ_1	γ_2
36.0558	1.60248	2.42625	0.061
γ_3	α_1	α_2	α_3
0.001	0.0017	0.3	1
k_{on}	k_{off}	ϵ	K_D
0.003	0.0016	0.01	5.56

Table 2.1: Parameter values corresponding to saddle-node bifurcation

established using CellASIC ONIX2 software as follows. (i) Pre-stimulus: Imaging media was flowed from well groups 2 (CellAsic Onix Manual - www.merckmillipore.com/) at high pressure (30 kPa) for 5 min. (ii) Pulse establishment: After closing well group 2, pre-loaded EGF^{647} (20 ng/ml) was flowed through well group 3 at high pressure (30 kPa) for 5 min (iii) Washout: After closing well groups 3, imaging media was flowed from well groups 2 again at high pressure (30 kPa) for 5 min and maintained at low pressure (7 kPa) for 80 min. For single gradient migration experiments, this protocol was modified as follows: in step (iii), gradient maintenance was done for 285 min. In step (iv), maintenance was at low pressure for 585 min. 30 ng/ml EGF^{647} was used. For $EGFR^{mCitrine}$ phosphorylation experiments upon double pulses of EGF stimulation, two extra steps were added to the previous protocol inbetween (ii) and (iii) - revised (iii) Inter-pulse washout: After closing well groups 3, imaging media was flowed from well groups 2 again at high pressure (30 kPa) for 10 min and revised (iv) Second pulse establishment: After closing well group 2, pre-loaded EGF^{647} (20 ng/ml) was flowed through well group 3 at high pressure (30 kPa) for 5 min.

2.2.10 Gradient establishment for polarization and migration experiments

2.2.10.1 Polarization protocol

The CellAsic Onix Microfluidic Platform (EMD Millipore) was used for gradient cell migration and $EGFR^{mCitrine}$ phosphorylation polarization experiments. The M04-G02 microfluidic gradient plates were primed for usage by flowing cell culture media through the cell chamber for 5 min according to manufacturer's instructions. For $EGFR^{mCitrine}$ phosphorylation polarization experiments, 1 h gradient stimulation was established using CellASIC ONIX2 software as follows. (i) Pre-stimulus: Imaging media was flowed from well groups 3 and 4 (CellAsic Onix Manual - www.merckmillipore.com/) at low

pressure (2.5 kPa) for 5 min. (ii) Gradient establishment: After closing well group 3, pre-loaded EGF^{647} (10 ng/ml) was flowed through well group 2 and imaging media from well group 4 at high pressure (15 kPa) for 15 min (iii) Gradient maintenance: The pressure was reduced to 10 kPa for 45 min. (iv) Washout: After closing well groups 2 and 4, imaging media was flowed from well groups 3 and 5 at high pressure (15 kPa) for 15 min and maintained at low pressure (7 kPa) for 165 min. For single gradient migration experiments, this protocol was modified as follows: in step (iii), gradient maintenance was done for 285 min. In step (iv), maintenance was at low pressure for 585 min. 30 ng/ml EGF^{647} was used. For polarization experiments with inhibitor, the same protocol as for polarization experiments was used, except well group 3 and 5 were filled with 1 uM Lapatinib solution and in step (i) well group 3 was kept closed. For single cell gradient migration experiment with inhibitor, 3 uM Lapatinib was used.

2.2.10.2 Migration protocol

For migration experiments under subsequent gradient stimuli / gradient quantification, the following changes in the steps were used: (ii) well group 2 with 30 ng/ml EGF^{647} / 2.5 uM Fluorescein was used. (iii) The gradient maintenance was done for 225 min. (iv) Washout: serum-free imaging media was flowed from well groups 3 and 4 at high pressure (15 kPa) for 15 min and maintained at low pressure (7 kPa) for 15 min. (v) Second gradient establishment: After closing well group 3, EGF^{647} (30 ng/ml) / 2.5 uM Fluorescein was flowed from well group 2 and imaging media from well group 4 at high pressure (15 kPa) for 15 min. (vi) The second gradient thus formed was maintained by reducing the pressure to 10 kPa for 45 min. (vii) Washout: imaging media was flowed from well groups 3 and 4 at high pressure (15 kPa) for 15 min and maintained at low pressure (7 kPa) for 15 min. (viii) Third gradient establishment: After closing well group 4, EGF^{647} (30 ng/ml) / 2.5 uM Fluorescein was flowed from well group 5 and imaging media from well group 3 at high pressure (15 kPa) for 15 min. (ix) The third reversed gradient was maintained by reducing the pressure to 10 kPa for 225 min. (x) Washout: imaging media was flowed from well groups 3 and 4 at high pressure (15 kPa) for 15 min and maintained at low pressure (7 kPa) for 285 min.

2.2.11 Cell migration assays

For single cell migration experiments with uniform EGF^{647} stimulation, 6-well Lab-Tek plates were coated with collagen (Sigma Aldrich) in 0.1 M Acetic acid (Sigma Aldrich) for MCF7 (100 µg/cm^2) and Fibronectin (Sigma Aldrich) in DPBS (PAN Biotech) for MCF10A cells (2 µg/ml). Coated plates were stored in incubator at 37°C overnight for evaporation. Excessive media was removed and wells were washed with DPBS before seeding cells. Gradient plates were respectively coated with the extracellular matrix proteins before loading cells.

2.2.12 Imaging

2.2.12.1 EGFR phosphorylation

Transfected MCF7-$EGFR^{mCitrine}$ cells transferred to M04G-02 gradient plates as described above were incubated for at least 3 h, followed by serum starvation for at least 6 h before imaging. Existing cell media was substituted right before imaging with imaging media. Confocal imaging for multiple positions at 1 min time interval using adaptive auto-focus system and the water objective was performed concurrently during the duration of the experiment using the Leica TCS SP8i.

2.2.12.2 Single cell migration

For migration experiments under EGF^{647} stimulation, confocal laser scanning microscopy / transmission imaging of live MCF7-$EGFR^{mCitrine}$ / MCF10A cells was done on a Leica TCS SP8i or Olympus IX81 for multiple positions at 1 min, 2 min and 3 min time interval respectively depending on the type of experiment and stage movement speed, using the 10x dry objective for 14 hours.

2.2.13 EGF^{647} / Fluorescein gradient quantification

To quantify the spatial extent of the EGF^{647} / Fluorescein gradient, gradients were generated following the protocol described in subsection 2.2.10 in plates without cells or matrix coating. Confocal images of Alexa647 / GFP channel were acquired at 1 min interval. A rectangular region of interest (including the perfusion channels and the culture chamber) was used to obtain an averaged pixel intensity profile using FIJI [168] at each time point. This spatial profile was averaged across multiple experiments and then scaled with the mean intensity value in the perfusion channel, which corresponds to the applied EGF^{647} / Fluorescein concentration.

2.2.14 Quantification of $EGFR^{mCitrine}$ phosphorylation in single cells

To quantify plasma membrane $EGFR^{mCitrine}$ phosphorylation in live MCF7-$EGFR^{mCitrine}$ cells, single cell masks were obtained from the $EGFR^{mCitrine}$ channel at each time-point using FIJI [168]. All pixels within the obtained boundary were radially divided into 2 segments of equal areas [92], and the outer segment was taken to represent the plasma membrane. For the kymograph analysis, at each time point, the plasma membrane segment was divided into 4 quadrants in anti-clockwise direction, and each was divided into 5 spatial bins (Figure 3.3A). The fraction of phosphorylated $EGFR^{mCitrine}$ in each bin, i was estimated as:

$$EGFR_p^i(t) = \frac{PTB_{PM}^i(t)/(PTB_T(t) - PTB_{endo}(t))}{EGFR_{PM}^i(t)/EGFR_T(t)} \tag{2.2}$$

where $PTB_{PM}^i(t)$ and $EGFR_{PM}^i(t)$ are respectively the $PTB^{mCherry}$ and $EGFR^{mCitrine}$ fluorescence at i^{th} plasma membrane bin, $PTB_T(t)$ and $EGFR_T(t)$ - respective total fluorescence in the whole cell, $PTB_{endo}(t)$ – the $PTB^{mCherry}$ fluorescence on vesicular structures in the cytoplasm. Endosomal structures were identified from the cytosol by intensity thresholding (1.5 × s.d. percentile) and $PTB^{mCherry}$ fluorescence from these structures was subtracted from the $PTB_T(t)$, to correct for the $PTB^{mCherry}$ fraction bound to the phosphorylated $EGFR^{mCitrine}$ on endosomes.

Temporal profile of the fraction of phosphorylated $EGFR^{mCitrine}$ on the plasma membrane was obtained using:

$$EGFR_p(t) = \frac{\frac{\sum_{i=1}^{20} PTB_{PM}^i(t)}{(PTB_T(t) - PTB_{endo}(t))}}{\frac{\sum_{i=1}^{20} EGFR_{PM}^i(t)}{(EGFR_T(t))}} \tag{2.3}$$

and then normalized as:

$$EGFR_p(t) = \frac{EGFR_p(t) - < EGFR_p >_{t\in[0,5min]}}{max_t(EGFR_p(t)) - < EGFR_p >_{t\in[0,5min]}} \tag{2.4}$$

with <> being the temporal average in the pre-stimulation interval $t \in [0, 5min]$. The fraction of liganded receptor was calculated using:

$$EGF - EGFR(t) = \frac{EGF_{PM}}{EGFR_{PM}}(t) \tag{2.5}$$

2.2.15 Method of classification of cell states

To classify single cells into non-activated, activated (polarized $EGFR^{mCitrine}$ phosphorylation) and pre-activated (uniformly distributed $EGFR^{mCitrine}$ phosphorylation) upon gradient EGF^{647} stimulation (Figure 3.4 A, B), the following method was applied. To identify pre-activated cells, a Gaussian Mixture Model (GMM) was fitted to the histogram of $(EGFR_p^i)_{t\in[0,5min]}$ values from all the analysed cells, and the intersection point between the two normal distributions was identified. If more than 30% of the $(EGFR_p^i)_{t\in[0,5min]}$ pixel intensity values for any cell lie above the intersection point, the cell is classified as pre-activated. To distinguish between the non-activated and activated cells in the remaining population, average $EGFR^{mCitrine}$ phosphorylation value ($EGFR_p$) per cell was estimated during the pre-stimulation ($t \in [0, 5min]$) and

the stimulation period ($t \in [5min, 65min]$) ($< EGFR_p >_{t\in[0,65]}$) from the temporal $EGFR^{mCitrine}$ phosphorylation profiles. Histogram of the respective $EGFR_p$ values was again fitted with a GMM model. All cells with an average $< EGFR_p >_{t\in[0,65]}$ value lying below the intersection point were considered to be non-activated, whereas those above - activated.

The average of the spatial projection of the fraction of phosphorylated $EGFR^{mCitrine}$ from single-cell kymographs (Figure 3.4 E) was generated from the 20 (from total of 21 cells) that were polarized in the direction of the EGF^{647} gradient. For each cell, a temporal average of $EGFR_p$ per bin was calculated for the duration of the gradient ($t \in [5min, 65min]$) and the bin with the maximal $EGFR_p$ value was translated to π. The profiles were then smoothened using a rolling average with a window of 7 bins. The resulting profiles were then averaged over all cells and mean±s.d. is shown.

2.2.16 Estimating memory duration in $EGFR^{mCitrine}$ phosphorylation polarization

The duration of memory in $EGFR^{mCitrine}$ phosphorylation polarization in single cells was estimated from the temporal profile of the fraction of plasma membrane area with high $EGFR^{mCitrine}$ phosphorylation during and after gradient removal (Figure 3.6). For this, the single-cell kymographs were normalized to a maximal value of 1 using

$$EGFR_p^i(t) = \frac{EGFR_p^i(t) - < EGFR_p >_{t\in[0,5min]}}{max_t(EGFR_p(t)) - < EGFR_p >_{t\in[0,5min]}} \tag{2.6}$$

yielding the value of phosphorylated $EGFR^{mCitrine}$ per bin i per time point t. Using the mean of $EGFR_p + s.d.$ over the whole experiment duration as a threshold, all $EGFR_p^i(t)$ lying above the threshold were taken to constitute the area of polarized $EGFR^{mCitrine}$ phosphorylation. To account for different bin sizes, at each timepoint, the area of all bins with $EGFR_p$ above the threshold was summed and divided by the respective total cell area, yielding the temporal evolution of the fraction of polarized cell area (FPA) (Figure 3.7). The end of the memory duration per cell was identified as the time point at which $FPA_{per-cell} < (FPA_{average} - s.d.)$ in 3 consecutive time points.

2.2.17 Quantification of morphological changes

Morphological changes of polarized cells were quantified using the solidity (Figure 3.9 B) of each cell at each time point and the directed protrusive area towards and away from the gradient (Figures 1.14; 3.9 A). The memory duration in cell morphology was calculated from the single-cell solidity profiles, and corresponds to the time-point at which the solidity is below $mean - s.d.$ estimated during gradient presence. The directed cell protrusion area was estimated by comparing single cell masks at two consecutive

time points. To reduce noise effects, the masks were first subjected to a 2D Gaussian filtering using the $filters.gaussian$ function from the *scipy* python package. Protrusions were considered if the area change was greater than 10 pixels or $1.2\mu m^2$ per time point. The front and the back of the cells were determined by identifying an axis that runs perpendicular to the gradient and through the cell nucleus of the initial time point. The directed cell protrusion area was then obtained using $\frac{A_{prot,front}}{A_{front}} - \frac{A_{prot,back}}{A_{back}}$. The final profiles of directed protrusive area were smoothed using 1D Gaussian filtering with the $filters.gaussian\_filter1d$ function from the *scipy* python package. For the equivalent quantification from the simulations, the same procedures were applied without an area threshold. The memory duration was estimated as the time point at which the directed protrusive area crosses zero after the gradient removal. Methods and codes for quantifying morphological changes were developed in-house by Robert Lott.

2.2.18 Quantification of single-cell migration

Single cell migration trajectories were extracted using Trackmate[169] in Fiji [168] using Hoechst 33342 / transmission channel. From the positional information (x and y coordinates) of individual cell tracks, quantities such as Motility, Directionality and $\cos\theta$ were extracted using custom Python (Python Software Foundation, versions 3.7.3, https://www.python.org/) script written in-house . Directionality was calculated as displacement over total distance and statistical significance was tested using two-sided Welch's t-test. To quantify the memory duration in directed single-cell migration, the Kernel Density Estimate (KDE) from $\cos\theta$ quantification in the continuous absence of EGF^{647} (uniform case, between 250 min-300 min) was compared with windowed KDE (5 time points moving window) from the gradient migration profile, using two sided Kolmogorov-Smirnov test.

2.2.19 Modelling of cell migration

To quantify the motility patterns of MCF10A cells in absence, uniform or gradient EGF^{647} stimulation, we fitted the experimentally obtained single cell migration trajectories using modified Ornstein-Uhlenbeck process (mOU) [170] that is defined by the Langevin equation for the velocity vector ν:

$$\frac{d\nu(t)}{dt} = -\frac{1}{\tau}\cdot\nu(t) + \frac{\sqrt{2D}}{\tau}\cdot(\xi(t) + b(t)) \tag{2.7}$$

where $\xi(t)$ represents a white noise component, D is a diffusion coefficient characteristic of a Brownian motion, τ is the persistence time and $b(t)$ models the contribution of the time-dependent bias. The experimental data was fitted to obtain values of D and τ. In order to estimate D, Mean Square Displacement (MSD) was

calculated from the single cell tracks using $MSD(t) = <|\mathbf{x}_i(t) - \mathbf{x}_i(0)|^2>$, where $\mathbf{x}_i(t)$ is the tracked position of i-th cell in the 2D plane, $<>$ is the average across all single cell tracks, and $|.|$ is the Euclidean distance [171]. To estimate D, the obtained MSD profile was fitted with a linear function ($= 4Dt$). Goodness of Fit for the different experimental conditions: $0ng/ml\ EGF^{647}$, $R^2 = 0.975$; for uniform $20ng/ml\ EGF^{647}$ stimulation, $R^2 = 0.995$. In order to estimate τ, Velocity Auto-Correlation Function $VACF(t) = <\nu_{i(t)} \cdot \nu_{i(0)}>$, where $\nu_{i(t)}$ is the measured velocity of i-th cell at time t, was fitted with a mono exponential function ($= \phi_0 \cdot e^{\frac{-t}{\tau}}$). Goodness of Fit : for $0ng/ml$ EGF^{647} case - Standard Error Of Estimate $SEOE = 0.0261$; for uniform $20ng/ml$ EGF^{647} stimulation case, $SEOE = 0.0570$. Fitted values: for $0ng/ml\ EGF^{647}$ case, $\tau = 11.105$, $D = 0.425$; for uniform $20ng/ml\ EGF^{647}$ stimulation case, $\tau = 38.143$, $D = 2.207$; bias $b(t) = 0.134$.

2.2.20 Reconstructing state-space trajectories from temporal $EGFR^{mCitrine}$ phosphorylation profiles

The state-space reconstruction in Figures 3.8 and 3.10 was performed using the method of time-delay. For a time series of a scalar variable, a vector $x(t_i)$, $i = 1, ..N$ in state-space in time t_i can be constructed as following

$$\mathbf{X}(t_i) = [x(t_i), x(t_i + \tau), .., x(t_i + (m-1)\tau)] \tag{2.8}$$

where $i = 1$ to $N - (m-1)\tau$, τ is the embedding delay, m - is a dimension of reconstructed space (embedding dimension). Following the embedding theorems by Takens [155] and Sauer et al. [156], if the sequence $X(t_i)$ consists of scalar measurements of the state of a dynamical system, then under certain genericity assumptions, the time delay embedding provides a one-to-one image of the original set, provided m is large enough.

The embedding delay was identified using the *timeLag* function (based on autocorrelation), the embedding dimension using the *estimateEmbeddingDims* function (based on the nearest-neighbours method) [172], and the state-space reconstruction using the *buildTakens* function, all from the *nonlinearTseries* package in R (https://cran.r-project.org/web/packages/nonlinearTseries/index.html). Before state-space reconstructions, time series were smoothened using the *Savitzky-Golay* filter function in Python. For Figure 3.8 D, $\tau = 26$, $d_e = 3$; for Figure 3.10 D, $\tau = 50$, $d_e = 3$.

3

Results

3.1 Phosphorylation response of EGFR upon uniform EGF stimulation

Summarizing the previous studies [84, 92, 142], the dynamics of the regulatory network of EGFR shown in Figure 3.1(A) shapes the phosphorylation response of EGFR to chemokine growth factors like EGF. Autocatalytic amplification of ligand-induced EGFR activation ensures robust receptor activation to extracellular signals as well as amplification of spontaneous phosphorylation events in the absence of growth factors. As the dimeric liganded EGFR fraction is increased upon EGF addition, it promotes autocatalysis and activation of the monomeric one. The dephosphorylation or EGFR or inhibition of activated EGFR is carried out by the phosphatases, which regulate the phosphorylation of EGFR at their distinct localisations in the cell. The major PTPs include PTPRG localised in the PM and PTPN2 localised in the ER. The essential role of the EGFR-PTP interdependence thus underlines the importance of determining the network motif of EGFR with each of its phosphatases. The reaction networks of the motif can be written uniquely as:

$$\begin{aligned}
\frac{d[EGFR_p]}{dt} &= EGFR_t(\alpha_1 \cdot ([EGFR] + \alpha_2 \cdot [EGFR_p] + \alpha_3 \cdot [EGF - EGFR_p]) \\
&\quad - \gamma_1 \cdot [PTPRG_a] \cdot [EGFR_p] - \gamma_3 \cdot [EGFR_p] - k_{on} \cdot ([EGFR_p] \\
&\quad + [EGFR]) \cdot [EGF_{free}] \ + k_{off} \cdot [EGF - EGFR_p]) \\
\frac{d[EGF - EGFR_p]}{dt} &= [EGFR_t] \cdot (k_{on} \cdot ([EGFR_p] + [EGFR]) \cdot [EGF_{free}] \\
&\quad - k_{off} \cdot [EGF - EGFR_p]) \\
\frac{d[PTPRG_a]}{dt} &= k_1 \cdot ([PTPRG_i] - k_2 \cdot [PTPRG_a] - \beta_1 \cdot [PTPRG_a] \cdot ([EGFR_p] \\
&\quad + [EGF - EGFR_p])) \\
\frac{d[PTPN2_a]}{dt} &= \epsilon \cdot (k_4 \cdot ([PTPN2_i] \cdot k_3 - [PTPN2_a] + \beta_2 \cdot [PTPN2i] \cdot ([EGFR_p] \\
&\quad + [EGF - EGFR_p]))) \quad (3.1)
\end{aligned}$$

with
$[EGFR] = ([EGFR_t] - [EGFR_p] - [EGF - EGFR_p])$; $[PTPRG_i] = ([PTPRG_t] - [PTPRG_a])$; $[PTPN2_i] = ([PTPN2_t] - [PTPN2_a])$; and $[EGF_{free}] = [EGF_t] - [EGF - EGFR_p]$

$[EGF - EGFR_p]$ is the phosphorylated ligand-bound dimeric EGFR, $[EGFR_p]$ - ligandless phosphorylated EGFR, $[EGFR_t]$ - total amount of EGFR, $[PTPRG_a], [PTPRG_t]$ and $[PTPN2_a], [PTPN2_t]$ - the active and total amount of the membrane localized PTPRG and the ER-bound PTPN2, respectively. Both, the receptor and the deactivating enzymes have active and inactive states, and the model equations describe their state transition rates. Therefore, mass is conserved in the system and the total protein concentrations of the three species ($[EGFR_t]$, $[PTPRG_t]$ and $[PTPN2_t]$) are constant parameters.

Autonomous, autocatalytic and ligand-bound-induced activation of ligandless EGFR takes place with distinct rate constants α_{1-3}, respectively. Other parameters are as follows: k_{1-4} — activation/inactivation rate constants of the phosphatases, β_1/β_2 - receptor-induced regulation rate constants of $PTPRG/PTPN2$, γ_1/γ_2 - specific reactivity of the enzymes ($PTPRG/PTPN2$) towards the receptor. The EGFR-PTPN2 negative feedback is on a time scale (ϵ) approximately two orders of magnitude slower than the phosphorylation-dephosphorylation reaction, as estimated from the $\sim 4min$ recycling time of $EGFR_p$ [92]. $[EGF_t]$ denotes the total ligand concentration. Ligand-binding unbinding for low EGF doses has been modeled explicitly using k_{on}, k_{off} in Eqns.3.1 [148]. All parameter values are described in Methods section 2.2.8.

How a single cell responds to time-varying cues will depend on the system's organization in the parameter space (PTPRG/EGFR). The response dynamics exhibit reversible but delayed phosphorylation relaxation when the system is organized close to the bifurcation point, just outside the irreversible bistable region. In previous theoretical work from the lab, it has been proposed that the memory that results from a "ghost" attractor is a dynamic transient memory, and it will enable signal integration for cell systems. I therefore performed stochastic simulations with suprathreshold EGF signals using Eqns. 3.1 for the organization of the system before the Saddle-Node (SN) bifurcation (Figure 1.12 B) to determine the duration and nature of the transient memory. Dimensionless time has been converted to minutes by equating the EGFR phosphorylation kinetics and duration in the simulations using the kinetic parameters to the experimental values in [92]. An adaptive step-size function [173] is used to mimic the 5 min EGF pulse. To model the contribution of random fluctuations in the activity dynamics of the network elements, an additive noise term ($\xi(t)$) was added to the $PTPN2$ term in the ODE system. $\xi(t)$ is a Gaussian white noise with zero mean and small autocorrelation. This noise term can incorporate both intrinsic and extrinsic sources. To avoid negative values of the protein concentrations due to the introduced stochasticity in the system, a custom-made adaptive step size algorithm [174] employed to Euler integration scheme for solving the ODE system.

In Figure 3.1 B (left), upon a simulated 5 min EGF pulse (grey area), the system jumps to a high EGFR phosphorylation state (blue line) along with a high fraction of ligand-bound EGFR (red dashed line). Removal of the pulse immediately decreases the ligand-bound fraction to the basal state. However, high EGFR phosphorylation persists for a significant period. Following the prolonged EGFR phosphorylation, the system converges back to the resting state and is susceptible to upcoming growth factor stimuli. The simulations reveal that higher EGFR phosphorylation is maintained for $\approx$ 25 minutes after removal of EGF pulse (Figure 3.1(B) left). However, for a cell to sense multiple time-varying signals, it is necessary to probe how the response is changed and how is the transient memory affected by a concurrent arrival of new EGF pulses. A subsequent EGF pulse is simulated within the duration of the transient memory 10 min after the first pulse (Figure 3.1 B right). Corresponding results show that with the second pulse, the system revisits the high EGFR phosphorylation steady state from the currently occupied narrow region of the metastable state. The system therefore senses the second signal within the memory interval of it's initial state and generates a memory after the second pulse. The total duration of high phosphorylation was extended to $\approx$ 40 mins (Figure 3.1 B right). Our observation showed that the combined memory duration of the two signals in this train of double pulses was longer than that of two independent pulses. Thus the transient activity allows real-time signal integration via temporal information storage while retaining responsiveness.

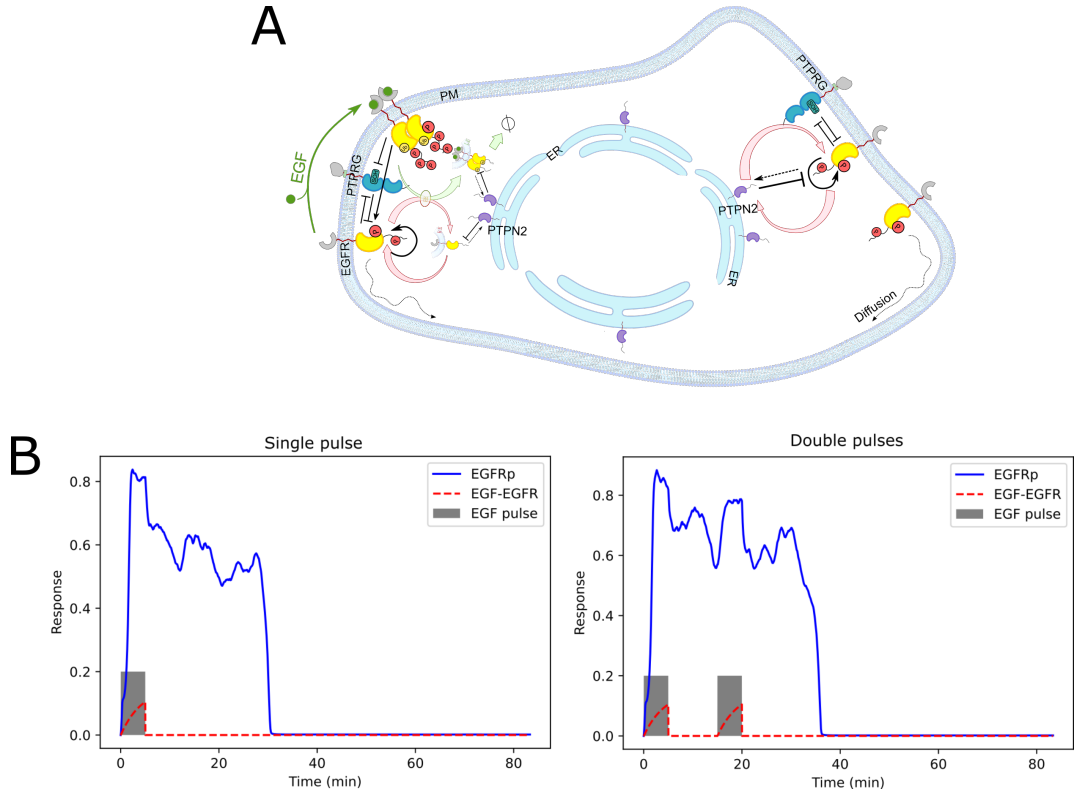

Figure 3.1: Phosphorylation response of EGFR to EGF - (A) Schematic of single cell with the EGFR-PTP network shown as EGFR and PTPRG on the membrane diffuse while the PTPN2 is localized on the ER of the cell. Activation of EGFR starts the signaling cascade and spatial regulation occurs via the Rabs (B) Stochastic simulations of the 5 min single pulse (left) and 5+5 min double pulse (right) in the EGFR-PTP system organized at criticality showing transient memory in EGFR phosphorylation

To test these simulation results experimentally, we use well-established EGFR-PTP network in engineered epithelial cells (Figure 3.1 A). MCF7 cells (human breast adenocarcinoma cell line with mutations in PIK3CA gene encoding for the catalytic domain of the PI3K complex) were cultured in the lab. Since MCF7 cells have low endogenous EGFR expression ($\sim 10^3$ molecules per cell), these cells had $EGFR^{mCitrine}$ ectopically expressed, which fell within the endogenous EGFR expression range of the non-tumorigenic $MCF10A$ cells (See Methods 2.2.3) [92]. Short 5 min EGF^{647} pulse of 20 ng/mL concentration was administered to starved engineered MCF7-$EGFR^{mCitrine}$ cells, followed by a quick washout with serum free IM. The fluorescently-tagged phosphotyrosine binding domain of Shc ($PTB^{mCherry}$) is recruited to the phosphorylated tyrosines 1086/1148 of EGFR upon EGF stimulation (Figure 3.2 A). Thus, the fraction of phosphorylated receptor ($EGFR_p$) is determined by the rapid translocation of $PTB^{mCherry}$ to the phosphorylated $EGFR^{mCitrine}$ at the plasma membrane (See Methods 2.2.14). The fraction of ligand-bound receptors at the plasma membrane was determined by ($EGF^{647}/EGFR^{mCitrine}$) (See Methods 2.2.14 for normalizations). Quantification of EGFR phosphorylation in single cells revealed that the phosphorylation was maintained for $\approx$ 20 minutes after the pulse removal in the case of a single 5 min

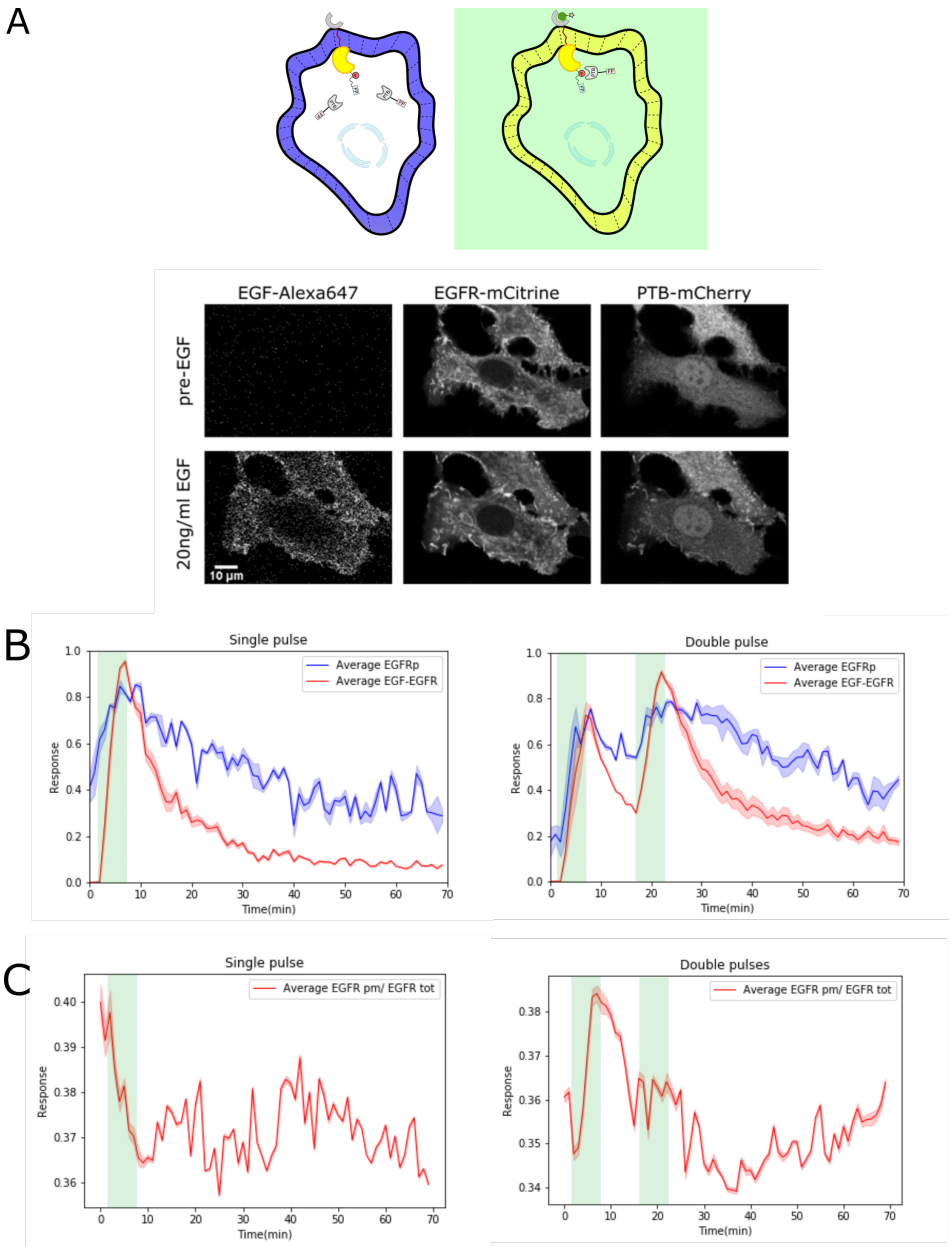

Figure 3.2: Temporal profiles of EGFR phosphorylation upon stimulation with EGF pulses - (A) (Top) Scheme depicting translocation and binding of $PTB^{mCherry}$ to $EGFR^{mCitrine}$ on the PM in presence of EGF^{647}. (Below) Exemplary single-cell confocal images recorded in EGF^{647}, $EGFR^{mCitrine}$ and $PTB^{mCherry}$ channels before, during and after stimulation with a single pulse of 20ng/ml EGF^{647} for 5 mins showing translocation of PTB to EGFR. (B) (Left) Quantification of $EGFR^{mCitrine}$ phosphorylation in single-cell 5 min pulse experiments from n=14. Mean +/- SD (Right) Quantification of $EGFR^{mCitrine}$ phosphorylation in single-cell double pulse experiments from n=11. Mean +/- SD. Blue line shows average EGFR phosphorylation, red line shows average EGF-EGFR. (C) (Left) Quantification of $EGFR^{mCitrine}$ on the membrane from (B-left). (Right) Quantification of $EGFR^{mCitrine}$ on the membrane from (B-right). Mean +/- SD. Green shaded areas show EGF^{647} stimulation.

pulse (Figure 3.2 B left - blue). The rapid decay profile of the ligand-bound fraction upon stimulus removal (Figure 3.2 B left - red) highlighted that the memory in receptor phosphorylation is not due to the EGF binding to the EGFR receptors but resides in

the active monomers. A decrease of EGFR on the PM during the pulse duration was also estimated (Figure 3.2 C left - red) which stabilized and remained at steady state over time after EGF removal. This decrease of receptor level can be related to the ligand-bound EGFR fraction which are unidirectionally endocytosed upon EGF binding.

In a second set of experiments, single cells were uniformly stimulated with two consecutive pulses of EGF which were separated by an interval. When the cells were stimulated with a second 5 min pulse of EGF (20 ng/ml), administered 10 min after washout of the initial pulse, EGFR phosphorylation response was prolonged and lasted $\approx$ 40 minutes (Figure 3.2 B right - blue). The system retained the ability to sense the upcoming signal while in the memory phase and eventually resetted to the basal level. The ligand-bound fraction showed a rapid exponential decay upon each pulse removal (Figure 3.2 B right - red). These experimental results were consistent with the simulation outputs. Again quantification of the level of $EGFR^{mCitrine}$ on the membrane (Figure 3.2 C right - red) showed that the receptors levels are decreased from the membrane after stimulation which indicates the system is pushed from the bistable state to the monostable state. Receptors are recruited to the membrane on stimulation with EGF but decay over time as the bound ones are degraded by the cell machinery.

3.2 Spatio-temporal phosphorylation response of EGFR to gradient of EGF stimulation

To demonstrate experimentally whether cells maintain a memory of the direction of encountered signals, MCF7 cells with ectopic expression of $EGFR^{mCitrine}$ were subjected to a gradient of fluorescently tagged EGF^{647} for an hour and imaged using confocal microscopy. Cells were seeded in a microfluidic plate in which stable gradients of EGF^{647} are established and controlled through pressure and diffusion through a perfusable channel of the chamber (Figure 3.3 A). Optimal flow conditions are described in Methods 2.2.10. Gradient measurements with EGF^{647} were found to be stable over an hour and approximately linear in nature across the cell seeding chamber with a width of 500 µm (Figure 3.3 B). Washout of gradient was quick and observed to be within 5 min. For the polarization experiments, a maximal amplitude of 10 ng/ml EGF was used to pass through one of the channels. This mimics the physiological concentration of EGF during human tissue secretions (0.4-20 ng/ml) [134]. Multichannel confocal images were recorded for 4 h (240 min) at every 1 min interval.

To determine the direction of growth factor sensing by cells and the corresponding polarization of the EGFR phosphorylation towards the EGF gradient, single cells were masked as regions of interest (ROI) using $EGFR^{mCitrine}$ channel (Figure 3.4 A). The masked cells are segmented and spatially divided into their plasma membrane and the cytoplasm using the methods described in Section 2.2.14. The cell mask area was

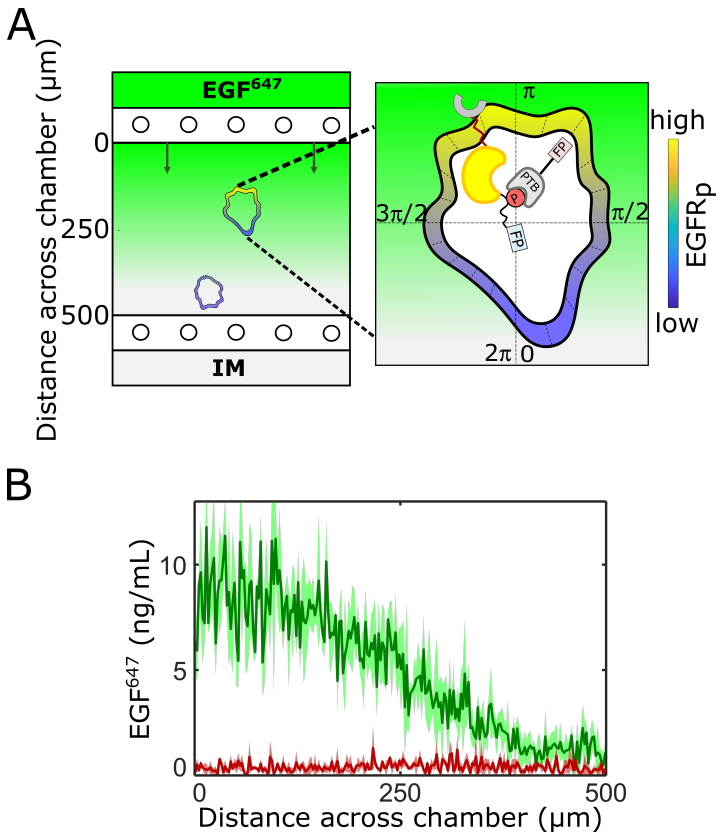

Figure 3.3: Setup of cell polarization experiments - (A) Schematic diagram of the microfluidic gradient chamber with single cells seeded. Zoom in: single-cell measurables. On stimulation with the gradient EGF^{647}, EGFR phosphorylation is estimated on the membrane by the ratiometric method of $PTB^{mCherry}$ over $EGFR^{mCitrine}$. Colorbar denotes level of phosphorylation change on the PM. (B) The linear nature of the gradient is identified at time point 60 min over the length of the gradient chamber. Maximal EGF concentration of 10ng/ml was used and the quick washout at time point 65 min is verified by the red line. Mean±s.d., N=4.

divided circularly into two equal areas and the outer area was defined to be the plasma membrane. The PM was then divided radially into 20 equal segments, and the EGFR phosphorylation amount was quantified in each radial segment using Eqn. 2.2. The EGF signal for each cell was quantified from ≈ 10 pixels area from the outer segmented cell contour.

To investigate whether the phosphorylation of EGFR in single cells polarizes towards the gradient direction, $EGFR^{mCitrine}$ phosphorylation on the plasma membrane in single cells was estimated (Figure 3.4 A). The experiments demonstrated that on an average, most cells responded to the external EGF^{647} gradient. Among all the single cells observed across seven independent replicates, only a few cells showed basal or symmetric $EGFR^{mCitrine}$ phosphorylation upon gradient stimulation (Figure 3.4 B). Fluorescent intensity from background corrected confocal images was utilized to characterize varied $EGFR^{mCitrine}$ expression in single cells. The $EGFR^{mCitrine}$ phosphorylation in the cells were plotted using kymographs. Kymographs are space–time plots which display intensity/measured values of a variable along a predefined path over time. The circular

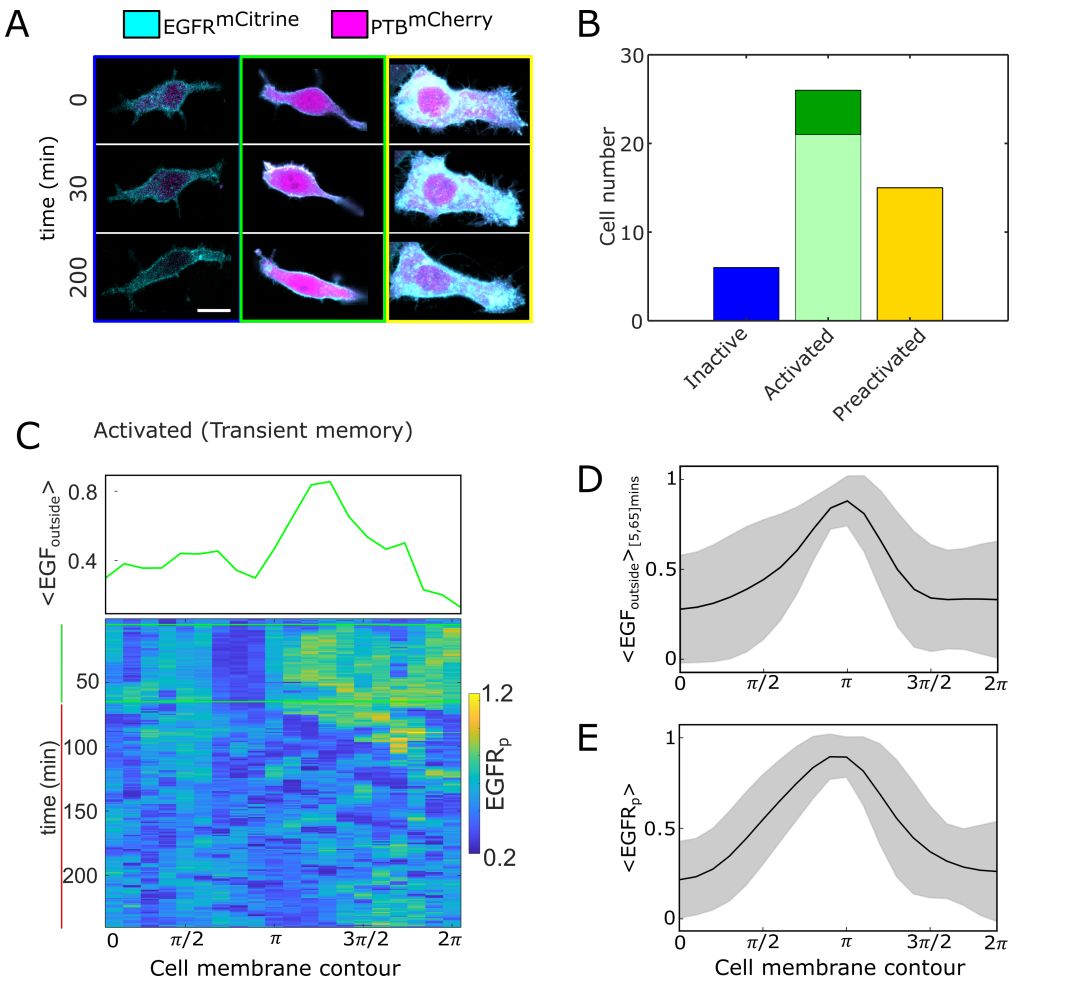

Figure 3.4: Quantification of spatial-temporal phosphorylation dynamics of EGFR upon EGF gradient stimulation - (A) Representative images/overlay of $EGFR^{mCitrine}$ (cyan) and $PTB^{mCherry}$ (magenta) prior to (0min), during (30min) and after (200min) MCF7-$EGFR^{mCitrine}$ cells were subjected to 60min EGF-647 gradient. Columns: non-activated (blue), transiently polarized (green) and uniformly pre-activated (yellow). Scale bar: 15 um. (B) Distribution of single-cell responses corresponding to A, N=7 wherein cells are broadly classified into 3 categories. Single cells undergoing activation in $EGFR^{mCitrine}$ phosphorylation upon EGF gradient stimulation were subdivided into "transient" (light green) and "permanent" (dark green) based on the activity profiles of the single cells over the duration of the recording of experiments. (C) Exemplary single-cell kymographs depicting polarized $EGFR^{mCitrine}$ phosphorylation. Data was acquired at 1 min intervals in live MCF7-$EGFR^{mCitrine}$ cells subjected for 60 min to an EGF^{647} gradient of source concentration 10 ng/ml. Top: Averaged EGF signal sensed across the outer periphery of cell over the duration of the static EGF gradient. Single cell kymograph shown from n=20, N=7. Green/red lines: stimulus presence/absence. (D) Average profile of the spatial EGF signal at the outside periphery of single cell contours as sensed by single cells over the duration of the EGF signal. For each cell temporal average per spatial bin is quantified and the final spatial profile was estimated via a smoothing Guassian function. Peaks of single cell EGF gradient distributions were shifted to π before averaging. Mean +/- SD from n=18, N=7 are shown. (E) Average profile of the spatial projection of the fraction of phosphorylated $EGFR^{mCitrine}$ from single-cell kymographs. For each cell, temporal average per bin is calculated, and the final spatial profile was estimated as an average of Gaussian smoothened profiles. Peaks of single-cell distributions were shifted to before averaging. Mean +/- SD from n=20, N=7 is shown.

PM was radially divided into equal bins (marked from 0-2π) (Figure 3.3 A - zoomed inset) and EGFR phosphorylation on the PM was plotted over time. The EGF^{647} gradient signal sensed by each of the cells was spatially mapped across the immediate outer boundary of the masked cell contour in Figure 3.4 C (top) (See Methods in Section 2.2.10). The kymograph plotted in Figure 3.4 C shows an exemplary cell where the $EGFR^{mCitrine}$ phosphorylation is polarized upon gradient stimulation and the polarization is shown to persist for a transient period even after removal of the external gradient. The spatial polarization of $EGFR^{mCitrine}$ phosphorylation was observed for gradients of EGF^{647} as shallow as 10% between the front and back of the cell. The maximal EGF^{647} gradient sensed by the single cells have been estimated and plotted across the cell membrane contour (Figure 3.4 D). It was observed that the average receptor phosphorylation across the PM of most of the cells polarized in the direction of the maximal EGF^{647} gradient (Figure 3.4 E).

The average $EGFR^{mCitrine}$ phosphorylation amount on the PM of the cells before and during the stimulation with EGF^{647} gradient correlated with the $EGFR^{mCitrine}$ expression levels. The receptor phosphorylation levels of single cells were mapped to the receptor expression amounts in the single cells. Single cell phosphorylation estimates $< EGFR_p >_{0,65mins}$ which fell below a threshold were classified as 'Inactive' cells. The exemplary kymograph of an inactive cell (Figure 3.5 A) shows basal EGFR phosphorylation across the membrane. Calculation of threshold for each cell was performed using Gaussian Mixture Models (Explained in Methods section 2.2.15). MCF7-$EGFR^{mCitrine}$ cells with continuously high symmetric receptor phosphorylation across the membrane even before stimulation were termed as 'Preactivated' cells (Figure 3.5 B). Kymograph of a preactivated cell shows high phosphorylation without any polarization all over the membrane (Figure 3.5 B). 'Activated' cells (shown in green in Figure 3.5 C and kymograph in Figure 3.4 C) showing characteristic high $< EGFR_p >_{0,65mins}$ upon EGF^{647} gradient reported $EGFR^{mCitrine}$ expression in-between inactive (blue) and preactivated cells (yellow). These cells were characterised by prolonged polarization in receptor phosphorylation even upon gradient removal. Cells with high $EGFR^{mCitrine}$ expression on the PM revealed higher average phosphorylation values ($< EGFR_p >_{0,65mins}$) as compared to cells with lower receptor expression levels (Figure 3.5 C). The results indicated the significance of abundance of receptor levels found in single cells during the sensing of extracellular growth factor gradients. Cell-cell variability in EGFR expression level affects the responsiveness of the system.

3.2.1 Identification of memory in EGFR phosphorylation polarization

From the kymographs, the polarization in $EGFR^{mCitrine}$ phosphorylation on the PM of activated cells was found to persist for a transient time even after complete washout of

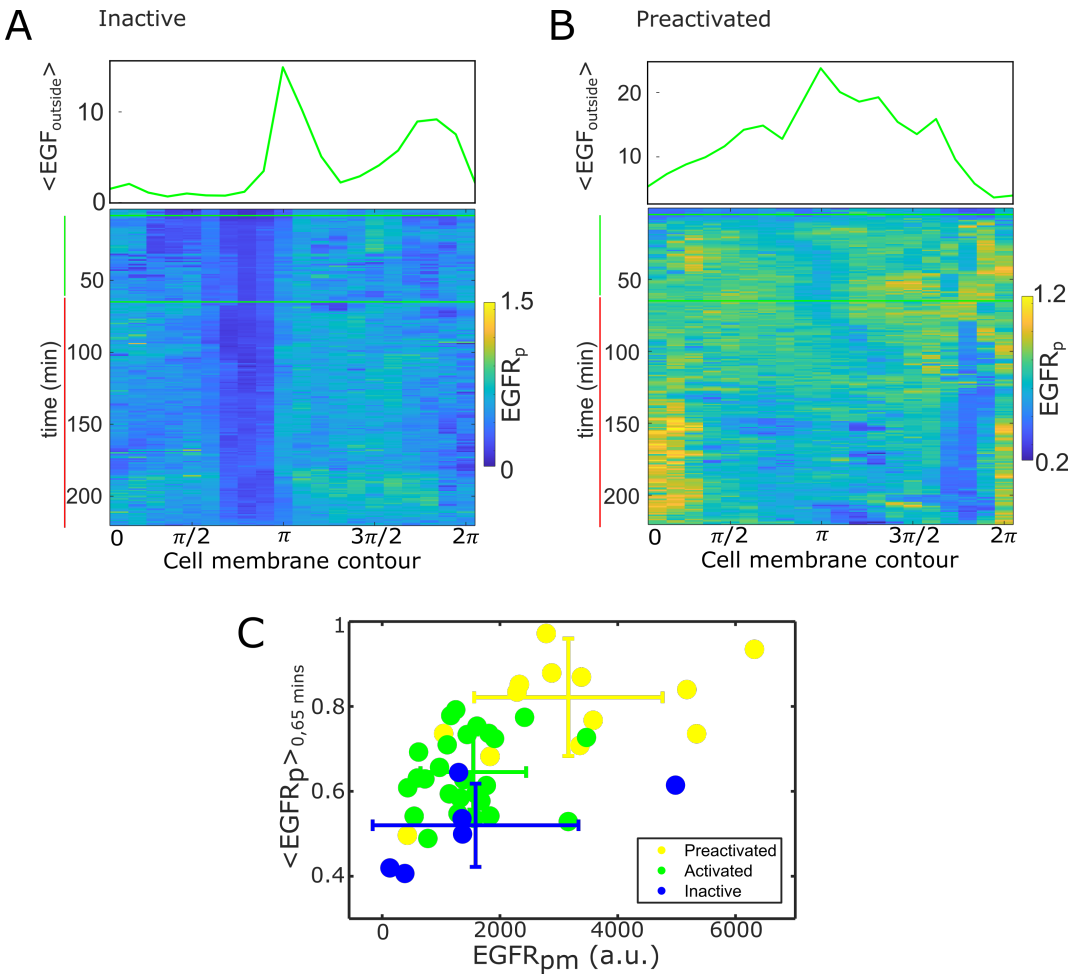

Figure 3.5: EGFR dependent spatial-temporal distribution of phosphorylated EGFR upon EGF gradient stimulation - (A) Additional exemplary single-cell kymograph depicting non-activation and as such non-polarization of EGFR-mCtrine phosphorylation upon stimulation with EGF gradient. (B) Single-cell kymograph depicting uniformly pre-activated EGFR-mCtirine phosphorylation even before stimulation with EGF gradient. Activity is shown not to be polarized in such cases. (C) An experimental bifurcation scatter plot showing the clustering of all single cells when the total $EGFR^{mCitrine}$ phosphorylation before and during the EGF gradient stimulation in single cells was plotted against the expression of $EGFR^{mCitrine}$ molecules on the plasma membrane of the cells. Colours denote the cell classification in Figure 3.4 A,B. Mean +/- SD across both axes from individual clusters from N=7.

EGF^{647} gradient. The washout was quick and occurred within 5 min indicated by red profile in Figure 3.3 B which proved that the high phosphorylation levels are not due to the presence of residual EGF in the chamber. In parallel, it was verified from the temporal profile of the ligand-bound $EGFR^{mCitrine}$ on the PM ($EGF-EGFR$) (Figure 3.6 A) estimated using Eqn. 2.5. $EGF-EGFR$ is normalized similar to phosphorylated $EGFR^{mCitrine}$ in Eqn. 2.3. The temporal profile of $EGFR^{mCitrine}$ phosphorylation ($EGFR_p$) from single cells showed duration of memory in receptor phosphorylation to be similar to the memory from single pulse experiments (Figure 3.6 A,B). Thus, a systemic approach utilizing the fraction of polarized cell area on the membrane was employed to

investigate memory in the polarization of the $EGFR^{mCitrine}$ phosphorylation (Figures 3.6 C, 3.7).

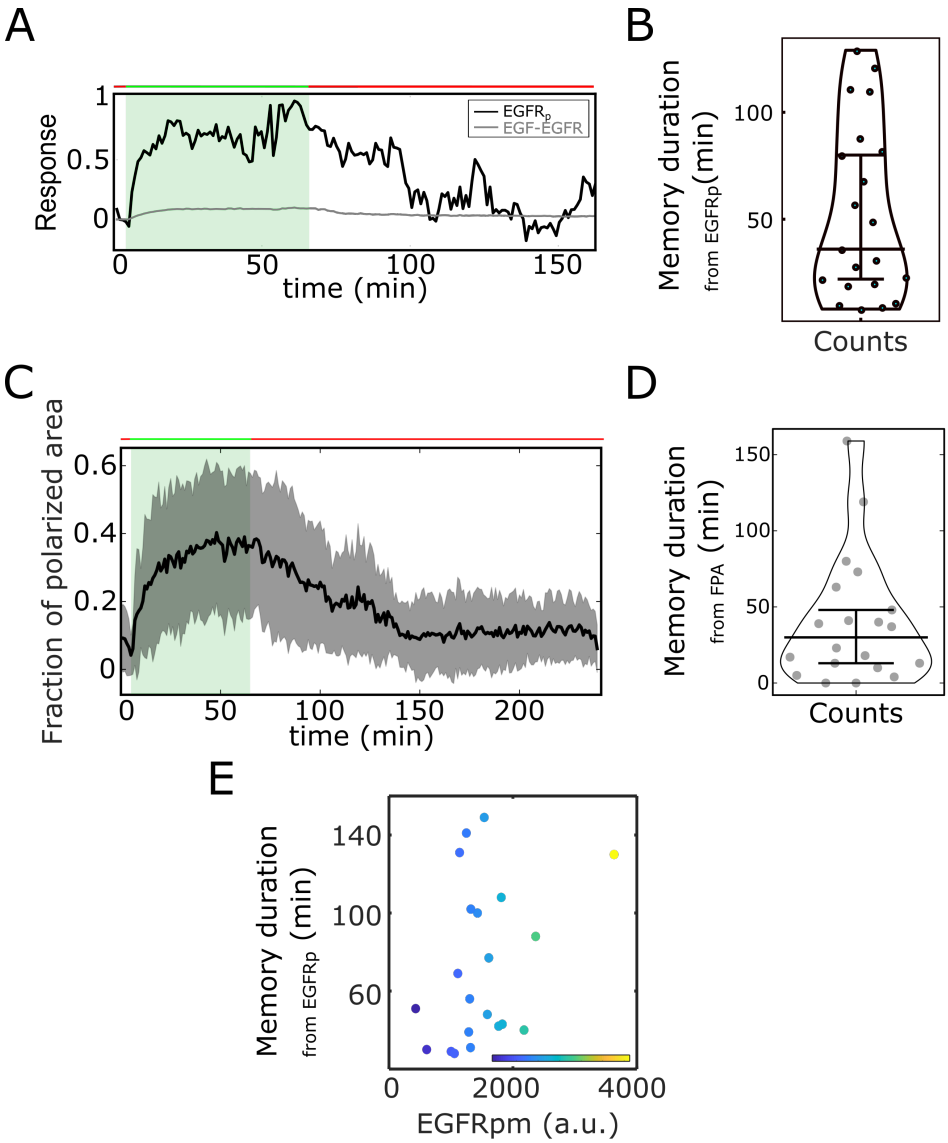

Figure 3.6: Estimation of memory duration in polarization of EGFR phosphorylation - (A) Temporal profile of $EGFR^{mCitrine}$ phosphorylation and EGF-EGFR (ligand bound fraction) corresponding to the single cell in Figure 3.4 A. (B) Quantification of memory duration in single cells (median + C.I.) from the temporal activity profiles of phosphorylated $EGFR^{mCitrine}$. (C) Average fraction of polarized plasma membrane area from single cells undergoing activation Mean +/- SD. n=20, N=7. (D) Quantification of memory duration in single cells (median + C.I.) from the fraction of polarized area in single cells.n=20, N=7. (E) Scatter plot showing the distribution of memory duration from the temporal profiles of single cells activated by EGF^{647} gradient against the expression levels of $EGFR^{mCitrine}$ on the PM of the cells.n=20, N=7.

The fraction of polarized cell area (FPA) for all the masked single cells was estimated from thresholded normalized kymographs of $EGFR^{mCitrine}$ phosphorylation (See Methods section 2.2.16) (Figure 3.7). The end of the memory duration per cell was identified as the time point at which $FPA_{per-cell} < (FPA_{average} - s.d.)$ in 3 consecutive time points. Most of the cells from Figure 3.7 revealed polarization upon EGF gradient

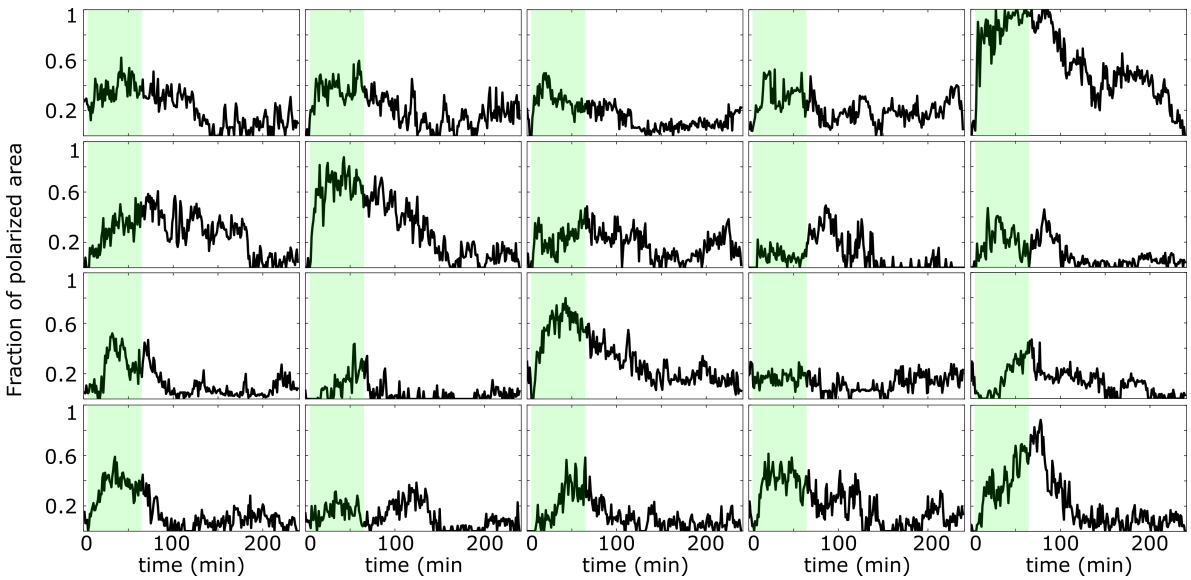

Figure 3.7: Temporal profiles of fraction of polarized area of activated cells upon stimulation with EGF gradient - Temporal profiles of the estimated fraction of polarized area for single cells. Green shaded area: EGF gradient duration. The mean +/- SD shown in Figure 3.6 A. n=20, N=7.

with a high FPA value which persisted for a transient period upon EGF removal. The average transient memory duration in polarization of $EGFR_p$ persisted was $\approx$ 40 min after the gradient removal (Figure 3.6 D). This observation showed that the single cells initially positioned in a homogeneous basal activity state breaks through the symmetrical state when stimulated with a stable gradient of growth factor and polarizes towards the direction of stimulus. Such polarization is retained by the cells to maintain a front and back polarity for a significant period even upon the removal of the stimulus.

Comparison of single cell memory duration estimated from the $EGFR_p$ temporal data with the $EGFR^{mCitrine}$ expression on the PM revealed a positive correlation between the amount of receptors and the memory (Figure 3.6 E). A higher number of EGFRs on the PM brings the system closer to the bifurcation regime and as such the memory duration scales with EGFR amount. Thus, a critical and balanced number of receptors are required to be maintained on the PM for cells to incorporate both the symmetry breaking mechanism as well as exhibit memory in polarization. The result experimentally validates the theoretical prediction of cellular polarization and information processing via the dynamical PB mechanism.

3.2.2 Reconstruction of state-space trajectory from temporal EGFR phosphorylation

The trajectory in state space from the reaction-diffusion simulations of the EGFR-PTP system described the change of state of the cellular system when plotted in 3 dimensions (Figure 1.13 D). It was conjectured that the temporal memory in polarization of $EGFR_p$ was caused due to transient trapping of the signaling state trajectory in state space.

Such transient trapping indicated the presence of metastable "ghost" states wherein the system is maintained away from time-invariant steady states. To identify whether the transient memory observed in polarization of $EGFR^{mCitrine}$ phosphorylation results from a metastable state it is necessary to reconstruct the state-space trajectory from our experimental data. Transient trapping of the trajectory indicated the presence of metastable "ghost" states wherein the system is maintained away from time-invariant steady states.

Taken's delay embedding theorem (See Introduction section [155, 156]) was utilized to verify the presence of such a metastable state experimentally, from a single observable. Using the delay embedding theorem, the state space trajectory was reconstructed from the measured single-cell temporal $EGFR^{mCitrine}$ phosphorylation profile (Figure 3.8 A). Optimal values of the time delay (τ=26) and the embedding dimension (m=3) were identified from the autocorrelation function (Figure 3.8 B) and the False Nearest Neighbourhood algorithm (Figure 3.8 C) (See Methods section 2.2.20 for details). The reconstructed phase space trajectory shows when the cells are stimulated with EGF gradient (depicted by thick line), the system jumps from a basal state (purple cloud) to a polarized state (cyan cloud). As the EGF is removed the trajectory (thin line) travels through a region in state-space and returns to the initial basal state. It was observed that the memory phase (magenta cloud) was characterized by the trajectory getting trapped in a state-space area distinct than that of the polarized and basal steady states (Figure 3.8 D). This experimental observation along with previous theoretical predictions corroborates that the memory in $EGFR^{mCitrine}$ phosphorylation polarization emerges from a saddle node of a pitchfork bifurcation (SN_{PB}) "ghost" that maintains the system away from the steady states.

3.2.3 Observation and estimation of memory in cell morphology

Quantification of confocal images reveal $EGFR^{mCitrine}$ phosphorylation polarization resulted in subsequent cell shape changes directed towards the EGF^{647} gradient (Figure 3.4 A). Although the memory in $EGFR^{mCitrine}$ phosphorylation polarization do not result from a stable, steady-state, it was observed that this memory effectively helps in maintaining a polarized cell shape even after the gradient removal. In order to quantify the phenotypic changes, the morphological differences of the polarized cells were quantified using two parallel methods – 1) the solidity measurements of each cell at each time point and 2) the directed protrusive area towards and away from the gradient (Figure 3.9 A). The solidity (σ) is the ratio between the cell's area A_{cell} and the area of the convex hull, which fits the cell A_{convex}. The memory duration in cell morphology was calculated from single-cell solidity profiles and corresponded to the time point at which the solidity is less than a threshold mark (mean-S.D.) estimated during the gradient

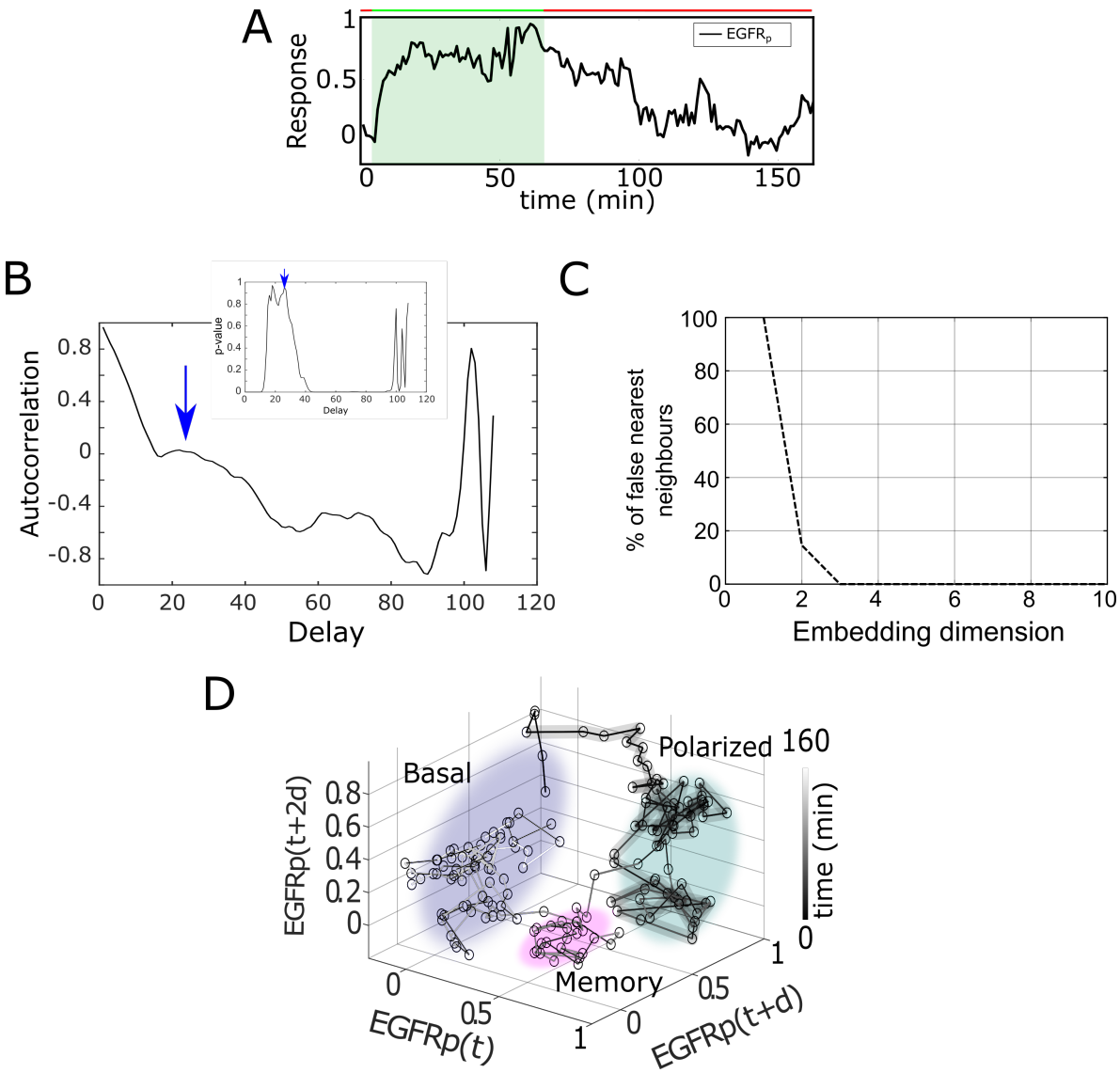

Figure 3.8: State-space reconstruction from experimental observables using Taken's delay embedding theorem - (A) Exemplary temporal profile of $EGFR^{mCitrine}$ phosphorylation ($EGFR_p$) corresponding to the single cell in Figure 3.4 C- used for reconstruction of state-space. (B) Optimal delay indicated by blue arrow from autocorrelation of $EGFR_p$. Inset: p-value of autocorrelation function plotted against the embedding delay for identification of proper embedding time delay value (= 26). (C) Estimation of appropriate embedding dimension based on false nearest-neighbours method (=3). (D) Corresponding state-space trajectory with denoted trapping state-spaces (arbitrarily coloured - basal - purple, memory - magenta, polarized - cyan). Thick/thin line: signal presence/absence, d – embedding time delay.

presence (Figure 3.9 B). The directed cell protrusion area was estimated by comparing filtered single-cell masks at two consecutive time points. The memory duration was estimated as the time point when the directed protrusive area crosses zero after the gradient removal (See Methods section 2.2.17 for details).

The memory of the polarized cell morphology was reflected through the exemplary temporal evolution of the cell protrusion area in the direction of the gradient (Figure 3.9 A), and it was found to be $\approx$ 43 mins for the exemplary cell shown in Figure 3.4 C. In

general, the cells were found to have an average duration of memory in the polarized cell morphology which directly corresponds to the average memory duration in the fraction of polarized cell area (Figure 3.6). This result shows that the transient memory in signaling is directly translated in the phenotypic cell shapes (Figure 3.9 B).

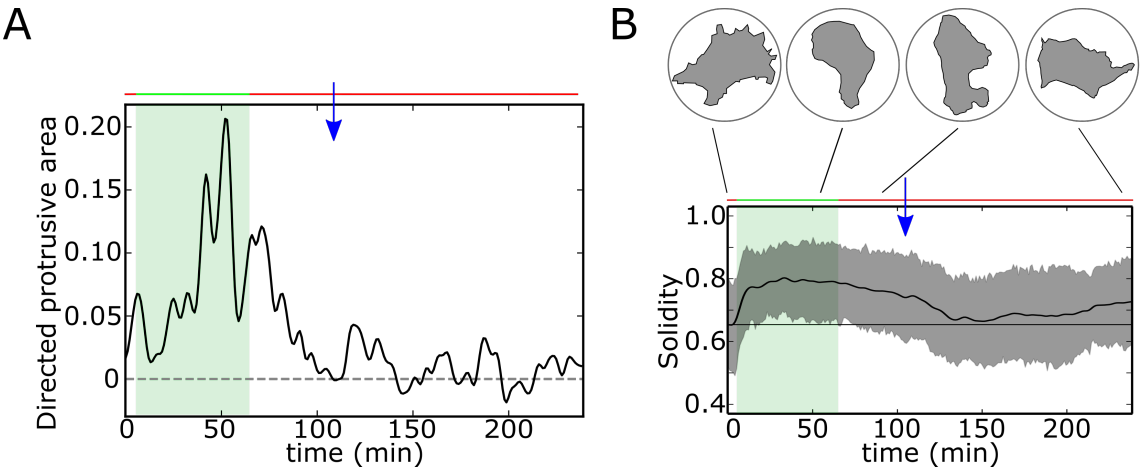

Figure 3.9: Quantification of changes in cell shapes during polarization - (A) Exemplary quantification of morphological changes, directed cell protrusion area, for the cell in Figure 3.4(A). Memory duration indicated by the blue arrow was found to be 43 min. (B) Averaged single-cell morphological changes (Solidity, mean+/- SD). Average memory duration was found to be 40 min (blue arrow). Top insets: representative cell masks at distinct time points. Green shaded area: EGF^{647} gradient duration; green/red lines: stimulus presence/absence. Custom morphological analysis was developed in-house by Robert Lott.

3.2.4 Inhibition of EGFR phosphorylation results in loss of memory in phosphorylation polarization

To examine whether the memory in cell morphology indeed is regulated on the level of the receptors, we probed the $EGFR_p$ response experimentally after inhibiting the EGFRs with a kinase inhibitor, Lapatinib (Lap.) [175]. Lapatinib is a small molecule drug that inhibits the EGFR phosphorylation within a few minutes by binding to the ATP-binding pocket of the receptor protein kinase domain, thus preventing self-phosphorylation of EGFR and subsequent activation of the signal transduction mechanism.

Similar to the previous polarization experiments, cells were seeded in the microfluidic plates and treated to a stable gradient of EGF^{647} for an hour. During washout of the gradient, the cells were supplied with a homogeneous solution of Lapatinib (1 µM) of physiological concentrations. As demonstrated in the exemplary single-cell kymograph, the phosphorylation response decays rapidly upon the receptor inhibitor addition (Figure 3.10 A). It results in an evident absence of transient memory in $EGFR^{mCitrine}$ phosphorylation polarization. This observation is sustained also across many cells as shown in Figure 3.10 B. Loss in polarized cell shape was also observed (Figure 3.10 C). Moreover, the absence of memory is reflected in the reconstructed

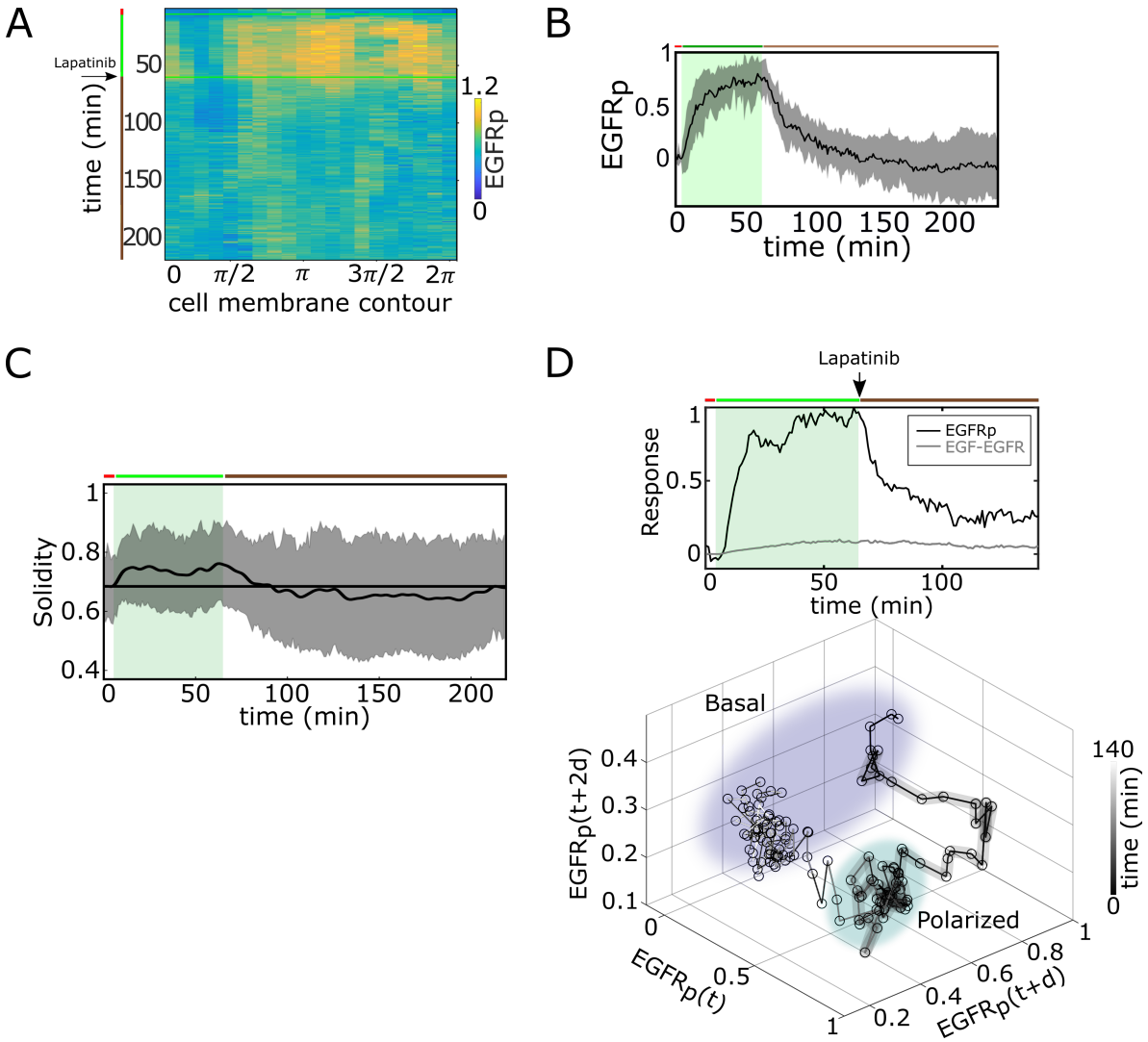

Figure 3.10: EGFR phosphorylation response upon EGFR inhibition - (A) Exemplary single-cell kymograph depicting phosphorylated $EGFR^{mCitrine}$ for data acquired at 1 min intervals in live MCF7-$EGFR^{mCitrine}$ cell subjected to 60 min EGF gradient, and 3 h after gradient wash-out with 1 µM Lapatinib. (B) Average temporal profiles of plasma membrane $EGFR^{mCitrine}$ phosphorylation of live MCF7-$EGFR^{mCitrine}$ cells subjected to 60 min EGF gradient, and 3 h after gradient wash-out with 1 µM Lapatinib. Mean +/- SD from n=9, N=2 is shown. (C) Average solidity in MCF7-$EGFR^{mCitrine}$ cells subjected to experimental conditions in (A, B). Mean +/- SD from n=9, N=2 cells. (D) Top: Exemplary profiles of phosphorylated $EGFR^{mCitrine}$ (black) and ligand bound fraction EGF-$EGFR^{mCitrine}$ (grey) in live MCF7-$EGFR^{mCitrine}$ cells subjected to the experimental conditions in (A, B). Bottom: Corresponding reconstructed state-space trajectory with state-space trapping (arbitrary colouring - in Figure 3.8 D). d – embedding time delay = 50 min. Green/red lines: stimulus presence/absence; brown lines: inhibitor presence.

state-space trajectory, from the corresponding $EGFR_p$, which smoothly transits from a polarized to a basal activity state, without the transient state-space trapping in-between that was the characteristic for the memory state emerging from the dynamical "ghost" (Figure 3.10 D). It showed the absence of trapping in state-space observed in Figure 3.8 D. These results therefore show that the memory in $EGFR^{mCitrine}$ phosphorylation

polarization is maintained on the level of the receptors and it also enables memory in cell shape. A possible mechanism could be the autocatalytic nature of the EGFR molecules, which gets self-activated and thus helps in maintaining the memory of the previously experienced EGF signal. Loss of autocatalysis due to EGFR inhibition disrupts the dynamical modes of the receptor network and results in the loss of memory.

3.3 Memory in $EGFR_p$ and cell shape is translated to memory in directed migration towards localized source

According to the working hypothesis, operating in the SN_{PB} vicinity enables sensing dynamic gradients, and translates this information to directed migration. To experimentally investigate whether the transient memory in cell polarization has implications on the phenotypic fate of the cell, we analyzed the motility features of the engineered MCF7-$EGFR^{mCitrine}$ cell line and the wild-type (WT) $MCF10A$ cells. Although EGF-induced migration have studied extensively, optimal dosage of EGF concentration for efficient migration have been missing. So we stimulated the cells with EGF doses ranging from low concentration like 2.5 ng/ml to saturating concentration of 100 ng/ml.

For this single epithelial cells were seeded in 6-well Lab-Teks coated with respective extracellular matrix proteins (fibronectin for $MCF10A$ and collagen for engineered MCF7) and subjected to uniform stimulation of varying EGF concentrations separately (See Methods section 2.2.11). The filtered single-cell movements was imaged and recorded for 14 h. Divergence plots of single cell tracks showed random migratory behavior upon EGF stimulation (Figure 3.11). However, the distance covered during the random movement was shown to be increasing with higher EGF doses (Figure 3.11 B,D). The individual single cell velocities reflected the increase in the random motion for increasing concentrations of EGF (Figure 3.12 C,D). Affect of extracellular matrix was also shown to play a role in the increase of velocity of cell migration (Figure 3.12 A,B) on uniform stimulation with 20ng/ml EGF.

To find the optimal EGF concentration along with optimal matrix coating for efficient cell migration, single-cell trajectories were tracked using the Hoechst 33342 fluorescent signal (used to demarcate cell nuclei) or the transmission channel. Physical quantities including 'Motility' and 'Directionality' were estimated from the positional information (x and y coordinates) of individual cell tracks. 'Motility' was defined as the percentage of single-cell tracks with track length greater than a threshold estimated from cell displacement. The directionality measure, which was defined as the ratio of displacement between initial and final positions over distance traveled by individual cells, showed that the cells' movement was random in nature. The motility estimates from cell tracks were

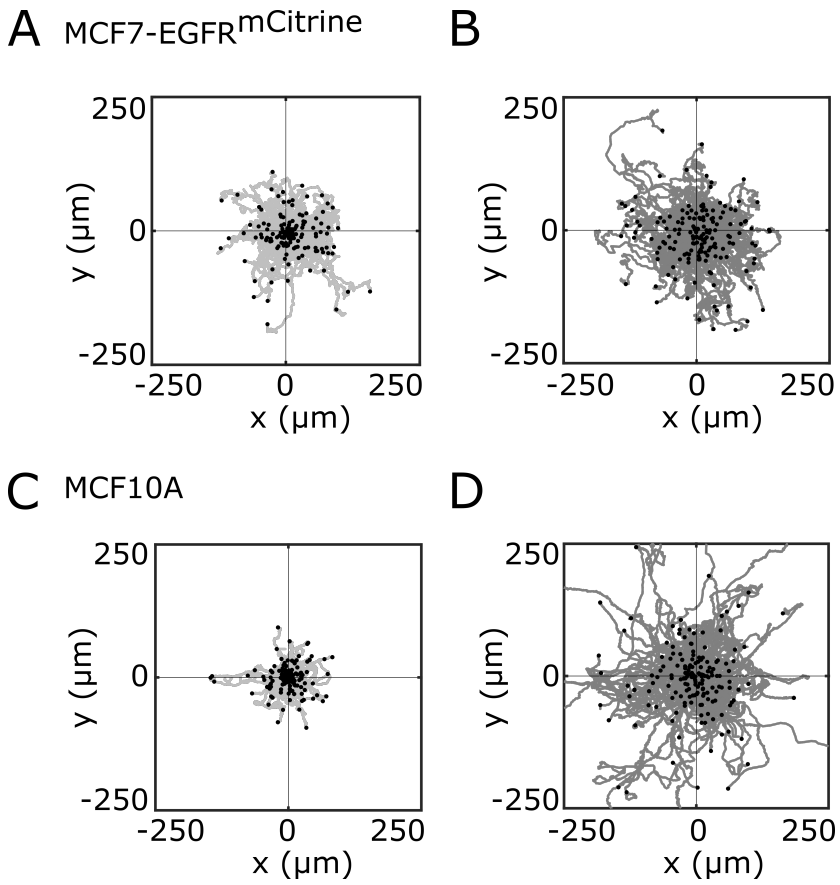

Figure 3.11: Single cell migration assays - Characterization of MCF-$EGFR^{mCitrine}$ and $MCF10A$ single-cell migration. (A) Divergence plots depicting MCF7-$EGFR^{mCitrine}$ single-cell trajectories quantified, left: 14 h of 0 ng/ml EGF (subset of n=207 from n=426 is shown, N=2); and right: 14 h of uniform 20 ng/ml EGF stimulation (subset of n=200 from n=456 is shown, N=2). (B) Similar experiments and plots for $MCF10A$ WT cells. Left: n=245, N=3; and right: n=297, N=3. Black dots denote end of tracks.

utilized to determine the most favourable extracellular matrix coating concentration for the cell migration assays. For MCF7-$EGFR^{mCitrine}$ cells, 100µg/cm^2 collagen coating concentration (Figure 3.13 A) and 20 ng/ml EGF^{647} (Figure 3.13 C) was observed to be optimal conditions for efficient migration. For $MCF10A$ cells 2 µg/ml fibronectin or 1:500 dilution (Figure 3.13 B) along with 15 ng/ml EGF^{647} was found to be optimal.

Both WT $MCF10A$ and engineered MCF7-$EGFR^{mCitrine}$ cells reported similar concentration of EGFR receptors on the cell membrane and similar binding affinity to EGF ([92]). However additional phenotypic quantification using velocity and directionality measures showed similar migratory features as well (Figure 3.14 A,B). The population behaviour of both the cell lines were found to be equivalent under absence of EGF and under uniform stimulation with 20 ng/ml with the median values showing no significant differences.

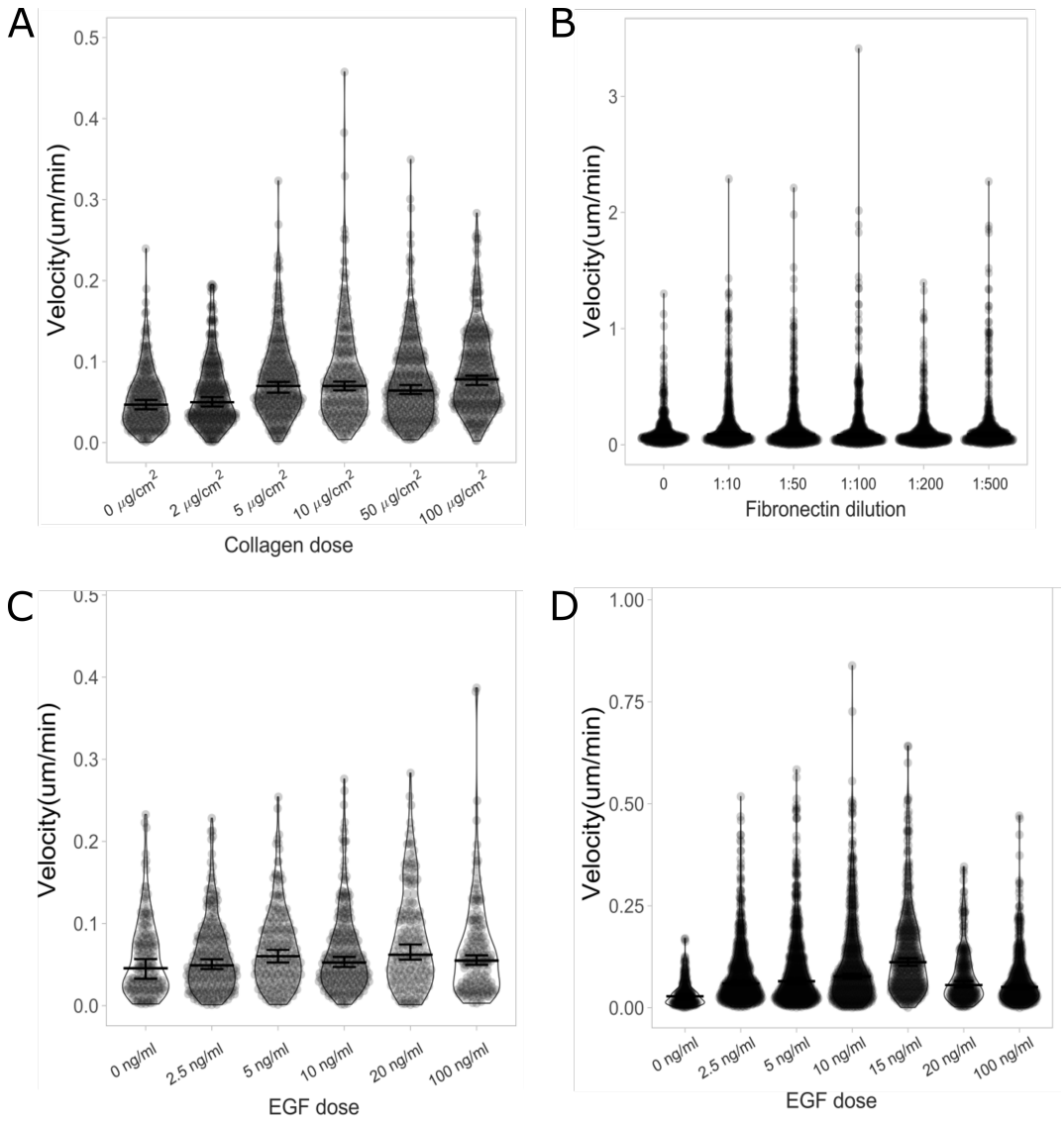

Figure 3.12: Identification of chemoattractant doses using velocity of single cells - (A) Identification of optimal collagen coating concentration for single-cell migration assay for MCF7-$EGFR^{mCitrine}$ cells on the basis of velocity of single cells under stimulation with uniform dose of 100 ng/ml EGF. (B) Similar to (A) identification of optimal fibronectin coating concentration for single-cell migration assay for $MCF10A$ cells. (C, D) Identification of EGF dose for single-cell migration assay for MCF7-$EGFR^{mCitrine}$ (left) and $MCF10A$ (right) cells.

3.3.1 Migrating cells display directional memory of recently encountered signals

To check whether the transient memory in $EGFR^{mCitrine}$ phosphorylation polarization is translated into memory of directional migration and whether cells can sense dynamic gradients we established first a gradient whose slope changes over time. In particular we created a EGF^{647} gradient that was linearly distributed within the width of the chamber (500 µm), ranging between 25-0 ng/ml (Figure 3.15 A). However, this was dynamic in time as well. The gradient steepness was progressively decreased in a controlled

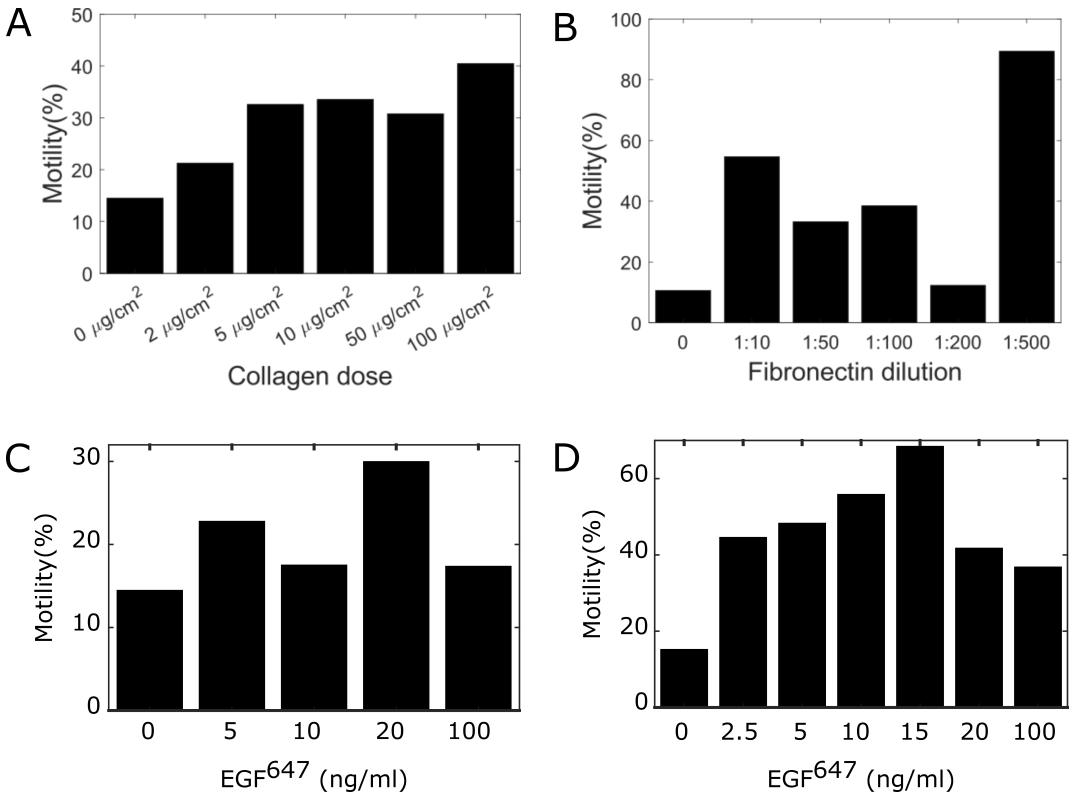

Figure 3.13: Identification of optimal conditions using motility measures - (A) Identification of optimal collagen coating concentration for single-cell migration assay for MCF7-$EGFR^{mCitrine}$ cells. Percentage of cell having motility greater than a displacement threshold ((Number of cell tracks with track length greater than threshold/ Total number of cells)·100) is shown. (B) Similar to (A) identification of optimal fibronectin coating concentration for single-cell migration assay for $MCF10A$ cells. (C, D) Identification of EGF dose for single-cell migration assay for MCF7-$EGFR^{mCitrine}$ (left) and $MCF10A$ (right) cells.

manner, rendering an evolution towards a 50% shallower gradient over 5 h (Figure 3.15 B). The gradient washout after 5 h was observed to be quick within 5 min, thus giving an accurate degree of control over the experimental conditions ensuring no remnant EGF levels inside the cell chamber. Single cells seeded on microfluidic plates were subjected to this 5 h dynamic gradient of EGF^{647}. Automated tracking of single-cell motility trajectories similar to the uniform migration experiments was performed for the entire duration of the imaging (14 h).

The migration tracks demonstrated that both the unperturbed $MCF10A$ cells as well as the engineered MCF7-$EGFR^{mCitrine}$ cells sensed the dynamic gradient and migrated in a directional manner towards the EGF^{647} source (Figure 3.16 A,B). Moreover, we observed that the directed migration of the single cells in the gradient chamber persisted for a transient period towards the source even after complete gradient washout. This observation indicated that cells retain the ability to maintain a memory of the location of previously encountered growth factor signal. Following the memory phase, the cells transited to a migration pattern which resembled the motility behaviour of cells without any stimulus. Compared to the uniform stimulation experiments, induced directed

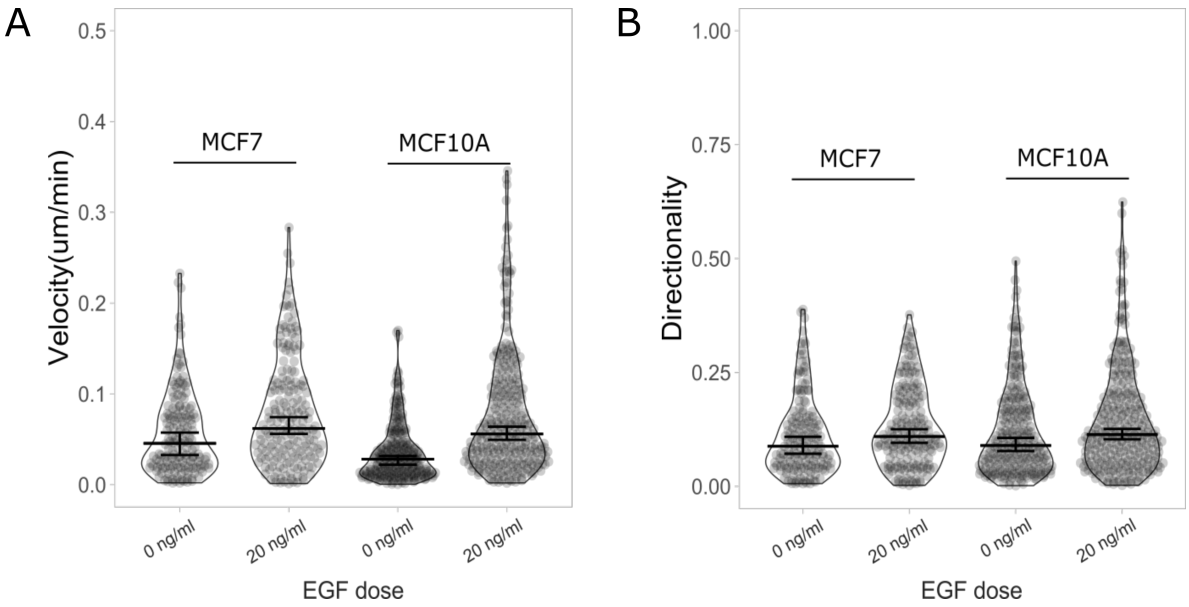

Figure 3.14: Evidence of directional memory cross cell-lines - (A) Comparison of velocity (displacement/time) distribution of single cells in MCF7-$EGFR^{mCitrine}$ and $MCF10A$ single cell migration during 14 h absence (0 ng/ml; MCF7 – n=207, N=2 and $MCF10A$ – n=245, N=3) or uniform 20 ng/ml EGF stimulation (MCF7 – n=200, N=2 and $MCF10A$ – n=297, N=3). Error bars: Median +/- 95% CI. (B) Comparison of directionality (displacement/distance) distribution of single cells in MCF7-$EGFR^{mCitrine}$ and $MCF10A$ single cell migration during 14 h absence (0 ng/ml; MCF7 – n=207, N=2 and $MCF10A$ – n=245, N=3) or uniform 20 ng/ml EGF stimulation (MCF7 – n=200, N=2 and $MCF10A$ – n=297, N=3). Error bars: Median +/- 95% CI.

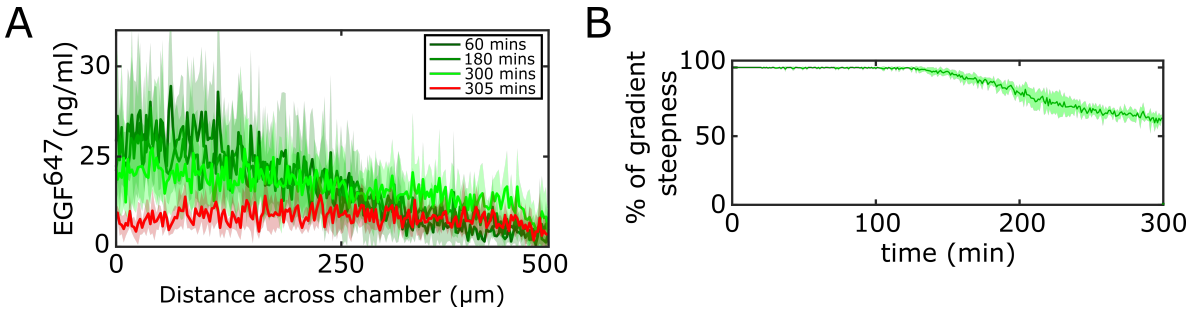

Figure 3.15: Single cell gradient migration experimental setup - (A) Quantification of 5 h dynamic EGF gradient at distinct time-points followed by gradient wash-out after 5 h. Different colors indicate gradient slope at different time points. Red line indicates washout. (B) Corresponding quantification of the temporal evolution of the gradient slope. Percentage of gradient steepness: [EGF(0) – EGF(L)]/EGF(0)×100 where L is the length across the chamber. Mean +/- SD from N=4 is shown.

migration was observed in both the cell lines in the gradient experiments, although the overall migration distance was lower due to lower duration of stimulation with EGF. Quantification of single cells' motion from the gradient experiments showed that the directionality was significantly higher during the gradient stimulation (5 h) as compared to the no – or uniform stimulation cases in both the cell lines (Figure 3.16 C). Moreover, the directionality estimated in the 9 h time-frame after the gradient removal was greater

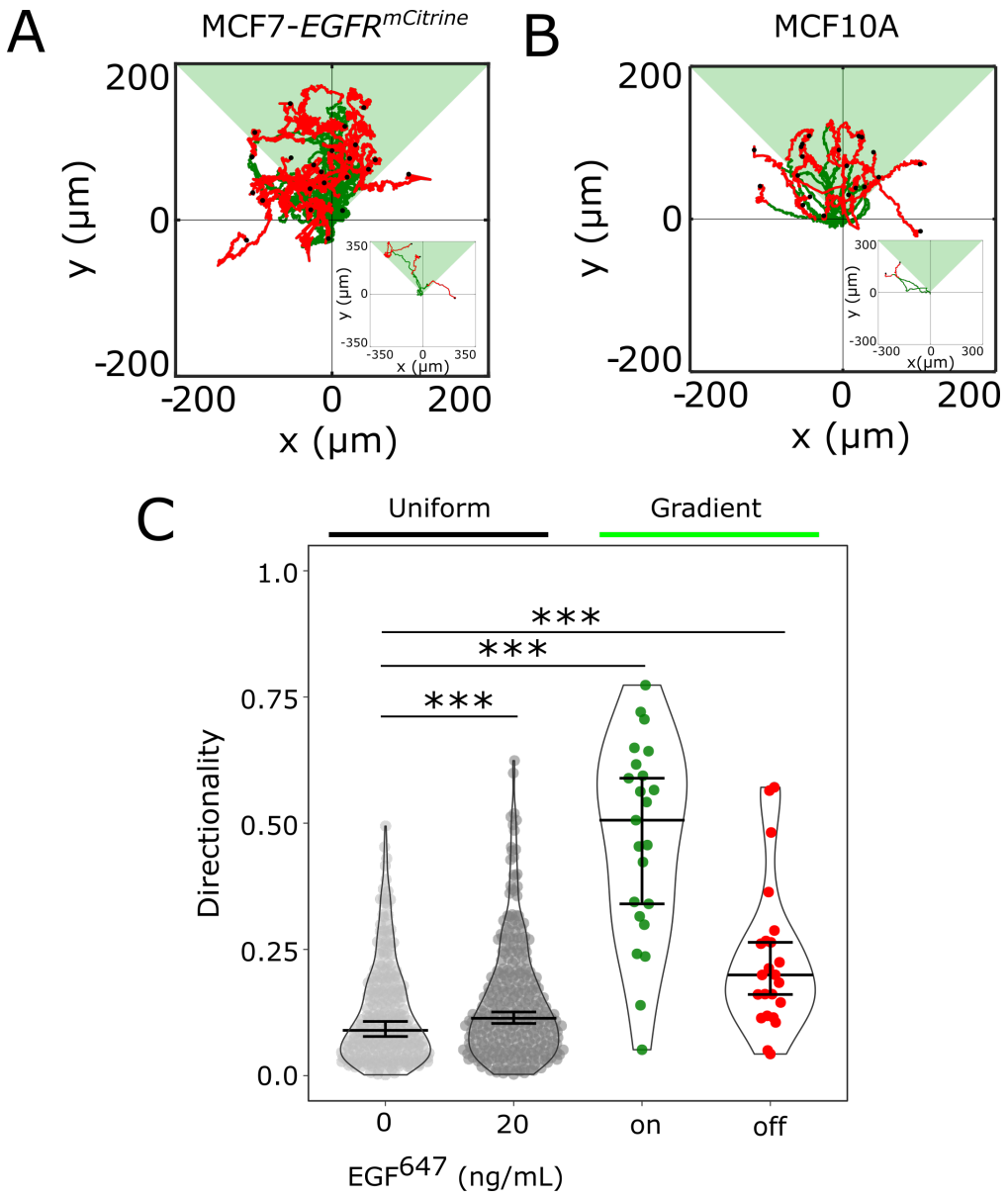

Figure 3.16: Single cell gradient migration assays - (A) Divergence plots depicting MCF7-$EGFR^{mCitrine}$ single-cell trajectories quantified, 5 h during (green) and 9 h after (red) dynamic EGF gradient duration (n=26, N=7). (B) Similar divergence plots as in (A) for $MCF10A$ cells (n=23, N=5). Black dots denote end of tracks. Insets capture long length cell tracks. (C) Directionality in $MCF10A$ single cell migration during 14 h absence (0 ng/ml) or uniform 20 ng/ml EGF stimulation; 5 h dynamic EGF gradient (green) and 9 h during wash-out (red; n=23, N=5). P-values: ***p≤0.001, two-sided Welch's t-test. Error bars: Median +/- 95% CI.

than the one in continuous stimulus absence, corroborating that the cells transiently maintain memory in directed migration (Figure 3.16 C) thus increasing the directionality.

3.3.2 Quantification of memory in directed motility

The motility results suggest that epithelial cells direct their motion according to the external dynamic signal's position and maintain temporal memory to preserve the directed motility transiently after the washout of the dynamic gradient. To verify this

observation and systematically find the duration of this memory in directional migration, we used the cell's relative turning angles (θ) estimated along the direction of the gradient source, i.e., the EGF^{647} flow channel, as a measure of the cells' directional motion. At each time point, the coordinates of the center of the cell were tracked using Trackmate [169], and the projection of the cells' relative turning angles ($cos(\theta)$) estimated along the gradient direction (π) was mapped and temporally profiled (Figure 3.17 A) (See Methods section 2.2.18 for details). The $cos(\theta)$ values or the straight-line projection towards the gradient, initially distributed around 0, approached 1 during gradient stimulation, and were temporally maintained after gradient removal before slowly decaying again to around 0. Similar temporal profiles of $cos(\theta)$ were also drawn for migration experiments with no- and uniform stimulation cases. Distribution of $cos(\theta)$ values around 0 were observed to be a vital characteristic in stimulus absence (Figure 3.17 B) or during uniform stimulation (Figure 3.17 C), although the spread of the distribution around 0 varied between individual cases. Higher variance reflecting non-directionality of cells was noticeable for uniform stimulation experiments.

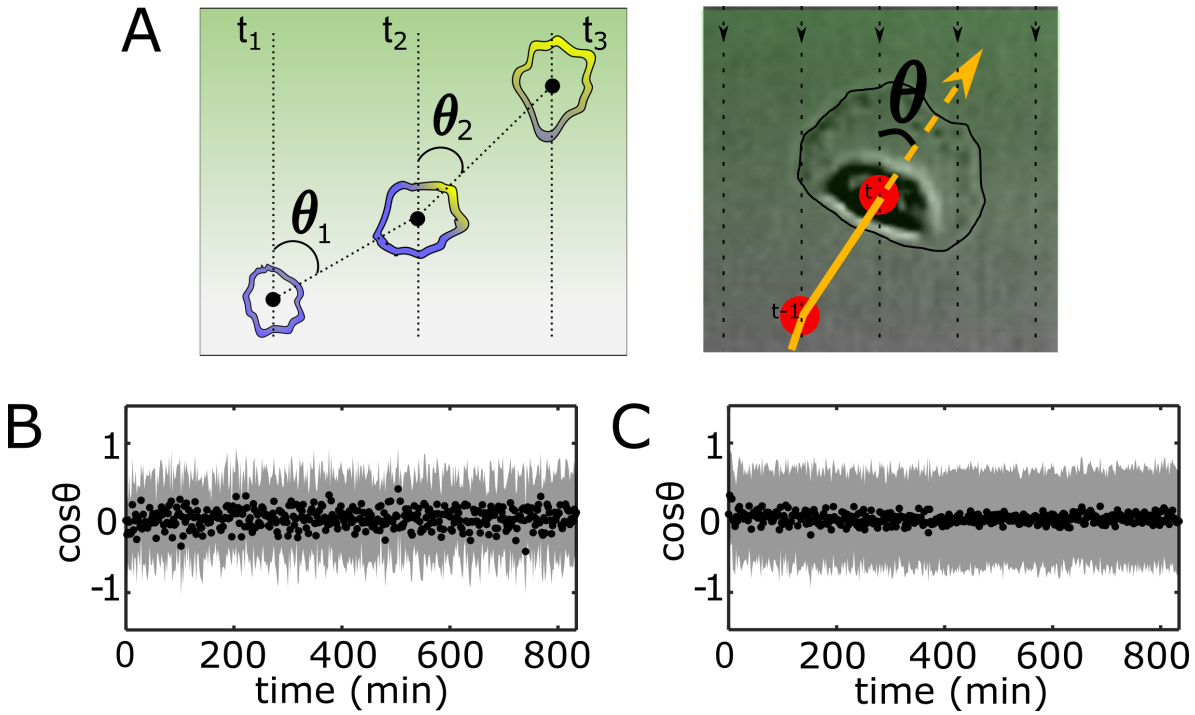

Figure 3.17: Estimation of single cells' relative turning angles - (A) (Left) Scheme of single-cell turning angle estimation (cos*theta*) from the cell migration trajectories at individual time points. (Right) Overlay of a migrating $MCF10A$ cell with the schematic of estimation of θ with respect to the direction of the gradient; (B) Average cos*theta* from single $MCF10A$ cell trajectories (mean +/- SD), estimated over a 2 min interval upon absence of EGF stimulation (0 ng/ml; n=245, N=3). (C) Similar to (B) upon uniform stimulation with 20 ng/ml of EGF (n=297, N=3).

The characteristic temporal evolution of $cos(\theta)$ was crucial in estimating the duration of memory in directional motility in the gradient migration experiments (Figure 3.18 A). To estimate the temporal interval in which $cos(\theta)$ was approximately distributed

around one after gradient removal, we tested whether the kernel density distribution estimate (KDE) of $cos(\theta)$ from all the analyzed single cells at each time point is statistically different to the characteristic KDE in the absence of stimulus employing a Kolmogorov-Smirnov (KS) test. Calculating the similarity between the KDEs shows that the distributions of $cos(\theta)$ during the gradient series and the no-stimulus case approach each other only $\approx$ 50 min after the gradient was washed out (Figure 3.18 A bottom). Additionally, the calculated similarity between the $cos(\theta)$ KDE distributions during the gradient (5 h) and the 50 min memory period further corroborated this finding (Figure 3.18 B(green and blue)). The average memory phase in directional motility thus corresponds to the time in which the memory in polarized $EGFR^{mCitrine}$ phosphorylation and single-cell shape is maintained (Figure 3.4, 3.6,3.9). The outcome demonstrates that memory in directed cell migration is likely resulting from the memory in receptor polarization that emerges from the SN_{PB} "ghost" or metastable state. It indicates that the metastable signaling state is translated to a stable prolonged migration response after the gradient removal.

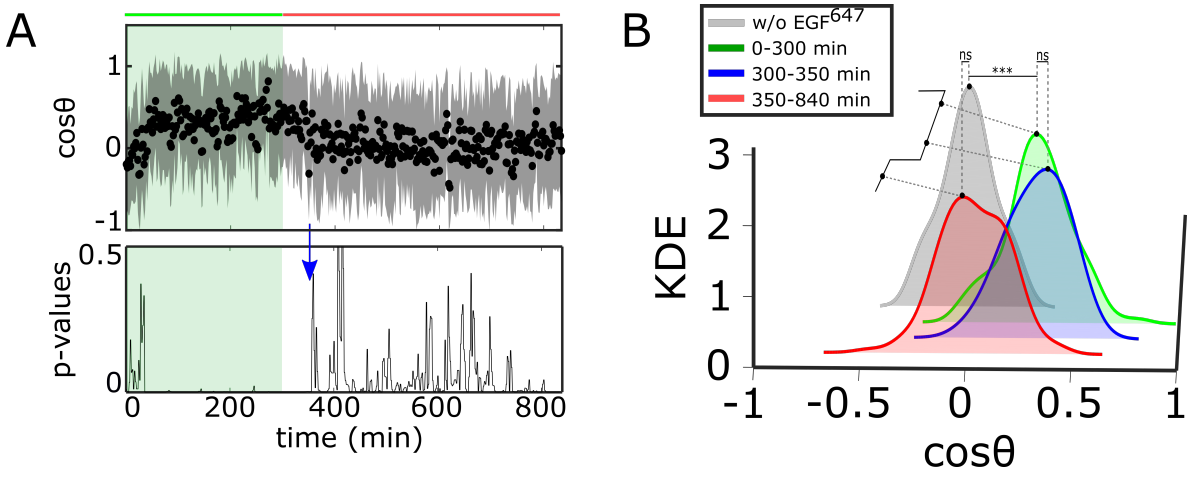

Figure 3.18: Single cells display directional memory of recently encountered signals - (A) Top: Projection of the cell's relative turning angles (mean +/- SD; n=23, N=5) during (green shaded) and after 5 h dynamic EGF gradient. Green/red lines: stimulus presence/absence. Bottom: Kolmogorov-Smirnov (KS) test p-values depicting end of memory in directional migration (blue arrow, t=350 min). Each KS test p-value estimated using 5 consecutive time points moving window. (B) Kernel density estimates (KDE) of the distributions in (A)-Top and Figure 3.17 B, in continuous EGF absence (grey), during 5 h dynamic EGF gradient (green), after gradient wash-out: $t \in [300min, 350min]$ (blue) and $t \in [350min, 840min]$ (red). P-values: ***, p$\leq$0.001, ns: not significant, KS test.

3.3.3 Inhibition of EGFR results in loss of memory in directional migration

To validate the link between the memory in polarized receptor activity observed, WT $MCF10A$ cells were treated with Lapatinib (Lap.) during the gradient washout similar to

the previous polarization experiments with the inhibitor. In the polarization experiments we showed that the addition of 1 µM Lap. inhibited the formation of memory in $EGFR^{mCitrine}$ phosphorylation polarization caused by an EGF^{647} gradient with a source concentration of 10 ng/ml. Hence for the gradient migration experiments with an EGF^{647} source concentration of 30 ng/ml, a Lap. concentration of 3 µM was chosen to satisfy the linearity change in concentrations. In the $MCF10A$ gradient migration assay, cells directly switched to a migration pattern described by the $cos(\theta)$ of cell migration in absence of EGF (Figures 3.11 A, 3.17 B) upon uniform gradient washout with Lapatinib (Figure 3.19 A). Thus, loss in directional motility was observed. The phenomenon was evident when the directionality estimates after gradient removal for the inhbitor treated cells were compared with directionality of cells exhibiting memory in directional motility (Figure 3.19 B). This result conclusively demonstrates that the memory in the EGFR phosphorylation polarization is translated into the memory in the directional motility through the spatio-temporal EGFR regulation on the cell membrane. It indicated that the transient memory arising from a metastable "ghost" signaling state is a core dynamical feature underlying transient memory in directional motility, which cannot be explained with slow relaxation kinetics in receptor dephosphorylation.

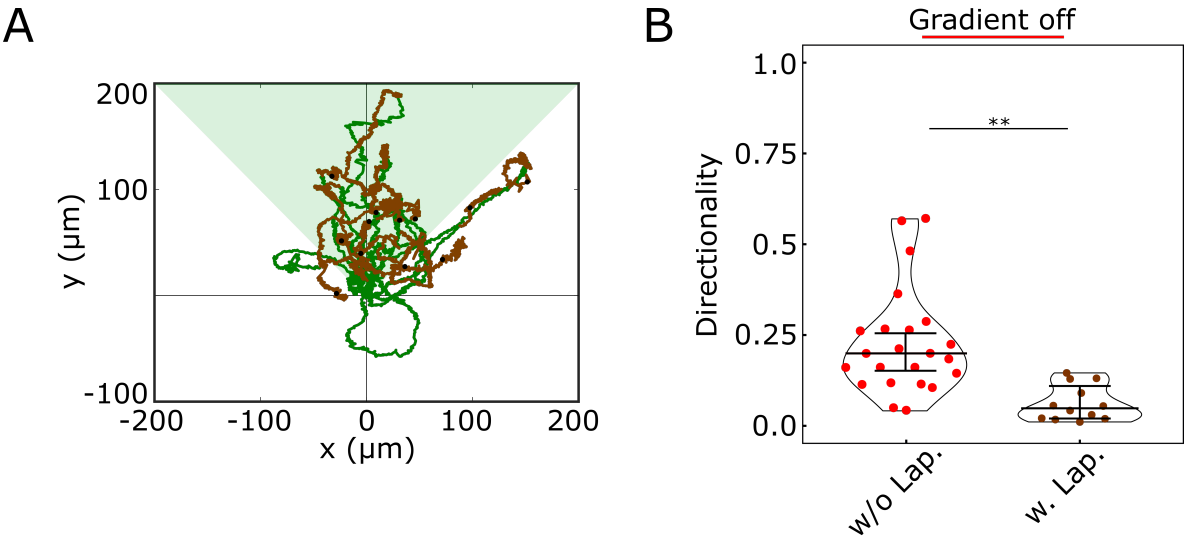

Figure 3.19: Absence of directional memory on treatment with receptor inhibitor - (A) $MCF10A$ single-cell trajectories quantified 5 h during (green) and 9 h after (brown) dynamic EGF gradient (green shading) wash-out with 3 µM Lapatinib. n=12, N=5. (B) Directionality in single-cell $MCF10A$ migration after gradient wash-out with (brown, n=12, N=5) and without Lapatinib (red, n=23, N=5). P-values: **p≤0.01, ns: not significant, KS test. Error bars: Median +/- 95%CI.

3.4 Characterization of cell migration tracks using modified Ornstein-Uhlenbeck process

It is crucial to identify what kind of motion cells exhibit in order to understand the cellular motility on stimulation with chemoattractants. To investigate and characterize the varied motility patterns observed in the cell migration assays, we used the Ornstein-Uhlenbeck process, originally used to describe the motion of a Brownian object/particle under an external force. The experimentally obtained single unperturbed $MCF10A$ cell migration trajectories were fitted using a modified Ornstein-Uhlenbeck process [146]. The Langevin equation defines the modified Ornstein-Uhlenbeck process (mOU) for the vector ν, which describes the velocity of a single cell using a motility coefficient and a random component of the motion. The expression can be written as:

$$\frac{d\nu(t)}{dt} = -\frac{1}{\tau} \cdot \nu(t) + \frac{\sqrt{2D}}{\tau} \cdot (\xi(t) + b(t)) \tag{3.2}$$

where $\xi(t)$ represents a white noise component, D is a diffusion coefficient characteristic of a Brownian motion, τ is the persistence time and $b(t)$ models the contribution of the time-dependent bias. The fitted values for D and τ can be obtained from the mean-square displacement (MSD) and velocity autocorrelation (VACF) functions of the tracked cells.

3.4.1 Characteristics of single cell migration in dynamic gradients

The experimental single MCF10A migration tracks data from the no- and uniform stimulation case of 20 ng/ml EGF was fitted to obtain values of D and τ. For 0 ng/ml EGF stimulation, fitted values are: D = 0.425, τ = 11.105. For 20 ng/ml EGF stimulation, fitted values are: D = 2.207, τ = 38.143. The bias value depicting the direction of EGF in the gradient migration experiments was fitted to the gradient migration tracks and found to be (0,0.134). The extracted motility parameters were then used to generate synthetic single-cell trajectories. In absence of any stimulus, the simulated divergence plot of the cell tracks resembled a random walk (RW) process (Figure 3.20 A). The corresponding $cos(\theta)$ distribution showed a mean value of 0 over time with high variance indicating non-directionality of cellular motion (Figure 3.20 C). For simulation of tracks with uniform stimulation with EGF, a persistent random walk (PRW) with higher persistence time was observed (Figure 3.20 B). The $cos(\theta)$ distribution from the PRW again resembled non-directionality with high variance (Figure 3.20 D). The single cell migration during the presence of the growth factor gradient was

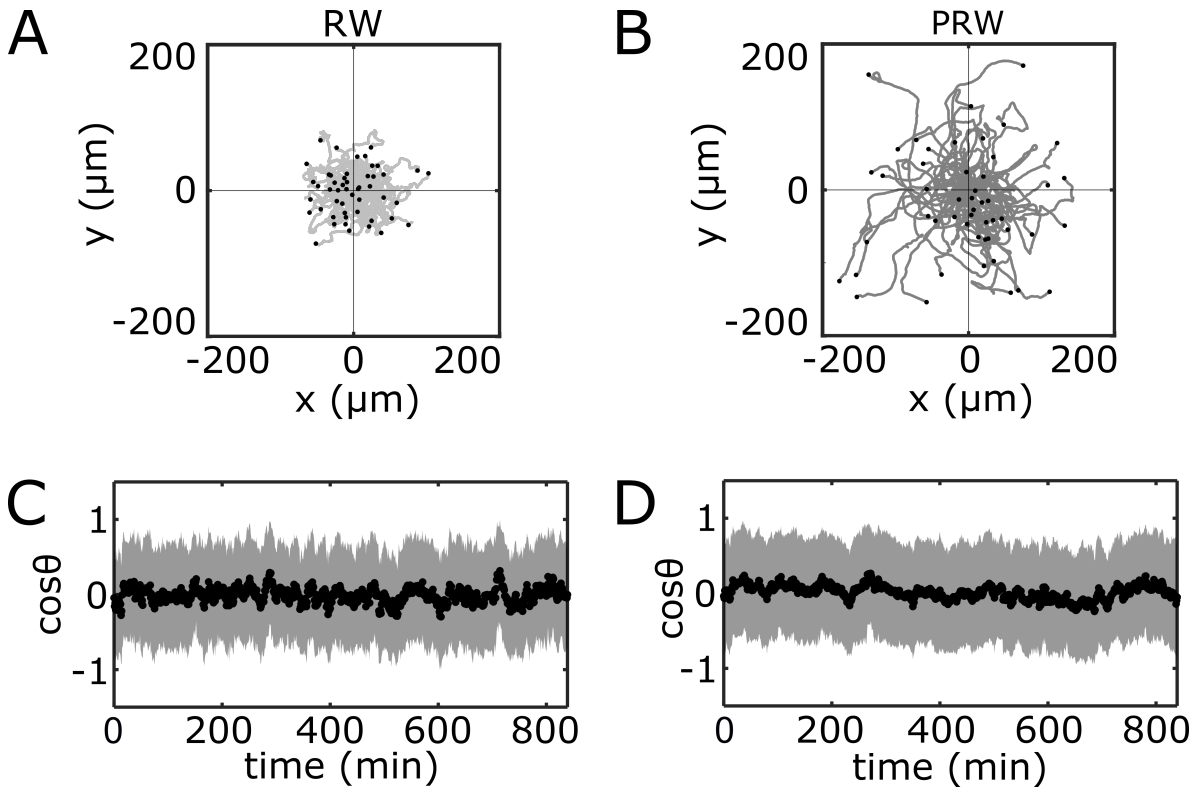

Figure 3.20: Identification of nature of single-cell migration - Synthetic single-cell trajectories (A) Random Walk (RW) (n=50), (B) Persistent Random Walk (PRW) (n=50). Parameters: for RW - $\tau = 11.105$, b(t) = 0, D = 0.425, and for PRW - $\tau = 38.143$, b(t) = 0, D = 2.207. (C, D) Average cosθ from synthetic cell trajectories (mean +/- SD) estimated over a 2 min interval from (A) and (B) respectively equivalent to experimental quantifications in Figure 3.17 B,C.

symbolized by a biased PRW (PBRW) wherein the bias indicated the direction of the source of the EGF (Figure 3.21 A). Extending the bias duration during the interval of the experimentally observed memory phase i.e. 50 min after the washout of the gradient thus simulating a time dependent bias (PB(t)RW) was able to reproduce the transient persistent motion after the gradient removal (Figure 3.21 C,D). The directionality estimates of the synthetic single cell tracks were extracted from a sample of repeated simulations and it was observed to be equivalent to the directionality calculations from the WT $MCF10A$ migration assays (Figure 3.21 B). The corresponding $cos(\theta)$ temporal profiles were shown to be comparable with their experimental counterparts.

The gradient migration with the receptor inhibitor washout was recapitulated synthetically using the mOU process by assuming the duration of the bias to be equal to the duration of the gradient of EGF (Figure 3.21 E,F). Altogether, these results demonstrate that single epithelial cells transiently maintain memory of the previous signal location and thereby display directed motility equivalent to that in the presence of the gradient characterized by PBRW, before reverting to a completely random walk migration pattern. Thus, the motility features of the single cell migration on chemokine stimulation can be understood using a modified Ornstein-Uhlenbeck process.

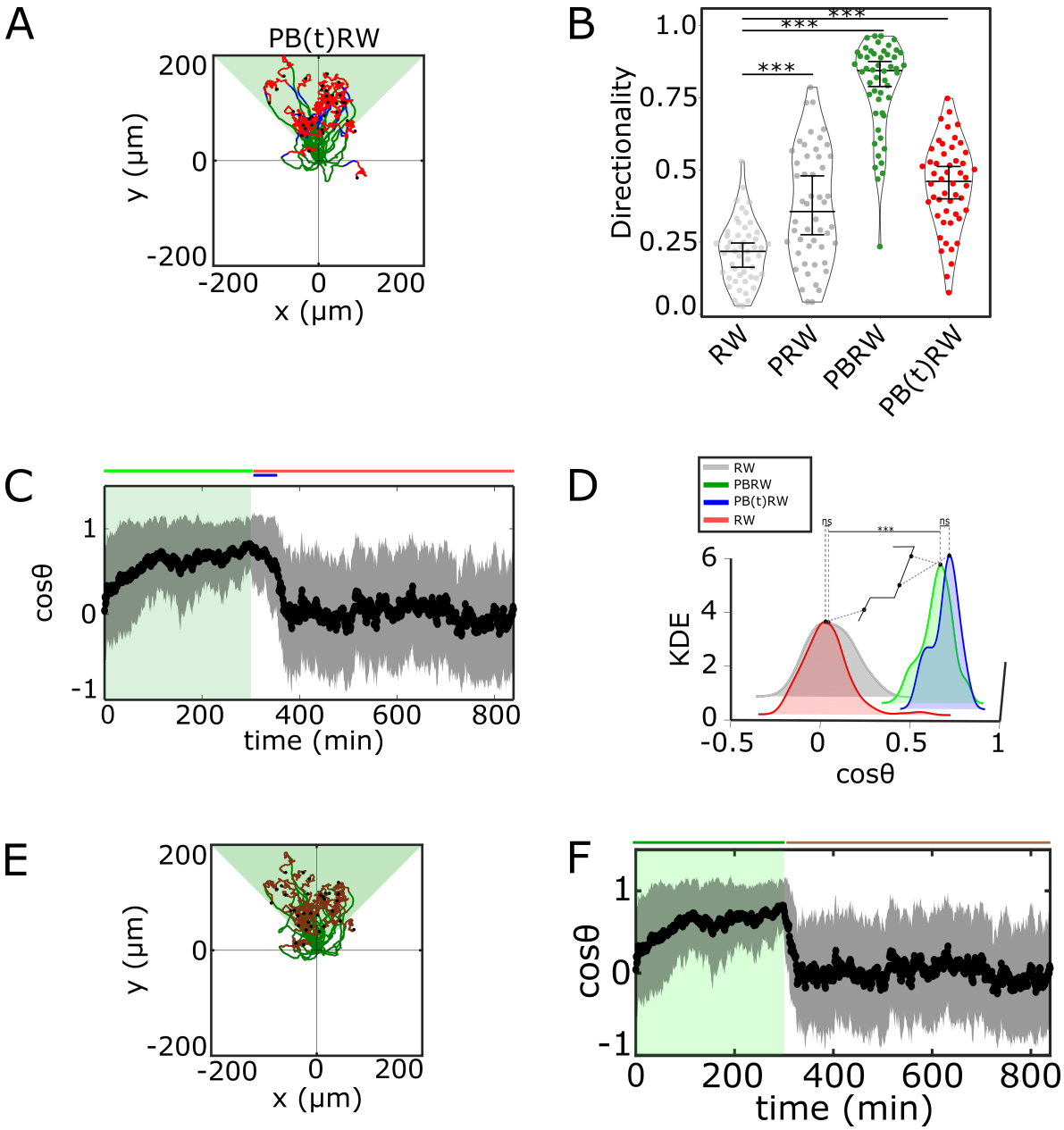

Figure 3.21: Characterisation of gradient migration using mOU process - (A) Representative in silico single cell trajectories for Persistent Biased Random Walk (PB(t)RW) where bias is a function of time (n=50). Parameters: τ = 38.143, b(t) = 0.134, D = 2.207 for t $\in$ [0 min, 350 min] (green, blue), τ = 11.105, b(t) = 0, D = 0.425 for t $\in$ [350 min, 840 min] (red). (B) Corresponding directionality estimates from n=50 samples of RW, PRW and PB(t)RW. P-values: ***p$\leq$0.001, two-sided Welch's t-test. Error bars: Median +/- 95%CI. (C) Projection of the synthetic cells' relative turning angles (mean +/- SD; n=50) during EGF gradient (green shaded), memory period (blue line) and after 5 h dynamic EGF gradient. Green/red lines: stimulus presence/absence. (D) Kernel density estimates (KDE) of the distributions in (C) similar to Figure 3.18 B. (E) Synthetic single cell trajectories generated when PBRW is considered only in the time frame during gradient duration mimicking the experimental data in Figure 3.19 A. (F) Same as in (C) but changed parameters to mimic inhibitor case in (E). Parameters:: τ = 38.143, b(t) = 0.134, D = 2.207 for t $\in$ [0 min, 300 min] (green), τ = 11.105, b(t) = 0, D = 0.425 for t $\in$ [300 min, 840 min] (brown). Brown line: inhibitor presence.

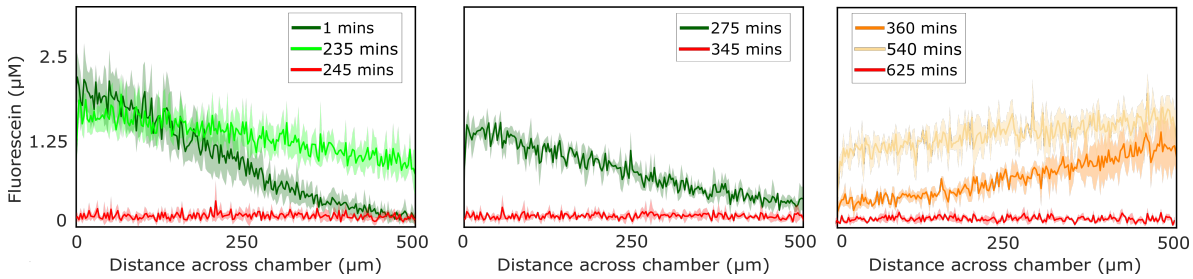

Figure 3.22: Experimental implementation of changing chemoattractant fields - Dynamic spatio-temporal growth factor field implemented in the experiments using microfluidic chambers. Quantification of a 15 h dynamic EGF gradient field at distinct time points. Mean ± SD from N=3 is shown. Green and orangish yellow/red: gradient presence/absence.

3.5 Single cell navigation in changing growth factor fields

From the combined results of the previous experiments, we have been able to conclude that single cells when stimulated with complex external signals are able to sense the direction of the signal via the membrane receptors, undergo symmetry breaking and polarize in the direction of the extracellular signals, and more importantly maintain such activity states even upon removal of external signal, thereby manifesting a form of molecular memory at the level of the receptor activity polarization. This transient memory, arising from the trapping of the cell system in a metastable "ghost" near the vicinity of the stable steady states as predicted from the theoretical description, translates to a transient memory in directional migration of single cells. Such phenotypic behaviour forms a core dynamical feature of the cellular sensing via receptor networks. To investigate how this transient molecular memory enables cells to sense and navigate in dynamic spatio-temporal growth factor fields, a systemic approach using multiple gradients was implemented.

3.5.1 Molecular working memory enables cells to navigate in dynamic chemoattractant fields

Since the memory in EGFR phosphorylation polarization and thereby memory in directional motility emerges from a dynamically metastable state, it has been proposed (See Dissertation by Akhilesh P. Nandan) that the system senses and quickly respond to subsequent chemical cues that vary both in space and time. Even if cells are subjected with new signals within the memory phase, cells can sense the novel signals and accordingly adapt the duration of EGFR phosphorylation polarization and subsequently directional motility, rendering history-dependent response in a changing environment. Experimentally, complex fields were tested and an optimal sequence of dynamic time-varying gradients was chosen to input in the simulation study (Figure 3.22). The field was

generated by a sequence of signals, starting with a dynamic 4 h gradient whose steepness changed over time, followed by a second 1 h static gradient from the same direction, that after an equivalent disruption period of washout was followed by a third dynamic 4 h gradient from the opposite direction to the initial two gradients. The sequence of signals was controlled and established using the automated microfluidic machine and quantified using Fluorescein (See Methods sections 2.2.10, 2.2.13 for details). To test whether the identified memory enables optimal cellular navigation in such a complex environment, where the signals are disrupted as well as changing in space and time, simulations of cell tracks were performed using the mOU process with fitted parameters (Methods section 2.2.19). Subset of simulated cell tracks in Figure 3.23 A- shows the response behaviour of cells under time-varying gradients. Despite the memory in cell polarization and subsequently in migration, cells remained responsive and adapted the duration of directional migration when presented with a second static gradient from the same direction, and subsequently prioritized the third, newly encountered signal with opposed orientation. Unperturbed $MCF10A$ cells seeded in the gradient microfluidic plates were also subjected to the changing growth factor field for experimental validation. A divergence plot (Figure 3.23 B) highlighted the migratory profile of the tracked single WT $MCF10A$ cells under the influence of such a complex field. The $MCF10A$ cells sensed the initial dynamic gradient field and migrated in the direction of the largest chemoattractant concentration, maintaining the directionality even when the signal was temporally disrupted.

The memory of the previously encountered signal localization enabled maintaining robust directional migration even when the signals were washed away, while still remaining sensitive to the newly emerging signals in the environment. The temporal memory in directional migration as well as the continuous adaptation of the $MCF10A$ cells to novel cues was also reflected in the projection of the cell's relative turning angles. Corresponding temporal evolution of the projection ($cos(\theta)$) from simulations (Figure 3.23 C) and the experiments (Figure 3.23 D) revealed that the cells also rapidly adapted their orientation when sensing the third signal with opposite localization. Such a dynamic memory which enables information of previous signals to be temporally maintained while retaining responsiveness to upcoming novel signals and thereby manipulate the stored information, in neuronal networks, is described as a working memory. These results demonstrate that single cells navigate in changing gradient fields by utilizing a molecular mechanism of working memory that is an intrinsic feature of the receptor tyrosine kinase networks namely, the EGFR network.

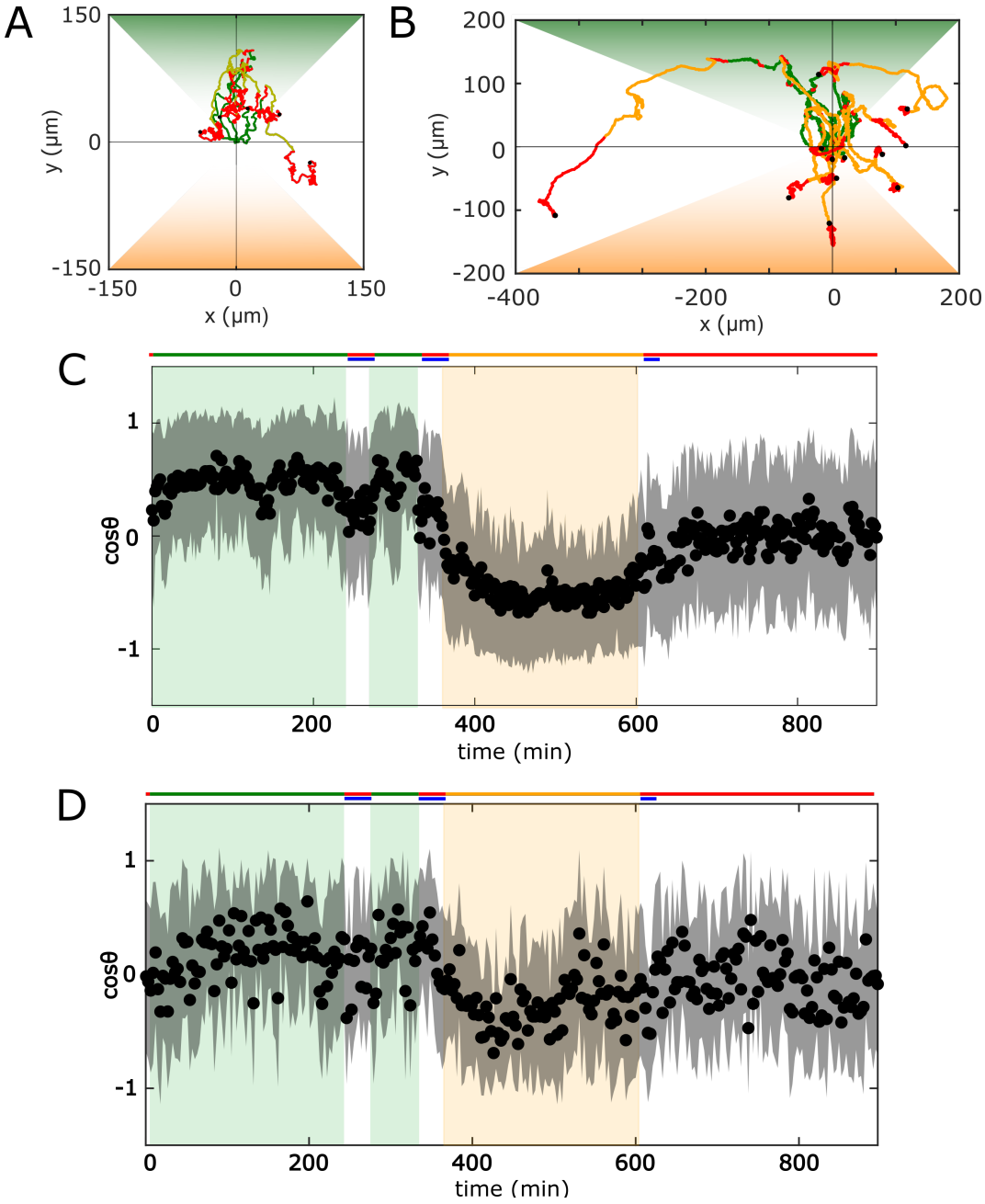

Figure 3.23: History-dependent single cell migration in complex field - (A) Representative *in silico* single cell trajectories for Persistent Biased Random Walk (PB(t)RW) where bias is a function of time (n=30). Parameters: τ = 38.143, b(t) = 0.134, D = 2.207 for t $\in$ [0 min, 360 min] (green, blue), τ = 38.143, b(t) = - 0.134, D = 2.207 for t $\in$ [360 min, 615 min] (yellow, blue), τ = 11.105, b(t) = 0, D = 0.425 for t $\in$ [615 min, 840 min] (red). (B) Divergence plots depicting $MCF10A$ single-cell trajectories quantified during migration in dynamic EGF gradient field shown in Figure 3.22. N=12, N=5 (C) Projection of cells' relative turning angles (cosθ) depicting their orientation towards the respective localized signals from simulation (n=30). (D) Same as (C) from experimental data. Mean $\pm$ SD from n=12, N=5 is shown.

4

Discussion

Essential cell migration has been shown as a coupled process of signaling events caused by PI3K and Rac1 mediated activation of Rho-GTPases by EGF-induced EGFR activation. In recent years, studies of the coupling interactions of EGFRs with the phosphatases have revealed a central EGFR-PTP network responsible for sensing and responding to extracellular EGF concentration [92, 84]. Although EGFR's phosphorylation regulation has been understood reasonably well, its role in processing spatial and temporal cues over time and optimal cellular migration as a response is essential in the real-time computation of single cells in complex environments. Under physiological conditions, a mechanism of cell polarization and migration using the dynamical symmetry breaking description of Subcritical pitchfork bifurcation ($SubPB$) has been proposed (See Dissertation by Akhilesh P. Nandan) [146], which can account for robust and rapid processing and maintenance of information from extracellular cues. The dynamical advantages of such a system arises from metastable states. In this thesis, the main objective was to reveal and verify the presence of such a metastable state in cell polarization and migration using the EGFR-PTP network motif.

4.1 Molecular mechanism of transient memory in cell polarization

How EGFR responds to EGF stimuli depends on the $PTPRG/EGFR$ abundance ratio at the PM of cells, i.e., the sensing and processing of the system depends on its positioning in parameter space [92, 142]. Optimal growth factor sensing of non-stationary signals has been identified to occur in the vicinity of the saddle-node (SN) bifurcation point, i.e., at criticality (Figure 1.12) where features like switch-like amplified activation and reversibility are presented [147, 142]. The dynamics of temporal EGFR phosphorylation responses at criticality on stimulation with EGF pulses show that

cells process and integrate time-varying signals using metastable states rather than time-invariant steady states. This results in maintenance of transient high EGFR phosphorylation even after signal removal (Figures 3.1, 3.2). Upon directed stimulation of cells with low physiological concentrations of EGF gradients, robust and rapid polarization of receptor phosphorylation occurs (Figures 3.4, 3.5). A temporal transient memory is realized on a molecular level by storing information about the direction of previously encountered signals through the maintenance of a prolonged polarized phosphorylation state of receptor tyrosine kinases (Figure 3.6). The short memory is highlighted in the maintenance of the polarized cell shape with a defined 'front' and 'back' towards the EGF gradient (Figure 3.9). Loss of memory in cell polarization upon addition of an EGFR inhibitor (Figure 3.10 A) results in a loss in polarized cell shape (Figure 3.10 C), which shows the importance of EGFR activity at the PM in regulating cellular memory in directional migration. This emphasizes that the geometry of cell membranes is tightly coupled with the signal processing capability of a cell that interprets its environment. Thus, to interpret the external gradient of EGF effectively a single cell reshapes its PM by polarizing the receptor activity in the direction of the gradient. The polarized cell morphology can persist due to stabilization by downstream protein reactivity, which in turn could be influenced by the geometry of the PM [26].

The activation mechanism triggering EGFR phosphorylation across the membrane includes EGFR activation of the ligand-bound dimers via trans-phosphorylation, along with the autocatalytic, autonomous, and ligand-bound induced activation of the unliganded EGFR (Section 1.2.1) [92]. Thus, initiation and signal propagation within the EGFR population can occur even in the absence of stimulus via the unliganded EGFR molecules. It has been shown in recent studies that under stimulation with suprathreshold EGF doses, unliganded EGFR undertakes a different trafficking route than the liganded EGFR upon activation at the PM and internalization. EGF-bound EGFRs are marked with ubiquitination tags and unidirectionally trafficked for lysosomal degradation. Transient stimulation with EGF doses has revealed the importance of the trafficking route of the unliganded receptor, which rapidly recycles to repopulate the PM. The recycling of the unliganded EGFR upon transient pulse stimulation results in prolonged phosphorylation on the PM due to the triggering of the autocatalytic mechanism of EGFR activation [84]. The unliganded EGFRs can get trans-phosphorylated in a transient complex by another unliganded receptor - comprising the autonomous or autocatalytic activation, or by an EGF-bound receptor that promotes the autocatalysis at a low dose. The basis for such phosphorylation propagation through autocatalytic EGFR activation is most likely the phosphorylation of the regulatory Y845 in the kinase activation loop, which stabilizes the active conformation of the receptor. This could be established by direct autophosphorylation in transient receptor complexes or by indirect phosphorylation via Src that is in turn activated by EGFR.

A double negative ROS-mediated EGFR-PTP feedback determines the ultrasensitive lateral phosphorylation propagation mechanism.

EGFR and PTP molecules are distributed across the PM, maintaining a critical balance [92]. PTPs are spatially localized in cellular compartments, i.e., PTPN2 in the ER, which does not diffuse, while PTPRG on the PM is free to diffuse with distinct constant. EGFR molecules on the PM occupy three distinct mobility states, free, confined, and immobile, with the occupations of the free and immobile states decreasing and increasing significantly after EGF stimulation [102]. In such a scenario, there could be two possibilities by which the cell can be organized in the critical organization of receptors and exhibit polarization features. One possibility is due to the heterogeneity in the EGFR signaling activity in the direction of the signal [86]. Upon directed stimulation with an external EGF gradient, higher ligand-binding effectively takes place on the side of the cell, sensing greater EGF molecules. Ligand-bound EGFRs are internalized and trafficked through the vesicles thus increasing the vesicular trafficking at one end of the cell. EGF-EGFR dimers can amplify the phosphorylation response of the recycled monomers on the PM in the direction of the stimuli. Effectively the signaling activity of EGFR is polarised towards the chemoattractant gradient. A second possibility by which cell polarization can arise is due to the nonuniform amount of EGFRs on the PM, which are free to sense the dynamic signal. While the EGF-EGFR dimers are unidirectionally internalized and trafficked for degradation, diffusion of unliganded EGFRs across the PM and recycled unliganded receptors can occur towards the gradient source for sensing the dynamic cue. As a consequence, a disparity in the distribution of EGFRs on the PM can arise, leading to an asymmetrical distribution of phosphorylated receptors on the membrane. Our preliminary investigation suggests it is likely via the former mechanism of EGFR activity as the number of receptors on the PM over time was estimated to be uniformly distributed. However, more detailed studies need to be performed for verification purposes. Thus an external gradient translates to an internal gradient within the cell, establishing a cell polarity towards the EGF source. Hence, when treated to a directional stimulus, a cell in a basal state breaks through the homogeneous symmetrical state to respond robustly and rapidly and attains a polarized state. This polarized state persists transiently even after removal of the external gradient and can translate to a memory in directional migration.

Such persistent motion requires continuous sensing of EGFRs along with corresponding polarization in EGFR phosphorylation. High levels of autonomous EGFR phosphorylation promote the phosphorylation of Akt via PI(3,4,5)P3-enriched membrane domains present at the PM. Phosphorylated Akt promotes vesicular recycling of EGFR generating positive feedback due to the autocatalytic nature of EGFR phosphorylation. An Akt-dependent EGFR recycling on the PM is promoted, which maintains further sensitivity to EGF and maintains a migratory mode of the cell by keeping an adequate number of receptors at the PM [137, 160]. Upon EGF gradient washout, the recycled

monomeric EGFRs can amplify and maintain high phosphorylation via autocatalysis, as described earlier. Such a mechanism can provide the molecular basis for persistent memory in the directional motility of single cells in gradient-driven systems.

4.1.1 Dynamical model of cell polarization using $SubPB$ mechanism

The polarized state has been shown to maintain even upon EGF removal due to the trapping of the trajectory in a region in the state-space, i.e., a transient memory. The mechanism of transient memory reported in this thesis is realized on a molecular level by storing information about the direction of previously encountered signals through the maintenance of a prolonged polarized phosphorylation state of receptor tyrosine kinases. Previously, the features of a saddle-node (SN) bifurcation 'ghost' were related with the emergence of dynamic memory crucial for processing time-varying signals [142]. It has now been conjectured that if the cell polarization network, i.e., the EGFR network is poised at criticality, i.e., the parameters correspond to an organization before a subcritical pitchfork bifurcation ($SubPB$) where a PB is stabilized through SN_{PB}, and the dynamical characteristics of both the bifurcations are uniquely manifested to render memory of the polarized state as well as plasticity in the responsiveness to dynamic spatial-temporal signals. The system's dynamical behavior was quantitatively studied by analyzing the evolution of the phase space trajectories in relation to the changes in the geometry of the underlying phase space (described by the system parameters) as a function of the gradient stimulus (See Dissertation by Akhilesh P. Nandan) [146]. Quasi-potential landscapes (See section 1.3) in Figure 4.1 describe energy-like levels associated with the states [142]. The EGF gradient induces a shift from the unpolarized state described by the homogeneous fixed point to the inhomogeneous state (IHSS) stabilized through the SN_{PB} (Figure 4.1 A [Top left]). The IHSS signifies the symmetry-broken polarized state, which underlies a mechanism of robust cell polarization (Figure 4.1 A [Top right]). Upon removal of gradient stimulus, due to the closeness of the nullclines [142] the system persists in a polarized state before returning to the basal level. Dynamically, the prolonged polarized state emerges for the organization of the EGFR network at criticality, where a slow-escaping remnant from the attractor state or a dynamical "ghost" is generated (Figure 4.1 A [Top middle]). The "ghost" metastable state maintains the EGFR system away from the steady-state, suggesting that in living cells, the information about the previous signals is encoded in the transient state-space trajectories rather than the steady states of the protein interaction network. Experimentally, we have shown that cellular sensing and processing of dynamic signals describe the dynamical mechanism of $SubPB$ where the PB confers the polarization features. In contrast, the metastable state from the SN_{PB} "ghost" allows for the memory of the polarized state and thereby capability for temporal signal integration. Such

features arise when EGFRs on the PM are maintained at a critical expression level (Figures 3.5 C; 3.6 E).

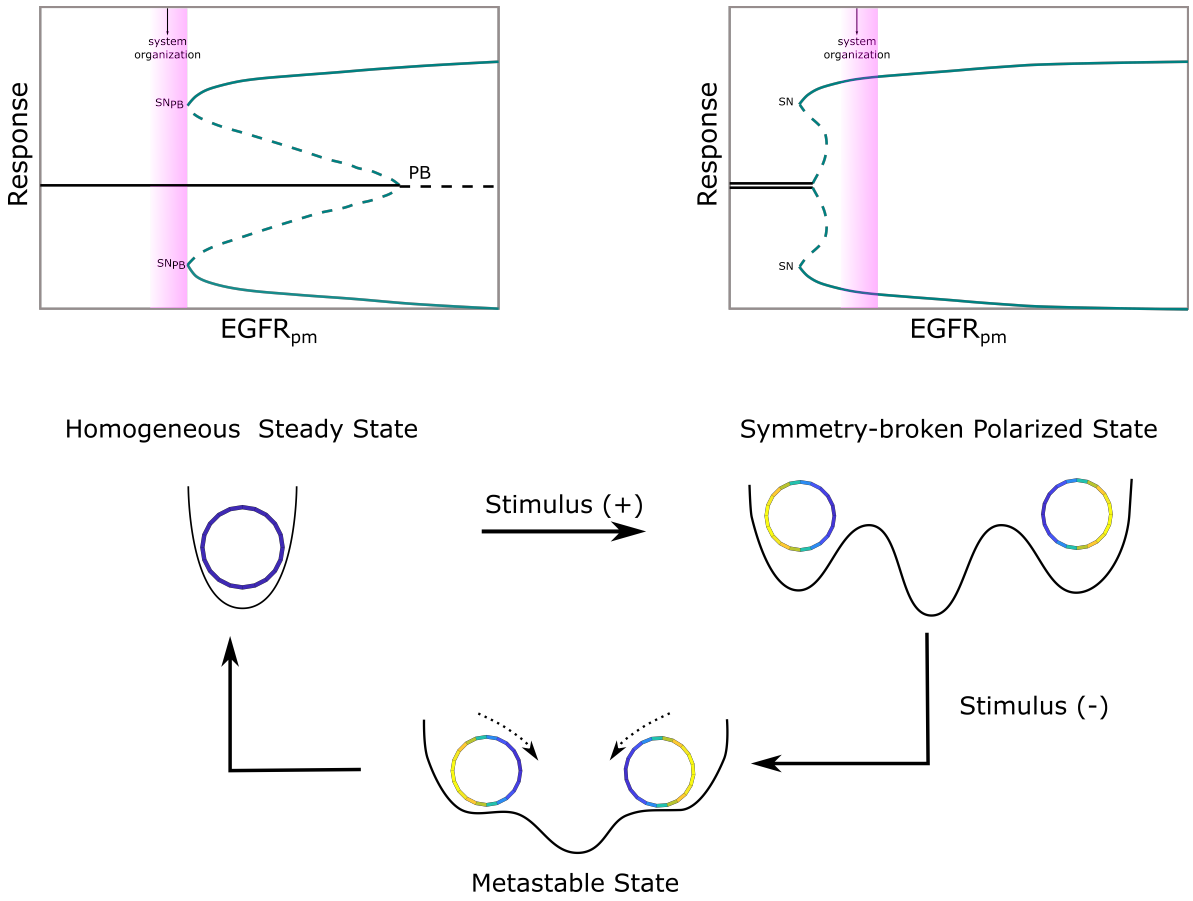

Figure 4.1: Dynamical mechanism of memory formation - (Left) Schematic bifurcation diagram depicting EGFR activity steady states with respect to system parameter, in the absence of EGF signals. (Right) Schematic bifurcation diagram depicting EGFR activity steady states with respect to system parameter, in the presence of EGF gradient. Stable/unstable steady states (solid/dashed lines): unpolarized (homogeneous, black) and polarized (inhomogeneous, dark cyan) EGFR activity. SN_{PB}: saddle-node bifurcation through which pitchfork bifurcation (PB) is stabilized. (Below) State-space transitions via a quasi-potential landscape depicting transition from a homogeneous steady state to a symmetry broken polarized state. Metastable state generated while transitioning back from polarized to homogeneous state with system poised at criticality.

4.2 Memory in directional motility of cells

Single cells within tissues and organisms rely on sensing local gradient cues, which are irregular, conflicting, and changing over time and space. However, a robust mechanistic validation for the generation of persistent directional migration when signals are disrupted while still remaining adaptive to external signal localization changes has not yet been shown. Processing of time-varying signals with a metastable state equips the system with unique features, which include allowing the cell to temporarily maintain the signaling state from the past. Thus a disrupted signal, e.g., in complex tissues, can still maintain

a proper receptor phosphorylation response. Such a transient memory in receptor phosphorylation have been demonstrated to guide directed migration in section 3.3.1. The two cell-lines, engineered MCF7-$EGFR^{mCitrine}$ and WT MCF10A, with similar expression levels of EGFRs on the membrane [92], exhibit similar phenotypic behaviour in their motility (Figure 3.14 A,B). Consequently, they provided us with a setup to test and compare the migratory features upon stimulation with EGF gradients. Our single-cell migration experiments under dynamic EGF fields (Figures 3.16; 3.22; 3.23) exemplify the translation of polarization in EGFR phosphorylation and cell morphology to a directional migration towards the chemoattractant source.

Chemotaxis requires that cells like leukocytes to remain responsive to stimuli for prolonged periods of time as they migrate toward the chemotactic source. Thus a migrating leukocyte must therefore distinguish between a hierarchy of signals within the tissue to successfully reach the site of inflammation. During wound healing processes, cells also operate in a complex, continuously changing environment with low physiological doses of growth factors. The motility features of single epithelial cells on an ECM coated surface showed optimal cell migration in the range of 15-30 ng/ml EGF stimulation (Figure 3.13). Under a 5 h gradient of EGF, the cells polarized and showed persisted migration in the direction of the source throughout the duration of the gradient (Figures 3.16). The EGF-induced directed motion was shown to persist towards the source direction for $\approx 50min$ even upon the washout of the gradient, which indicated a directional memory duration equivalent to the memory duration in polarization. Characterization of the cellular motion using Langevin dynamics revealed the migration to be of unique nature dissimilar to the natural RWs or PRWs. The migration under the gradient stimulation was described using a persistent random biased walk where the bias, given by the direction of EGF binding with EGFR, is a function of time (PB(t)RW) (Figure 3.20). Hence the memory in directional motility is encoded in the bias.

4.3 Importance of memory in realtime computation

For neuronal networks, short-term working memory has been shown to be a main requirement to integrate temporal dependencies from changing signals [176, 177]. Working memory is widely regarded to play a critical role in cognition by acting as a workspace on which information can be held, processed, and used to guide the behavior of neurons or the brain [178]. The popular model of working memory is that recurrent network interactions, either within or between brain regions, give rise to persistent neural activity [179, 180]. Most of these models present a limited capacity of sensing and processing of stimuli due to the processing with a fixed number of stable state attractors. On the other hand, experimental demonstration of 'working memory'-like features of non-neuronal networks has not been reported.

In this thesis, we have experimentally demonstrated that the positioning of the EGFR system in the vicinity of a SN_{PB} bifurcation provides a unique mechanism for processing cellular sensing of time-varying growth factor signals as well as cell polarization. The metastable state that is thereby generated facilitates a dynamic transient memory that encodes information about previous signals. Observation of single cells in changing chemoattractant fields (Figure 3.22) show that this information encoding is necessary to ensure constant adaptation shown in Figure 3.23. Constant adaptation is required to accommodate a large range of possible scenarios that can occur in complex environments. Cells integrate changing signals, as well as transform the extracellular information for the guidance of memory-directed migration. Such a type of memory-guided navigation is advantageous when the migration is realized over long and complex trajectories through dense tissues where the chemical cues are disrupted or only locally organized (Figure 1.1 B). Furthermore, EGFR signaling plays an essential role during embryogenesis, adult physiology, and pathophysiology [181] during which processing time-varying growth factor signals are prevalent, and hence a memory in EGFR phosphorylation due to the critical organization in parameter space can ensure proper cellular fate or outcome. Our data establish that mammalian cells use a mechanism of working memory to navigate in complex environments where the chemical signals are disrupted or vary over time and space.

On the other hand, receptor overexpression leads to an increase in EGFR density at the PM along with the kinase activity in the system. Hence, in the dynamical space, system can shift to either the bistable or preactivated monostable regime. As such, EGFR hyperphosphorylation can take place even upon subthreshold EGF signals. Such an aberrant signaling system will be devoid of memory, and cells won't be able to process time-varying signals and respond optimally. This can be caused by genetic mutations. In tumor cells, growth factor sensing and processing via EGFR is affected by point mutations on EGFR allele, e.g., L834R/T766M mutation in lung cancer [182]. Such mutations result in gene amplification/overexpression of the receptors.

4.4 Evolutionary context of integration of working memory within network topology

Understanding how the phenotypes and behaviors of single cells are controlled is one of the major challenges in biological research. Traditionally, the focus has been given to the characterization of individual genes/proteins or individual interactions during cellular events. However, many phenotypes and behaviors cannot be attributed to isolated components. Instead, they arise from characteristic modulation of cellular networks, which represent connections between molecules in cells [183]. Small patterns of interconnections occurring in higher frequency than random network connections

in larger complex networks are defined as network motifs. The organization of such network motifs described by the protein-protein interactions (PPI) can be examined from an evolutionary perspective. In *Saccharomyces cerevisiae*, proteins organized in cohesive patterns of interactions are conserved to a substantially higher degree than those that do not participate in such motifs [184]. Using bioinformatics approaches of comparing gene sequences across species, a repertoire of protein interaction complexes and pathways has been shown to be conserved across all multiple species [185]. Cellular network motifs contain characteristic topological patterns that enable their functionality and biological output. The same signaling networks are reused for different purposes at an evolutionary scale and in different cell types of the same organism.

The EGFR-MAPK complex pathway has been extensively studied as a crucial signaling system with critical roles in stimulating cell proliferation and suppressing apoptosis. Using transcriptional profiling and targeted proteomics, the core EGFR network motifs have been shown to same with equivalent protein concentrations in cancer-specific cell lines as well as normal epithelial cells and fibroblasts [186]. Cell-type-specific responses have been attributed to the variable amount of EGFRs and feedback regulators. Aberrant signaling has been shown to occur in the absence of ligands under high EGFR concentrations in tumor cells [187]. The abundance of adaptor proteins, which facilitate large signaling complexes via protein-binding modules, is a rate-limiting step in regulating differential cancer cell responses. Amplification of Grb2 and Shc1 with high Grb2/EGFR abundance ratios have been reported in human breast cancer cell lines [188, 186]. Differences in the abundance of proteins change signaling outputs because these proteins compete for binding to the main receptors at critical network branch points. Enabling flexibility in a pattern of activation from a binary switch to a gradient response by changing the concentration of kinases has also been demonstrated in synthetic MAPK cascades in yeast [189]. Variation in the abundance of proteins that compete for binding to the same receptor can also contribute to context-specific signaling plasticity [190, 191].

We have demonstrated in this thesis, utilizing the minimal EGFR network, that the transient memory in cell polarization and, therefore, the capabilities of cells to navigate in a complex environment is an emergent feature of receptor networks organized at criticality. Such a mechanism cannot be explained using computations with stable states but rather requires a generic mechanism of $SubPB$ for real-time cellular information processing. The criticality is highlighted by the PTPRG/EGFR abundance ratio, which must be kept in a defined interval near the SN bifurcation. Unidirectional removal of EGFR upon EGF binding disrupts the PTPRG/EGFR abundance at the PM. However, for optimal functioning of the network after EGF gradient, the PTPRG/EGFR parameter organization is dynamically maintained via vesicular trafficking. The possibility of Akt-induced EGFR recycling also provides a feedback regulation as a fluctuation sensor that maintains the EGFR concentration on the PM such that it remains at the criticality

(Figure 1.10). The context-dependent regulation of the network can be dynamically manipulated by changes of the PTPRG/EGFR abundance on the PM. Changes in PTPRG/EGFR ratio may occur due to perturbation to the vesicular trafficking of EGFRs on the membrane upon cell-cell contact-induced EphA2-receptor activity [137]. As such, the cellular response switches from a mobile phase to a stationary phase via Erk-dependent signaling, promoting cell proliferation (Figure 1.10) [40]. Such context-dependent plasticity is crucial in physiological conditions such as efficient wound closure and shown to arise due to the network architecture.

4.5 Future outlook

In this thesis, we have been able to verify how dynamical state transitions give rise to the features of flexible working memory. We have demonstrated for a simple non-neuronal EGFR-PTP network the features of such working memory. It would be interesting to study whether receptor networks are self-organized at criticality or these features arose through evolution as a means for optimizing the computational capabilities of cells. The identification of a molecular working memory also opens avenues of research in the single-cell migration and tissue homeostasis to study whether cells can integrate and interpret even sub-threshold environmental signals, leading to release of cells from a tissue and long-distance single cell migration, as during cancer metastasis.

References

[1] Yulia Artemenko et al. “Chemical and mechanical stimuli act on common signal transduction and cytoskeletal networks”. In: *Proceedings of the National Academy of Sciences of the United States of America* 113 (47 Nov. 2016), E7500–E7509. ISSN: 10916490. DOI: 10.1073/PNAS.1608767113/-/DCSUPPLEMENTAL/PNAS.1608767113.SM09.AVI. URL: https://www.pnas.org/content/113/47/E7500%20https://www.pnas.org/content/113/47/E7500.abstract.

[2] Paul A. Janmey and Christopher A. McCulloch. “Cell Mechanics: Integrating Cell Responses to Mechanical Stimuli”. In: *http://dx.doi.org/10.1146/annurev.bioeng.9.060906.151927* 9 (July 2007), pp. 1–34. ISSN: 15239829. DOI: 10.1146/ANNUREV.BIOENG.9.060906.151927. URL: https://www.annualreviews.org/doi/abs/10.1146/annurev.bioeng.9.060906.151927.

[3] Hyunryul Ryu et al. “Frequency modulation of ERK activation dynamics rewires cell fate”. In: *Molecular Systems Biology* 11 (11 Nov. 2015), p. 838. ISSN: 1744-4292. DOI: 10.15252/MSB.20156458. URL: https://onlinelibrary.wiley.com/doi/full/10.15252/msb.20156458%20https://onlinelibrary.wiley.com/doi/abs/10.15252/msb.20156458%20https://www.embopress.org/doi/abs/10.15252/msb.20156458.

[4] Amy Y. Chang and Wallace F. Marshall. “Dynamics of living cells in a cytomorphological state space”. In: *Proceedings of the National Academy of Sciences of the United States of America* 116 (43 Oct. 2019), pp. 21556–21562. ISSN: 10916490. DOI: 10.1073/PNAS.1902849116/-/DCSUPPLEMENTAL. URL: https://www.pnas.org/content/116/43/21556%20https://www.pnas.org/content/116/43/21556.abstract.

[5] Robert Olby. “Schrödinger’s Problem: What Is Life?” In: *Journal of the History of Biology* 4.1 (1971), pp. 119–148. ISSN: 00225010, 15730387. URL: http://www.jstor.org/stable/4330552.

[6] Shuvasree SenGupta, Carole A. Parent, and James E. Bear. “The principles of directed cell migration”. In: *Nature Reviews Molecular Cell Biology 2021 22:8* 22 (8 May 2021), pp. 529–547. ISSN: 1471-0080. DOI: 10.1038/s41580-021-00366-6. URL: https://www.nature.com/articles/s41580-021-00366-6.

[7] Laura Lara Rodriguez and Ian C. Schneider. "Directed cell migration in multi-cue environments". In: *Integrative biology : quantitative biosciences from nano to macro* 5 (11 2013), pp. 1306–1323. ISSN: 1757-9708. DOI: 10.1039/C3IB40137E. URL: https://pubmed.ncbi.nlm.nih.gov/24089107/.

[8] Ellen F. Foxman, Eric J. Kunkel, and Eugene C. Butcher. "Integrating Conflicting Chemotactic Signals: The Role of Memory in Leukocyte Navigation". In: *Journal of Cell Biology* 147.3 (Nov. 1999), pp. 577–588. ISSN: 0021-9525. DOI: 10.1083/jcb.147.3.577. eprint: https://rupress.org/jcb/article-pdf/147/3/577/1287387/9906013.pdf. URL: https://doi.org/10.1083/jcb.147.3.577.

[9] Sofia De Oliveira, Emily E. Rosowski, and Anna Huttenlocher. "Neutrophil migration in infection and wound repair: going forward in reverse". In: *Nature reviews. Immunology* 16 (6 June 2016), p. 378. ISSN: 14741741. DOI: 10.1038/NRI.2016.49. URL: /pmc/articles/PMC5367630/%20/pmc/articles/PMC5367630/?report=abstract%20https://www.ncbi.nlm.nih.gov/pmc/articles/PMC5367630/.

[10] Krishna Rajarathnam et al. "How do chemokines navigate neutrophils to the target site: Dissecting the structural mechanisms and signaling pathways". In: *Cellular signalling* 54 (Feb. 2019), p. 69. ISSN: 18733913. DOI: 10.1016/J.CELLSIG.2018.11.004. URL: /pmc/articles/PMC6664297/%20/pmc/articles/PMC6664297/?report=abstract%20https://www.ncbi.nlm.nih.gov/pmc/articles/PMC6664297/.

[11] Mieke Metzemaekers, Mieke Gouwy, and Paul Proost. "Neutrophil chemoattractant receptors in health and disease: double-edged swords". In: *Cellular Molecular Immunology 2020 17:5* 17 (5 Apr. 2020), pp. 433–450. ISSN: 2042-0226. DOI: 10.1038/s41423-020-0412-0. URL: https://www.nature.com/articles/s41423-020-0412-0.

[12] Hannah M. Olson and Alex V. Nechiporuk. "Using zebrafish to study collective cell migration in development and disease". In: *Frontiers in Cell and Developmental Biology* 6 (AUG Aug. 2018), p. 83. ISSN: 2296634X. DOI: 10.3389/FCELL.2018.00083/BIBTEX.

[13] Andy Aman and Tatjana Piotrowski. "Cell migration during morphogenesis". In: *Developmental Biology* 341 (1 May 2010), pp. 20–33. ISSN: 0012-1606. DOI: 10.1016/J.YDBIO.2009.11.014.

[14] Cecilia Grimaldi and Erez Raz. "Germ cell migration-Evolutionary issues and current understanding". In: *Seminars in cell developmental biology* 100 (Apr. 2020), pp. 152–159. ISSN: 1096-3634. DOI: 10.1016/J.SEMCDB.2019.11.015. URL: https://pubmed.ncbi.nlm.nih.gov/31864795/.

[15] Anne Aalto, Adan Olguin-Olguin, and Erez Raz. "Zebrafish Primordial Germ Cell Migration". In: *Frontiers in Cell and Developmental Biology* 9 (June 2021), p. 1477. ISSN: 2296634X. DOI: 10.3389/FCELL.2021.684460/BIBTEX.

[16] Adan Olguin-Olguin et al. "Chemokine-biased robust self-organizing polarization of migrating cells in vivo". In: *Proceedings of the National Academy of Sciences* 118 (7 Feb. 2021). ISSN: 0027-8424. DOI: 10.1073/PNAS.2018480118. URL: https://www.pnas.org/content/118/7/e2018480118.

[17] Zhijian Luo, Yan Dai, and Huile Gao. "Development and application of hyaluronic acid in tumor targeting drug delivery". In: *Acta Pharmaceutica Sinica B* 9 (6 Nov. 2019), pp. 1099–1112. ISSN: 2211-3835. DOI: 10.1016/J.APSB.2019.06.004.

[18] Vinata B. Lokeshwar, Summan Mirza, and Andre Jordan. "Targeting Hyaluronic Acid Family for Cancer Chemoprevention and Therapy". In: *Advances in cancer research* 123 (2014), p. 35. ISSN: 0065230X. DOI: 10.1016/B978-0-12-800092-2.00002-2. URL: /pmc/articles/PMC4791948/%20/pmc/articles/PMC4791948/?report=abstract%20https://www.ncbi.nlm.nih.gov/pmc/articles/PMC4791948/.

[19] Ilaria Caon et al. "Revisiting the hallmarks of cancer: The role of hyaluronan". In: *Seminars in Cancer Biology* 62 (2020). Translating Extracellular Matrix, pp. 9–19. ISSN: 1044-579X. DOI: https://doi.org/10.1016/j.semcancer.2019.07.007. URL: https://www.sciencedirect.com/science/article/pii/S1044579X19300422.

[20] Man Wu et al. "A novel role of low molecular weight hyaluronan in breast cancer metastasis". In: *FASEB journal : official publication of the Federation of American Societies for Experimental Biology* 29 (4 Apr. 2015), pp. 1290–1298. ISSN: 1530-6860. DOI: 10.1096/FJ.14-259978. URL: https://pubmed.ncbi.nlm.nih.gov/25550464/.

[21] Chuan-Hsiang Huang and Pablo A. Iglesias. "Cell memory and adaptation in chemotaxis". In: *Proceedings of the National Academy of Sciences* 111 (43 Oct. 2014), pp. 15287–15288. ISSN: 0027-8424. DOI: 10.1073/PNAS.1418077111. URL: https://www.pnas.org/content/111/43/15287.

[22] T. Schreier, E. Degen, and W. Baschong. "Fibroblast migration and proliferation during in vitro wound healing. A quantitative comparison between various growth factors and a low molecular weight blood dialysate used in the clinic to normalize impaired wound healing". In: *Research in experimental medicine. Zeitschrift fur die gesamte experimentelle Medizin einschliesslich experimenteller Chirurgie* 193 (4 Dec. 1993), pp. 195–205. ISSN: 0300-9130. DOI: 10.1007/BF02576227. URL: https://pubmed.ncbi.nlm.nih.gov/8235072/.

[23] Erik S. Welf et al. “Migrating fibroblasts reorient directionality: By a metastable, PI3K-dependent mechanism”. In: *Journal of Cell Biology* 197 (1 Apr. 2012), pp. 105–114. ISSN: 00219525. DOI: 10.1083/JCB.201108152/VIDEO-8. URL: www.jcb.org/cgi/doi/10.1083/jcb.201108152.

[24] Samer Hanna and Mirvat El-Sibai. “Signaling networks of Rho GTPases in cell motility”. In: *Cellular signalling* 25 (10 Oct. 2013), pp. 1955–1961. ISSN: 1873-3913. DOI: 10.1016/J.CELLSIG.2013.04.009. URL: https://pubmed.ncbi.nlm.nih.gov/23669310/.

[25] Monica Skoge et al. “Cellular memory in eukaryotic chemotaxis”. In: *Proceedings of the National Academy of Sciences* 111.40 (2014), pp. 14448–14453. ISSN: 0027-8424. DOI: 10.1073/pnas.1412197111. eprint: https://www.pnas.org/content/111/40/14448.full.pdf. URL: https://www.pnas.org/content/111/40/14448.

[26] Malte Schmick and Philippe I.H. Bastiaens. “The Interdependence of Membrane Shape and Cellular Signal Processing”. In: *Cell* 156 (6 Mar. 2014), pp. 1132–1138. ISSN: 0092-8674. DOI: 10.1016/J.CELL.2014.02.007. URL: http://www.cell.com/article/S0092867414001986/fulltext%20http://www.cell.com/article/S0092867414001986/abstract%20https://www.cell.com/cell/abstract/S0092-8674(14)00198-6.

[27] Aneta Koseska and Philippe IH Bastiaens. “Cell signaling as a cognitive process”. In: *The EMBO journal* 36 (5 Mar. 2017), pp. 568–582. ISSN: 1460-2075. DOI: 10.15252/EMBJ.201695383. URL: https://pubmed.ncbi.nlm.nih.gov/28137748/.

[28] Mark Larance and Angus I Lamond. “Proteins form the structural fabric of cells and under-pin all metabolic processes and regulatory mechanisms. Protein properties, including abundance levels, protein-protein interactions, post-translational modifications”. In: (2015). DOI: 10.1038/nrm3970. URL: www.nature.com/reviews/molcellbio.

[29] Peter Devreotes and Alan Rick Horwitz. “Signaling Networks that Regulate Cell Migration”. In: *Cold Spring Harbor Perspectives in Biology* 7 (8 Aug. 2015), a005959. ISSN: 19430264. DOI: 10.1101/CSHPERSPECT.A005959. URL: http://cshperspectives.cshlp.org/content/7/8/a005959.full%20http://cshperspectives.cshlp.org/content/7/8/a005959%20http://cshperspectives.cshlp.org/content/7/8/a005959.abstract.

[30] Wouter Jan Rappel and Leah Edelstein-Keshet. “Mechanisms of Cell Polarization”. In: *Current opinion in systems biology* 3 (June 2017), p. 43. ISSN: 24523100. DOI: 10.1016/J.COISB.2017.03.005. URL: /pmc/articles/PMC5640326/%20/pmc/

articles/PMC5640326/?report=abstract%20https://www.ncbi.nlm.nih.gov/pmc/articles/PMC5640326/.

[31] Francisco Sánchez-Madrid and Miguel Angel Del Pozo. "Leukocyte polarization in cell migration and immune interactions". In: *The EMBO Journal* 18 (3 Feb. 1999), pp. 501–511. ISSN: 1460-2075. DOI: 10.1093/EMBOJ/18.3.501. URL: https://onlinelibrary.wiley.com/doi/full/10.1093/emboj/18.3.501%20https://onlinelibrary.wiley.com/doi/abs/10.1093/emboj/18.3.501%20https://www.embopress.org/doi/abs/10.1093/emboj/18.3.501.

[32] Shailaja Seetharaman and Sandrine Etienne-Manneville. "Cytoskeletal Crosstalk in Cell Migration". In: *Trends in Cell Biology* 30 (9 Sept. 2020), pp. 720–735. ISSN: 0962-8924. DOI: 10.1016/J.TCB.2020.06.004. URL: http://www.cell.com/article/S0962892420301227/fulltext%20http://www.cell.com/article/S0962892420301227/abstract%20https://www.cell.com/trends/cell-biology/abstract/S0962-8924(20)30122-7.

[33] Florian Huber et al. "Cytoskeletal crosstalk: when three different personalities team up". In: *Current opinion in cell biology* 32 (Feb. 2015), pp. 39–47. ISSN: 1879-0410. DOI: 10.1016/J.CEB.2014.10.005. URL: https://pubmed.ncbi.nlm.nih.gov/25460780/.

[34] Thomas D. (Thomas Dean) Pollard and Robert D. Goldman. "The cytoskeleton". In: (), p. 391.

[35] Gary J. Brouhard and Luke M. Rice. "Microtubule dynamics: an interplay of biochemistry and mechanics". In: *Nature Reviews Molecular Cell Biology 2018 19:7* 19 (7 Apr. 2018), pp. 451–463. ISSN: 1471-0080. DOI: 10.1038/s41580-018-0009-y. URL: https://www.nature.com/articles/s41580-018-0009-y.

[36] Satish Bodakuntla et al. "Microtubule-Associated Proteins: Structuring the Cytoskeleton". In: *Trends in Cell Biology* 29 (10 Oct. 2019), pp. 804–819. ISSN: 0962-8924. DOI: 10.1016/J.TCB.2019.07.004. URL: http://www.cell.com/article/S0962892419301205/fulltext%20http://www.cell.com/article/S0962892419301205/abstract%20https://www.cell.com/trends/cell-biology/abstract/S0962-8924(19)30120-5.

[37] Henrik Daub et al. "Rac/Cdc42 and p65PAK regulate the microtubule-destabilizing protein stathmin through phosphorylation at serine 16". In: *The Journal of biological chemistry* 276 (3 Jan. 2001), pp. 1677–1680. ISSN: 0021-9258. DOI: 10.1074/JBC.C000635200. URL: https://pubmed.ncbi.nlm.nih.gov/11058583/.

[38] Ed Manser. "The Rho GTPases". In: *RHO Family GTPases* (Oct. 2005), pp. 1–18. DOI: 10.1007/1-4020-3462-8_1.

[39] Konstantin Gavriljuk et al. “A self-organized synthetic morphogenic liposome responds with shape changes to local light cues”. In: *Nature communications* 12 (1 Dec. 2021). ISSN: 2041-1723. DOI: 10.1038/S41467-021-21679-2. URL: https://pubmed.ncbi.nlm.nih.gov/33750780/.

[40] Aneta Koseska and Philippe I.H. Bastiaens. “Processing Temporal Growth Factor Patterns by an Epidermal Growth Factor Receptor Network Dynamically Established in Space”. In: *https://doi.org/10.1146/annurev-cellbio-013020-103810* 36 (Oct. 2020), pp. 359–383. ISSN: 15308995. DOI: 10.1146/ANNUREV-CELLBIO-013020-103810. URL: https://www.annualreviews.org/doi/abs/10.1146/annurev-cellbio-013020-103810.

[41] Maria Zeitz and Jan Kierfeld. “Feedback mechanism for microtubule length regulation by stathmin gradients”. In: *Biophysical Journal* 107 (12 Dec. 2014), pp. 2860–2871. ISSN: 15420086. DOI: 10.1016/J.BPJ.2014.10.056. URL: http://arxiv.org/abs/1412.2906%20http://dx.doi.org/10.1016/j.bpj.2014.10.056.

[42] P. R. Ebrahimzadeh, C. Hogfors, and M. Braide. “Neutrophil chemotaxis in moving gradients of fMLP”. In: *Journal of leukocyte biology* 67 (5 2000), pp. 651–661. ISSN: 0741-5400. DOI: 10.1002/JLB.67.5.651. URL: https://pubmed.ncbi.nlm.nih.gov/10811005/.

[43] Robert J. Eddy, Lynda M. Pierini, and Frederick R. Maxfield. “Microtubule asymmetry during neutrophil polarization and migration”. In: *Molecular Biology of the Cell* 13 (12 Dec. 2002), pp. 4470–4483. ISSN: 10591524. DOI: 10.1091/MBC.E02-04-0241/ASSET/IMAGES/LARGE/MK1222053008.JPEG. URL: https://www.molbiolcell.org/doi/abs/10.1091/mbc.e02-04-0241.

[44] Richard C. Chou et al. “Lipid-Cytokine-Chemokine Cascade Drives Neutrophil Recruitment in a Murine Model of Inflammatory Arthritis”. In: *Immunity* 33 (2 Aug. 2010), p. 266. ISSN: 10747613. DOI: 10.1016/J.IMMUNI.2010.07.018. URL: /pmc/articles/PMC3155777/%20/pmc/articles/PMC3155777/?report=abstract%20https://www.ncbi.nlm.nih.gov/pmc/articles/PMC3155777/.

[45] Philippe V. Afonso et al. “LTB4 Is a Signal-Relay Molecule during Neutrophil Chemotaxis”. In: *Developmental Cell* 22 (5 May 2012), pp. 1079–1091. ISSN: 1534-5807. DOI: 10.1016/J.DEVCEL.2012.02.003.

[46] E. K. Kim et al. “Selective activation of Akt1 by mammalian target of rapamycin complex 2 regulates cancer cell migration, invasion, and metastasis”. In: *Oncogene 2011 30:26* 30 (26 Feb. 2011), pp. 2954–2963. ISSN: 1476-5594. DOI: 10.1038/onc.2011.22. URL: https://www.nature.com/articles/onc201122.

[47] Natalie Ann Mack and Marios Georgiou. "The interdependence of the Rho GTPases and apicobasal cell polarity". In: *Small GTPases* 5 (2 Dec. 2014). ISSN: 2154-1256. DOI: 10.4161/21541248.2014.973768. URL: https://pubmed.ncbi.nlm.nih.gov/25469537/.

[48] Yasushi Izumi et al. "An Atypical PKC Directly Associates and Colocalizes at the Epithelial Tight Junction with ASIP, a Mammalian Homologue of Caenorhabditis elegans Polarity Protein PAR-3". In: *The Journal of Cell Biology* 143 (1 Oct. 1998), p. 95. ISSN: 00219525. DOI: 10.1083/JCB.143.1.95. URL: /pmc/articles/PMC2132825/%20/pmc/articles/PMC2132825/?report=abstract%20https://www.ncbi.nlm.nih.gov/pmc/articles/PMC2132825/.

[49] S. Etienne-Manneville. "Polarity proteins in migration and invasion". In: *Oncogene 2008 27:55* 27 (55 Nov. 2008), pp. 6970–6980. ISSN: 1476-5594. DOI: 10.1038/onc.2008.347. URL: https://www.nature.com/articles/onc2008347.

[50] Naël Osmani et al. "Scrib controls Cdc42 localization and activity to promote cell polarization during astrocyte migration". In: *Current biology : CB* 16 (24 Dec. 2006), pp. 2395–2405. ISSN: 0960-9822. DOI: 10.1016/J.CUB.2006.10.026. URL: https://pubmed.ncbi.nlm.nih.gov/17081755/.

[51] I. J. Uings and S. N. Farrow. "Cell receptors and cell signalling". In: *Molecular pathology : MP* 53 (6 2000), pp. 295–299. ISSN: 1366-8714. DOI: 10.1136/MP.53.6.295. URL: https://pubmed.ncbi.nlm.nih.gov/11193047/.

[52] Joseph Schlessinger. "Cell signaling by receptor tyrosine kinases". In: *Cell* 103 (2 Oct. 2000), pp. 211–225. ISSN: 0092-8674. DOI: 10.1016/S0092-8674(00)00114-8. URL: https://pubmed.ncbi.nlm.nih.gov/11057895/%20https://pubmed.ncbi.nlm.nih.gov/11057895/?dopt=Abstract.

[53] Mark A. Lemmon and Joseph Schlessinger. "Cell signaling by receptor tyrosine kinases". In: *Cell* 141 (7 2010), pp. 1117–1134. ISSN: 1097-4172. DOI: 10.1016/J.CELL.2010.06.011. URL: https://pubmed.ncbi.nlm.nih.gov/20602996/.

[54] Tony Hunter. "Signaling–2000 and beyond". In: *Cell* 100 (1 Jan. 2000), pp. 113–127. ISSN: 0092-8674. DOI: 10.1016/S0092-8674(00)81688-8. URL: https://pubmed.ncbi.nlm.nih.gov/10647936/%20https://pubmed.ncbi.nlm.nih.gov/10647936/?dopt=Abstract.

[55] Axel Ullrich and Joseph Schlessinger. "Signal transduction by receptors with tyrosine kinase activity". In: *Cell* 61 (2 Apr. 1990), pp. 203–212. ISSN: 0092-8674. DOI: 10.1016/0092-8674(90)90801-K. URL: https://pubmed.ncbi.nlm.nih.gov/2158859/.

[56] Theodorus W.J. Gadella and Thomas M. Jovin. "Oligomerization of epidermal growth factor receptors on A431 cells studied by time-resolved fluorescence imaging microscopy. A stereochemical model for tyrosine kinase receptor activation". In: *The Journal of cell biology* 129 (6 June 1995), pp. 1543–1558. ISSN: 0021-9525. DOI: 10.1083/JCB.129.6.1543. URL: https://pubmed.ncbi.nlm.nih.gov/7790353/.

[57] Katherine A. Fantauzzo and Philippe Soriano. "Receptor Tyrosine Kinase Signaling: Regulating Neural Crest Development One Phosphate at a Time". In: *Current Topics in Developmental Biology* 111 (Jan. 2015), pp. 135–182. ISSN: 0070-2153. DOI: 10.1016/BS.CTDB.2014.11.005.

[58] Bhuminder Singh, Graham Carpenter, and Robert J. Coffey. "EGF receptor ligands: recent advances". In: *F1000Research* 5 (2016). ISSN: 1759796X. DOI: 10.12688/F1000RESEARCH.9025.1. URL: /pmc/articles/PMC5017282/%20/pmc/articles/PMC5017282/?report=abstract%20https://www.ncbi.nlm.nih.gov/pmc/articles/PMC5017282/.

[59] Mark A. Lemmon, Joseph Schlessinger, and Kathryn M. Ferguson. "The EGFR family: not so prototypical receptor tyrosine kinases". In: *Cold Spring Harbor perspectives in biology* 6 (4 2014). ISSN: 1943-0264. DOI: 10.1101/CSHPERSPECT.A020768. URL: https://pubmed.ncbi.nlm.nih.gov/24691965/.

[60] Daniel J. Leahy. "Structure and function of the epidermal growth factor (EGF/ErbB) family of receptors". In: *Advances in protein chemistry* 68 (2004), pp. 1–27. ISSN: 0065-3233. DOI: 10.1016/S0065-3233(04)68001-6. URL: https://pubmed.ncbi.nlm.nih.gov/15500857/.

[61] Kathryn M. Ferguson. "Structure-based view of epidermal growth factor receptor regulation". In: *Annual review of biophysics* 37 (2008), pp. 353–373. ISSN: 1936-122X. DOI: 10.1146/ANNUREV.BIOPHYS.37.032807.125829. URL: https://pubmed.ncbi.nlm.nih.gov/18573086/.

[62] Tove Ringerike et al. "High-affinity Binding of Epidermal Growth Factor (EGF) to EGF Receptor Is Disrupted by Overexpression of Mutant Dynamin (K44A) *". In: *Journal of Biological Chemistry* 273 (27 July 1998), pp. 16639–16642. ISSN: 0021-9258. DOI: 10.1074/JBC.273.27.16639. URL: http://www.jbc.org/article/S0021925818805877/fulltext%20http://www.jbc.org/article/S0021925818805877/abstract%20https://www.jbc.org/article/S0021-9258(18)80587-7/abstract.

[63] Wei Ting Kuo et al. "Quantitative Analysis of Ligand-EGFR Interactions: A Platform for Screening Targeting Molecules". In: *PLoS ONE* 10 (2 Feb. 2015). ISSN: 19326203. DOI: 10.1371/JOURNAL.PONE.0116610. URL: /pmc/articles/

PMC4344348/%20/pmc/articles/PMC4344348/?report=abstract%20https://www.ncbi.nlm.nih.gov/pmc/articles/PMC4344348/.

[64] Melany J. Wagner et al. "Molecular mechanisms of SH2- and PTB-domain-containing proteins in receptor tyrosine kinase signaling". In: *Cold Spring Harbor perspectives in biology* 5 (12 Dec. 2013). ISSN: 1943-0264. DOI: 10.1101/CSHPERSPECT.A008987. URL: https://pubmed.ncbi.nlm.nih.gov/24296166/.

[65] Sara Barberán and Francesc Cebrià. "The role of the EGFR signaling pathway in stem cell differentiation during planarian regeneration and homeostasis". In: *Seminars in cell developmental biology* 87 (Mar. 2019), pp. 45–57. ISSN: 1096-3634. DOI: 10.1016/J.SEMCDB.2018.05.011. URL: https://pubmed.ncbi.nlm.nih.gov/29775660/.

[66] Susanna Fraguas, Sara Barberán, and Francesc Cebrià. "EGFR signaling regulates cell proliferation, differentiation and morphogenesis during planarian regeneration and homeostasis." In: *Developmental biology* 354 (1 June 2011), pp. 87–101. ISSN: 1095-564X. DOI: 10.1016/j.ydbio.2011.03.023. URL: http://www.ncbi.nlm.nih.gov/pubmed/21458439.

[67] Ji Zhu et al. "Amphiregulin-EGFR signaling mediates the migration of bone marrow mesenchymal progenitors toward PTH-stimulated osteoblasts and osteocytes". In: *PloS one* 7 (12 Dec. 2012). ISSN: 1932-6203. DOI: 10.1371/JOURNAL.PONE.0050099. URL: https://pubmed.ncbi.nlm.nih.gov/23300521/.

[68] Shuhao Lin et al. "Redundant roles of EGFR ligands in the ERK activation waves during collective cell migration". In: *Life Science Alliance* 5 (1 Jan. 2022). ISSN: 25751077. DOI: 10.26508/LSA.202101206/VIDEO-4. URL: https://www.life-science-alliance.org/content/5/1/e202101206%20https://www.life-science-alliance.org/content/5/1/e202101206.abstract.

[69] Thorsten Maretzky et al. "Migration of growth factor-stimulated epithelial and endothelial cells depends on EGFR transactivation by ADAM17". In: *Nature Communications 2011 2:1* 2 (1 Mar. 2011), pp. 1–11. ISSN: 2041-1723. DOI: 10.1038/ncomms1232. URL: https://www.nature.com/articles/ncomms1232.

[70] Yuichi Ohnishi et al. "Regulation of cell migration via the EGFR signaling pathway in oral squamous cell carcinoma cells". In: *Oncology Letters* 13 (2 Feb. 2017), pp. 930–936. ISSN: 17921082. DOI: 10.3892/OL.2016.5500/DOWNLOAD. URL: /pmc/articles/PMC5351309/%20/pmc/articles/PMC5351309/?report=abstract%20https://www.ncbi.nlm.nih.gov/pmc/articles/PMC5351309/.

[71] Susumu Kobayashi et al. "EGFR Mutation and Resistance of Non–Small-Cell Lung Cancer to Gefitinib". In: *http://dx.doi.org/10.1056/NEJMoa044238* 352 (8 Oct. 2009), pp. 786–792. ISSN: 0028-4793. DOI: 10.1056/NEJMOA044238. URL: https://www.nejm.org/doi/full/10.1056/$%5C%$E2NEJMoa044238.

[72] Xiaoping Wang et al. "EGFR signaling promotes inflammation and cancer stem-like activity in inflammatory breast cancer". In: *Oncotarget* 8 (40 Sept. 2017), pp. 67904–67917. ISSN: 1949-2553. DOI: 10.18632/ONCOTARGET.18958. URL: https://pubmed.ncbi.nlm.nih.gov/28978083/.

[73] Kathryn M. Ferguson et al. "EGF activates its receptor by removing interactions that autoinhibit ectodomain dimerization". In: *Molecular cell* 11 (2 Feb. 2003), pp. 507–517. ISSN: 1097-2765. DOI: 10.1016/S1097-2765(03)00047-9. URL: https://pubmed.ncbi.nlm.nih.gov/12620237/.

[74] Morgan Huse and John Kuriyan. "The conformational plasticity of protein kinases". In: *Cell* 109 (3 May 2002), pp. 275–282. ISSN: 0092-8674. DOI: 10.1016/S0092-8674(02)00741-9. URL: https://pubmed.ncbi.nlm.nih.gov/12015977/.

[75] Huaibin Chen et al. "A molecular brake in the kinase hinge region regulates the activity of receptor tyrosine kinases". In: *Molecular cell* 27 (5 Sept. 2007), pp. 717–730. ISSN: 1097-2765. DOI: 10.1016/J.MOLCEL.2007.06.028. URL: https://pubmed.ncbi.nlm.nih.gov/17803937/.

[76] Stevan R. Hubbard. "Juxtamembrane autoinhibition in receptor tyrosine kinases". In: *Nature reviews. Molecular cell biology* 5 (6 June 2004), pp. 464–470. ISSN: 1471-0072. DOI: 10.1038/NRM1399. URL: https://pubmed.ncbi.nlm.nih.gov/15173825/.

[77] Erika Kovacs et al. "Analysis of the Role of the C-Terminal Tail in the Regulation of the Epidermal Growth Factor Receptor". In: *Molecular and cellular biology* 35 (17 Sept. 2015), pp. 3083–3102. ISSN: 1098-5549. DOI: 10.1128/MCB.00248-15. URL: https://pubmed.ncbi.nlm.nih.gov/26124280/.

[78] Jessica P. Dawson et al. "Epidermal growth factor receptor dimerization and activation require ligand-induced conformational changes in the dimer interface". In: *Molecular and cellular biology* 25 (17 Sept. 2005), pp. 7734–7742. ISSN: 0270-7306. DOI: 10.1128/MCB.25.17.7734-7742.2005. URL: https://pubmed.ncbi.nlm.nih.gov/16107719/.

[79] Xuewu Zhang et al. "An allosteric mechanism for activation of the kinase domain of epidermal growth factor receptor". In: *Cell* 125 (6 2006), pp. 1137–1149. ISSN: 0092-8674. DOI: 10.1016/J.CELL.2006.05.013. URL: https://pubmed.ncbi.nlm.nih.gov/16777603/.

[80] Yibing Shan et al. “Transitions to catalytically inactive conformations in EGFR kinase”. In: *Proceedings of the National Academy of Sciences of the United States of America* 110 (18 Apr. 2013), pp. 7270–7275. ISSN: 1091-6490. DOI: 10.1073/PNAS.1220843110. URL: https://pubmed.ncbi.nlm.nih.gov/23576739/.

[81] Yibing Shan et al. “Oncogenic mutations counteract intrinsic disorder in the EGFR kinase and promote receptor dimerization”. In: *Cell* 149 (4 May 2012), pp. 860–870. ISSN: 1097-4172. DOI: 10.1016/J.CELL.2012.02.063. URL: https://pubmed.ncbi.nlm.nih.gov/22579287/.

[82] Ping Wee and Zhixiang Wang. “Epidermal Growth Factor Receptor Cell Proliferation Signaling Pathways”. In: *Cancers* 9 (5 May 2017). ISSN: 20726694. DOI: 10.3390/CANCERS9050052. URL: /pmc/articles/PMC5447962/%20/pmc/articles/PMC5447962/?report=abstract%20https://www.ncbi.nlm.nih.gov/pmc/articles/PMC5447962/.

[83] Gil Levkowitz et al. “c-Cbl/Sli-1 regulates endocytic sorting and ubiquitination of the epidermal growth factor receptor”. In: *Genes development* 12 (23 Dec. 1998), pp. 3663–3674. ISSN: 0890-9369. DOI: 10.1101/GAD.12.23.3663. URL: https://pubmed.ncbi.nlm.nih.gov/9851973/.

[84] M. Baumdick et al. “EGF-dependent re-routing of vesicular recycling switches spontaneous phosphorylation suppression to EGFR signaling”. In: *eLife* 4 (2015), e12223. ISSN: 2050-084X (Electronic)2050-084X (Linking). DOI: 10.7554/eLife.12223. URL: https://www.ncbi.nlm.nih.gov/pubmed/26609808.

[85] Christopher Y. Thomas et al. “Spontaneous activation and signaling by overexpressed epidermal growth factor receptors in glioblastoma cells”. In: *International journal of cancer* 104 (1 Mar. 2003), pp. 19–27. ISSN: 0020-7136. DOI: 10.1002/IJC.10880. URL: https://pubmed.ncbi.nlm.nih.gov/12532415/.

[86] AR. Reynolds et al. “EGFR activation coupled to inhibition of tyrosine phosphatases causes lateral signal propagation”. In: *Nat Cell Biol* 5 (2003), pp. 447–453. DOI: https://doi:10.1038/ncb981.

[87] Martin Baumdick et al. “A conformational sensor based on genetic code expansion reveals an autocatalytic component in EGFR activation”. In: *Nature Communications 2018 9:1* 9 (1 Sept. 2018), pp. 1–13. ISSN: 2041-1723. DOI: 10.1038/s41467-018-06299-7. URL: https://www.nature.com/articles/s41467-018-06299-7.

[88] P. J. Verveer et al. “Quantitative Imaging of Lateral ErbB1 Receptor Signal Propagation in the Plasma Membrane”. In: *Science* 290 (5496 Nov. 2000), pp. 1567–1570. ISSN: 00368075. DOI: 10.1126/SCIENCE.290.5496.1567. URL: https://www.science.org/doi/abs/10.1126/science.290.5496.1567.

[89] Nir Osherov and Alexander Levitzki. "Epidermal-growth-factor-dependent activation of the src-family kinases". In: *European journal of biochemistry* 225 (3 1994), pp. 1047–1053. ISSN: 0014-2956. DOI: 10.1111/J.1432-1033.1994.1047B.X. URL: https://pubmed.ncbi.nlm.nih.gov/7525285/.

[90] Thomas N. Sato et al. "Distinct roles of the receptor tyrosine kinases Tie-1 and Tie-2 in blood vessel formation". In: *Nature* 376 (6535 July 1995), pp. 70–74. ISSN: 0028-0836. DOI: 10.1038/376070A0. URL: https://pubmed.ncbi.nlm.nih.gov/7596437/.

[91] Youngjoo Kim et al. "Temporal Resolution of Autophosphorylation for Normal and Oncogenic Forms of EGFR and Differential Effects of Gefitinib†". In: *Biochemistry* 51 (25 June 2012), p. 5212. ISSN: 00062960. DOI: 10.1021/BI300476V. URL: /pmc/articles/PMC3390174/%20/pmc/articles/PMC3390174/?report=abstract%20https://www.ncbi.nlm.nih.gov/pmc/articles/PMC3390174/.

[92] A. Stanoev et al. "Interdependence between EGFR and Phosphatases Spatially Established by Vesicular Dynamics Generates a Growth Factor Sensing and Responding Network". In: *Cell Systems* 7.3 (2018), 295–309.e11. ISSN: 2405-4712. DOI: 10.1016/j.cels.2018.06.006. URL: https://www.sciencedirect.com/science/article/pii/S2405471218302461.

[93] Ping Liu et al. "A single ligand is sufficient to activate EGFR dimers". In: *Proceedings of the National Academy of Sciences of the United States of America* 109 (27 July 2012), pp. 10861–10866. ISSN: 00278424. DOI: 10.1073/PNAS.1201114109/-/DCSUPPLEMENTAL/APPENDIX.PDF. URL: https://pubmed.ncbi.nlm.nih.gov/22699492/.

[94] Jennifer L. Macdonald and Linda J. Pike. "Heterogeneity in EGF-binding affinities arises from negative cooperativity in an aggregating system". In: *Proceedings of the National Academy of Sciences* 105 (1 Jan. 2008), pp. 112–117. ISSN: 0027-8424. DOI: 10.1073/PNAS.0707080105. URL: https://www.pnas.org/content/105/1/112%20https://www.pnas.org/content/105/1/112.abstract.

[95] Linda J. Pike. "Negative Cooperativity in the EGF Receptor". In: *Biochemical Society transactions* 40 (1 Feb. 2012), p. 15. ISSN: 03005127. DOI: 10.1042/BST20110610. URL: /pmc/articles/PMC3711752/%20/pmc/articles/PMC3711752/?report=abstract%20https://www.ncbi.nlm.nih.gov/pmc/articles/PMC3711752/.

[96] Diego Alvarado, Daryl E. Klein, and Mark A. Lemmon. "Structural basis for negative cooperativity in growth factor binding to an EGF receptor". In: *Cell* 142 (4 2010), pp. 568–579. ISSN: 1097-4172. DOI: 10.1016/J.CELL.2010.07.015. URL: https://pubmed.ncbi.nlm.nih.gov/20723758/.

[97] Emanuel Salazar-Cavazos et al. “Multisite EGFR phosphorylation is regulated by adaptor protein abundances and dimer lifetimes”. In: *Molecular Biology of the Cell* 31 (7 Mar. 2020), p. 695. ISSN: 19394586. DOI: 10.1091/MBC.E19-09-0548. URL: /pmc/articles/PMC7202077/%20/pmc/articles/PMC7202077/?report=abstract%20https://www.ncbi.nlm.nih.gov/pmc/articles/PMC7202077/.

[98] Daniel M. Freed et al. “EGFR Ligands Differentially Stabilize Receptor Dimers to Specify Signaling Kinetics”. In: *Cell* 171 (3 Oct. 2017), 683–695.e18. ISSN: 1097-4172. DOI: 10.1016/J.CELL.2017.09.017. URL: https://pubmed.ncbi.nlm.nih.gov/28988771/.

[99] Akihiro Kusumi and Yasushi Sako. “Cell surface organization by the membrane skeleton”. In: *Current opinion in cell biology* 8 (4 1996), pp. 566–574. ISSN: 0955-0674. DOI: 10.1016/S0955-0674(96)80036-6. URL: https://pubmed.ncbi.nlm.nih.gov/8791449/.

[100] Akihiro Kusumi et al. “Paradigm Shift of the Plasma Membrane Concept from the Two-Dimensional Continuum Fluid to the Partitioned Fluid: High-Speed Single-Molecule Tracking of Membrane Molecules”. In: *http://dx.doi.org/10.1146/annurev.biophys.34.040204.144637* 34 (May 2005), pp. 351–378. ISSN: 10568700. DOI: 10.1146/ANNUREV.BIOPHYS.34.040204.144637. URL: https://www.annualreviews.org/doi/abs/10.1146/annurev.biophys.34.040204.144637.

[101] Christian Tischer and Philippe I.H. Bastiaens. “Lateral phosphorylation propagation: an aspect of feedback signalling?” In: *Nature Reviews Molecular Cell Biology 2003 4:12* 4 (12 Dec. 2003), pp. 971–975. ISSN: 1471-0080. DOI: 10.1038/nrm1258. URL: https://www.nature.com/articles/nrm1258.

[102] J. Ibach et al. “Single Particle Tracking Reveals that EGFR Signaling Activity Is Amplified in Clathrin-Coated Pits”. In: *PLoS One* 10.11 (2015), e0143162. ISSN: 2050-084X (Electronic)2050-084X (Linking). DOI: 10.1371/journal.pone.0143162. URL: https://www.ncbi.nlm.nih.gov/pubmed/26609808.

[103] Andrew H.A. Clayton et al. “Ligand-induced dimer-tetramer transition during the activation of the cell surface epidermal growth factor receptor-A multidimensional microscopy analysis”. In: *The Journal of biological chemistry* 280 (34 Aug. 2005), pp. 30392–30399. ISSN: 0021-9258. DOI: 10.1074/JBC.M504770200. URL: https://pubmed.ncbi.nlm.nih.gov/15994331/.

[104] Hernán E. Grecco, Malte Schmick, and Philippe I.H. Bastiaens. “Signaling from the Living Plasma Membrane”. In: *Cell* 144 (6 Mar. 2011), pp. 897–909. ISSN: 0092-8674. DOI: 10.1016/J.CELL.2011.01.029.

[105] Nicholas K. Tonks. "Protein tyrosine phosphatases: from genes, to function, to disease". In: *Nature reviews. Molecular cell biology* 7 (11 Nov. 2006), pp. 833–846. ISSN: 1471-0072. DOI: 10.1038/NRM2039. URL: https://pubmed.ncbi.nlm.nih.gov/17057753/.

[106] Karin Kolmodin and Johan Åqvist. "The catalytic mechanism of protein tyrosine phosphatases revisited". In: *FEBS Letters* 498 (2-3 June 2001), pp. 208–213. ISSN: 0014-5793. DOI: 10.1016/S0014-5793(01)02479-6.

[107] Wiljan J.A.J. Hendriks and Rafael Pulido. "Protein tyrosine phosphatase variants in human hereditary disorders and disease susceptibilities". In: *Biochimica et Biophysica Acta (BBA) - Molecular Basis of Disease* 1832 (10 Oct. 2013), pp. 1673–1696. ISSN: 0925-4439. DOI: 10.1016/J.BBADIS.2013.05.022.

[108] Tasneem Motiwala and Samson T. Jacob. "Role of Protein Tyrosine Phosphatases in Cancer". In: *Progress in nucleic acid research and molecular biology* 81 (2006), p. 297. ISSN: 00796603. DOI: 10.1016/S0079-6603(06)81008-1. URL: /pmc/articles/PMC3077959/%20/pmc/articles/PMC3077959/?report=abstract%20https://www.ncbi.nlm.nih.gov/pmc/articles/PMC3077959/.

[109] Fatima Ardito et al. "The crucial role of protein phosphorylation in cell signalingand its use as targeted therapy (Review)". In: *International Journal of Molecular Medicine* 40 (2 Aug. 2017), pp. 271–280. ISSN: 1791244X. DOI: 10.3892/IJMM.2017.3036/HTML. URL: http://www.spandidos-publications.com/10.3892/ijmm.2017.3036/abstract%20https://www.spandidos-publications.com/10.3892/ijmm.2017.3036.

[110] John V. Frangioni et al. "The nontransmembrane tyrosine phosphatase PTP-1B localizes to the endoplasmic reticulum via its 35 amino acid C-terminal sequence". In: *Cell* 68 (3 Feb. 1992), pp. 545–560. ISSN: 0092-8674. DOI: 10.1016/0092-8674(92)90190-N. URL: https://pubmed.ncbi.nlm.nih.gov/1739967/.

[111] D. E. Cool et al. "cDNA isolated from a human T-cell library encodes a member of the protein-tyrosine-phosphatase family". In: *Proceedings of the National Academy of Sciences of the United States of America* 86 (14 1989), pp. 5257–5261. ISSN: 0027-8424. DOI: 10.1073/PNAS.86.14.5257. URL: https://pubmed.ncbi.nlm.nih.gov/2546150/.

[112] Martin Offterdinger and Philippe I. Bastiaens. "Prolonged EGFR signaling by ERBB2-mediated sequestration at the plasma membrane". In: *Traffic (Copenhagen, Denmark)* 9 (1 Jan. 2008), pp. 147–155. ISSN: 1398-9219. DOI: 10.1111/J.1600-0854.2007.00665.X. URL: https://pubmed.ncbi.nlm.nih.gov/17956594/.

[113] Erica Novo and Maurizio Parola. "Redox mechanisms in hepatic chronic wound healing and fibrogenesis". In: *Fibrogenesis tissue repair* 1 (1 Oct. 2008). ISSN: 1755-1536. DOI: 10.1186/1755-1536-1-5. URL: https://pubmed.ncbi.nlm.nih.gov/19014652/.

[114] Benoît D'Autréaux and Michel B. Toledano. "ROS as signalling molecules: mechanisms that generate specificity in ROS homeostasis". In: *Nature Reviews Molecular Cell Biology 2007 8:10* 8 (10 Oct. 2007), pp. 813–824. ISSN: 1471-0080. DOI: 10.1038/nrm2256. URL: https://www.nature.com/articles/nrm2256.

[115] Milena Bertolotti et al. "AQP8 transports NOX2-generated H2O2 across the plasma membrane to promote signaling in B cells". In: *Journal of leukocyte biology* 100 (5 Nov. 2016), pp. 1071–1079. ISSN: 1938-3673. DOI: 10.1189/JLB.2AB0116-045R. URL: https://pubmed.ncbi.nlm.nih.gov/27256569/.

[116] Jeroen Den Hertog, Arnoud Groen, and Thea Van Der Wijk. "Redox regulation of protein-tyrosine phosphatases". In: (2004). DOI: 10.1016/j.abb.2004.05.024. URL: www.elsevier.com/locate/yabbi.

[117] Angel Stanoev. "Spatial unification of coupling interactions between EGFR and PTPs establishes a growth factor sensing network". In: (Aug. 2018). DOI: 10.17877/DE290R-20110. URL: https://eldorado.tu-dortmund.de/handle/2003/38129.

[118] Joshua Z. Rappoport and Sanford M. Simon. "Endocytic trafficking of activated EGFR is AP-2 dependent and occurs through preformed clathrin spots". In: *Journal of cell science* 122 (Pt 9 May 2009), pp. 1301–1305. ISSN: 0021-9533. DOI: 10.1242/JCS.040030. URL: https://pubmed.ncbi.nlm.nih.gov/19351721/.

[119] Lai Kuan Goh et al. "Multiple mechanisms collectively regulate clathrin-mediated endocytosis of the epidermal growth factor receptor". In: *The Journal of cell biology* 189 (5 May 2010), pp. 871–883. ISSN: 1540-8140. DOI: 10.1083/JCB.201001008. URL: https://pubmed.ncbi.nlm.nih.gov/20513767/.

[120] Fangtian Huang et al. "Analysis of Clathrin-mediated Endocytosis of Epidermal Growth Factor Receptor by RNA Interference". In: *Journal of Biological Chemistry* 279 (16 Apr. 2004), pp. 16657–16661. ISSN: 00219258. DOI: 10.1074/JBC.C400046200/ATTACHMENT/55C11EC0-6CDC-41BA-851A-67E4908BAF1A/MMC1.PDF. URL: http://www.jbc.org/article/S0021925820883963/fulltext%20http://www.jbc.org/article/S0021925820883963/abstract%20https://www.jbc.org/article/S0021-9258(20)88396-3/abstract.

[121] Alejandra Tomas, Clare E. Futter, and Emily R. Eden. "EGF receptor trafficking: consequences for signaling and cancer". In: *Trends in Cell Biology* 24 (1 Jan. 2014), p. 26. ISSN: 09628924. DOI: 10.1016/J.TCB.2013.11.002. URL: /pmc/articles/

PMC3884125/%20/pmc/articles/PMC3884125/?report=abstract%20https://www.ncbi.nlm.nih.gov/pmc/articles/PMC3884125/.

[122] Harald Stenmark. "Rab GTPases as coordinators of vesicle traffic". In: *Nature Reviews Molecular Cell Biology 2009 10:8* 10 (8 July 2009), pp. 513–525. ISSN: 1471-0080. DOI: 10.1038/nrm2728. URL: https://www.nature.com/articles/nrm2728.

[123] Samantha L. Schwartz et al. "Rab GTPases at a glance". In: *Journal of Cell Science* 120 (22 Nov. 2007), pp. 3905–3910. ISSN: 0021-9533. DOI: 10.1242/JCS.015909.

[124] Bruce Alberts et al. "Molecular Biology of Cell". In: (5 2014), pp. 591–595.

[125] Marko Jovic et al. "The early endosome: a busy sorting station for proteins at the crossroads". In: *Histology and histopathology* 25 (1 Jan. 2010), pp. 99–112. ISSN: 1699-5848. DOI: 10.14670/HH-25.99. URL: https://pubmed.ncbi.nlm.nih.gov/19924646/.

[126] Roberto Villaseñor, Yannis Kalaidzidis, and Marino Zerial. "Signal processing by the endosomal system". In: *Current opinion in cell biology* 39 (Apr. 2016), pp. 53–60. ISSN: 1879-0410. DOI: 10.1016/J.CEB.2016.02.002. URL: https://pubmed.ncbi.nlm.nih.gov/26921695/.

[127] Lene Melsæther Grøvdal et al. "Direct interaction of Cbl with pTyr 1045 of the EGF receptor (EGFR) is required to sort the EGFR to lysosomes for degradation". In: *Experimental cell research* 300 (2 Nov. 2004), pp. 388–395. ISSN: 0014-4827. DOI: 10.1016/J.YEXCR.2004.07.003. URL: https://pubmed.ncbi.nlm.nih.gov/15475003/.

[128] Sara Sigismund et al. "Threshold-controlled ubiquitination of the EGFR directs receptor fate". In: *The EMBO journal* 32 (15 July 2013), pp. 2140–2157. ISSN: 1460-2075. DOI: 10.1038/EMBOJ.2013.149. URL: https://pubmed.ncbi.nlm.nih.gov/23799367/.

[129] Xuejun Jiang et al. "Grb2 regulates internalization of EGF receptors through clathrin-coated pits". In: *Molecular biology of the cell* 14 (3 Mar. 2003), pp. 858–870. ISSN: 1059-1524. DOI: 10.1091/MBC.E02-08-0532. URL: https://pubmed.ncbi.nlm.nih.gov/12631709/.

[130] Ivan A. Yudushkin et al. "Live-cell imaging of enzyme-substrate interaction reveals spatial regulation of PTP1B". In: *Science (New York, N.Y.)* 315 (5808 Jan. 2007), pp. 115–119. ISSN: 1095-9203. DOI: 10.1126/SCIENCE.1134966. URL: https://pubmed.ncbi.nlm.nih.gov/17204654/.

[131] A. Sorkin et al. “Recycling of epidermal growth factor-receptor complexes in A431 cells: identification of dual pathways”. In: *The Journal of cell biology* 112 (1 1991), pp. 55–63. ISSN: 0021-9525. DOI: 10.1083/JCB.112.1.55. URL: https://pubmed.ncbi.nlm.nih.gov/1986007/.

[132] Oliver Ullrich et al. “Rab11 regulates recycling through the pericentriolar recycling endosome”. In: *The Journal of Cell Biology* 135 (4 1996), p. 913. ISSN: 00219525. DOI: 10.1083/JCB.135.4.913. URL: /pmc/articles/PMC2133374/?report=abstract%20https://www.ncbi.nlm.nih.gov/pmc/articles/PMC2133374/.

[133] Robert C. Piper and David J. Katzmann. “Biogenesis and Function of Multivesicular Bodies”. In: *Annual review of cell and developmental biology* 23 (2007), p. 519. ISSN: 10810706. DOI: 10.1146/ANNUREV.CELLBIO.23.090506.123319. URL: /pmc/articles/PMC2911632/%20/pmc/articles/PMC2911632/?report=abstract%20https://www.ncbi.nlm.nih.gov/pmc/articles/PMC2911632/.

[134] J. W. Konturek et al. “Distribution and release of epidermal growth factor in man”. In: *Gut* 30 (9 1989), pp. 1194–1200. ISSN: 0017-5749. DOI: 10.1136/GUT.30.9.1194. URL: https://pubmed.ncbi.nlm.nih.gov/2806986/.

[135] Elaine M. Khan et al. “Epidermal growth factor receptor exposed to cigarette smoke is aberrantly activated and undergoes perinuclear trafficking”. In: *FASEB journal : official publication of the Federation of American Societies for Experimental Biology* 22 (3 Mar. 2008), pp. 910–917. ISSN: 1530-6860. DOI: 10.1096/FJ.06-7729COM. URL: https://pubmed.ncbi.nlm.nih.gov/17971399/.

[136] Yannick Brueggemann et al. “Growth factor-dependent ErbB vesicular dynamics couple receptor signaling to spatially and functionally distinct Erk pools”. In: *Science Signaling* 14 (2021), eabd9943. DOI: 10.1126/scisignal.abd9943.

[137] Wayne Stallaert et al. “Contact inhibitory Eph signaling suppresses EGF-promoted cell migration by decoupling EGFR activity from vesicular recycling”. In: *Science signaling* 11 (541 July 2018). ISSN: 1937-9145. DOI: 10.1126/SCISIGNAL.AAT0114. URL: https://pubmed.ncbi.nlm.nih.gov/30065026/.

[138] F. Bellot et al. “High-affinity epidermal growth factor binding is specifically reduced by a monoclonal antibody, and appears necessary for early responses”. In: *The Journal of cell biology* 110 (2 1990), pp. 491–502. ISSN: 0021-9525. DOI: 10.1083/JCB.110.2.491. URL: https://pubmed.ncbi.nlm.nih.gov/2298813/.

[139] L. H.K. Defize et al. “Signal transduction by epidermal growth factor occurs through the subclass of high affinity receptors”. In: *The Journal of cell biology* 109 (5 1989), pp. 2495–2507. ISSN: 0021-9525. DOI: 10.1083/JCB.109.5.2495. URL: https://pubmed.ncbi.nlm.nih.gov/2553748/.

[140] Vibor Laketa et al. “PIP induces the recycling of receptor tyrosine kinases”. In: *Science signaling* 7 (308 Jan. 2014). ISSN: 1937-9145. DOI: 10.1126/SCISIGNAL.2004532. URL: https://pubmed.ncbi.nlm.nih.gov/24425787/.

[141] Hui Miao et al. “EphA2 mediates ligand-dependent inhibition and ligand-independent promotion of cell migration and invasion via a reciprocal regulatory loop with Akt”. In: *Cancer cell* 16 (1 July 2009), pp. 9–20. ISSN: 1878-3686. DOI: 10.1016/J.CCR.2009.04.009. URL: https://pubmed.ncbi.nlm.nih.gov/19573808/.

[142] Angel Stanoev, Akhilesh P. Nandan, and Aneta Koseska. “Organization at criticality enables processing of time-varying signals by receptor networks”. In: *Mol Syst Biol* 16 (2020), e8870. ISSN: 1079-7114 (Electronic)0031-9007 (Linking). DOI: 10.15252/msb.20198870.

[143] Steven H Strogatz. *Nonlinear dynamics and chaos: with applications to physics, biology, chemistry, and engineering*. CRC Press, 2018. ISBN: 0429961111.

[144] Berta Verd, Anton Crombach, and Johannes Jaeger. “Classification of transient behaviours in a time-dependent toggle switch model”. In: *BMC Systems Biology* 8 (1 Apr. 2014), pp. 1–19. ISSN: 17520509. DOI: 10.1186/1752-0509-8-43/FIGURES/8. URL: https://bmcsystbiol.biomedcentral.com/articles/10.1186/1752-0509-8-43.

[145] Heath E. Johnson and Jared E. Toettcher. “Signaling Dynamics Control Cell Fate in the Early Drosophila Embryo”. In: *Developmental cell* 48 (3 Feb. 2019), 361–370.e3. ISSN: 1878-1551. DOI: 10.1016/J.DEVCEL.2019.01.009. URL: https://pubmed.ncbi.nlm.nih.gov/30753836/.

[146] Akhilesh Nandan et al. “Cells use molecular working memory to navigate in changing chemoattractant fields”. In: *bioRxiv* (Nov. 2021), p. 2021.11.11.468222. DOI: 10.1101/2021.11.11.468222. URL: https://www.biorxiv.org/content/10.1101/2021.11.11.468222v1%20https://www.biorxiv.org/content/10.1101/2021.11.11.468222v1.abstract.

[147] A. Koseska, E. Volkov, and J. Kurths. “Transition from amplitude to oscillation death via Turing bifurcation”. In: *Phys Rev Lett* 111.2 (2013), p. 024103. ISSN: 1079-7114 (Electronic)0031-9007 (Linking). DOI: 10.1103/PhysRevLett.111.024103.

[148] D. Lauffenburger and J.J. Linderman. *"Receptors: model for binding, trafficking and signaling"*. Oxford University Press, 1996, pp. 366–381. ISBN: 0-19-506466-6.

[149] Paul Becherer, Alexander N. Morozov, and Wim van Saarloos. “Probing a subcritical instability with an amplitude expansion: An exploration of how far one can get”. In: *Physica D: Nonlinear Phenomena* 238.18 (2009), pp. 1827–1840. ISSN: 0167-2789. DOI: https://doi.org/10.1016/j.physd.2009.

03.009. URL: https://www.sciencedirect.com/science/article/pii/S0167278909000979.

[150] Christine Chiasson-MacKenize and Andrea I. McClatchey. "EGFR-induced cytoskeletal changes drive complex cell behavior: The tip of the iceberg". In: *Science Signaling* 11 (2018), eaas9473. DOI: 10.1126/scisignal.aas9473.

[151] A.J. Ridley and A. Hall. "The small GTP-binding protein rho regulates the assembly of focal adhesions and actin stress fibers in response to growth factors". In: *Cell* 70 (1992), pp. 389–399. DOI: 10.1016/0092-8674(92)90163-7.

[152] Liu Yang et al. "Modeling cellular deformations using the level set formalism". In: *BMC Syst Biol* 2.68 (2008), pp. 1–16. ISSN: 2050-084X (Electronic)2050-084X (Linking). DOI: 10.1186/1752-0509-2-68. URL: https://www.ncbi.nlm.nih.gov/pubmed/26609808.

[153] Marta Strani. "Nonlinear metastability for a parabolic system of reaction-diffusion equations". In: (Dec. 2013). URL: https://arxiv.org/abs/1312.0754v5.

[154] Peter Hanggi. "Escape from a Metastable State". In: *Journal of Statistical Physics* 42 (2 1986).

[155] Floris Takens. *"Detecting strange attractors in turbulence", in "Dynamical systems and turbulence", Editors David Rand and Lai-Sang Young.* Springer Nature, 1980, pp. 366–381. ISBN: 978-3-540-11171-9.

[156] T. Sauer, J. Yorke, and M. Casdagli. "Embedology". In: *J. Stat. Phys.* 65 (1991), p. 579.

[157] Mariano Matilla-García et al. "Selection of Embedding Dimension and Delay Time in Phase Space Reconstruction via Symbolic Dynamics". In: *Entropy 2021, Vol. 23, Page 221* 23 (2 Feb. 2021), p. 221. ISSN: 10994300. DOI: 10.3390/E23020221. URL: https://www.mdpi.com/1099-4300/23/2/221/htm%20https://www.mdpi.com/1099-4300/23/2/221.

[158] Anna Krakovská, Kristína Mezeiová, and Hana Budáčová. "Use of False Nearest Neighbours for Selecting Variables and Embedding Parameters for State Space Reconstruction". In: *Journal of Complex Systems* 2015 (Mar. 2015), pp. 1–12. ISSN: 2356-7244. DOI: 10.1155/2015/932750.

[159] Christopher G. Sip, Nirveek Bhattacharjee, and Albert Folch. "Microfluidic transwell inserts for generation of tissue culture-friendly gradients in well plates". In: *Lab on a chip* 14 (2 Jan. 2014), pp. 302–314. ISSN: 1473-0189. DOI: 10.1039/C3LC51052B. URL: https://pubmed.ncbi.nlm.nih.gov/24225908/.

[160] Yannick Brüggemann et al. "Growth factor-dependent ErbB vesicular dynamics couple receptor signaling to spatially and functionally distinct Erk pools". In: *Science signaling* 14 (683 May 2021). ISSN: 1937-9145. DOI: 10.1126/SCISIGNAL.ABD9943. URL: https://pubmed.ncbi.nlm.nih.gov/34006609/.

[161] C. Svensson et al. “Untangling cell tracks: Quantifying cell migration by time lapse image data analysis”. In: *Cytometry Part A, J. of Quantitative Cell Science* 93A (2017), pp. 357–370. ISSN: 2050-084X (Electronic)2050-084X (Linking). DOI: 10.1002/cyto.a.23249. URL: https://www.ncbi.nlm.nih.gov/pubmed/26609808.

[162] Brian D. Harms et al. “Directional Persistence of EGF-Induced Cell Migration Is Associated with Stabilization of Lamellipodial Protrusions”. In: *Biophysical Journal* 88 (2 Feb. 2005), pp. 1479–1488. ISSN: 0006-3495. DOI: 10.1529/BIOPHYSJ.104.047365.

[163] Peter Dieterich et al. “Anomalous dynamics of cell migration”. In: *Proceedings of the National Academy of Sciences* 105 (2 Jan. 2008), pp. 459–463. ISSN: 0027-8424. DOI: 10.1073/PNAS.0707603105. URL: https://www.pnas.org/content/105/2/459%20https://www.pnas.org/content/105/2/459.abstract.

[164] Daniel Campos, Vicenç Méndez, and Isaac Llopis. “Persistent random motion: uncovering cell migration dynamics”. In: *Journal of Theoretical Biology* 267 (4 2010). DOI: 10.1016/j.jtbi.2010.09.022Ãŕ. URL: www.elsevier.com/locate/yjtbi.

[165] Cesare Usai and Alberto Diaspro. “Fluorescence: General Aspects”. In: *Encyclopedia of Biophysics* (2013), pp. 826–832. DOI: 10.1007/978-3-642-16712-6_823. URL: https://link.springer.com/referenceworkentry/10.1007/978-3-642-16712-6_823.

[166] M. R. Tadross et al. “Robust approaches to quantitative ratiometric FRET imaging of CFP/YFP fluorophores under confocal microscopy”. In: *Journal of microscopy* 233 (1 Jan. 2009), p. 192. ISSN: 00222720. DOI: 10.1111/J.1365-2818.2008.03109.X. URL: /pmc/articles/PMC2877369/%20/pmc/articles/PMC2877369/?report=abstract%20https://www.ncbi.nlm.nih.gov/pmc/articles/PMC2877369/.

[167] M.H. Sonntag et al. “Site-Specific Protection and Dual Labeling of Human Epidermal Growth Factor (hEGF) for Targeting, Imaging, and Cargo Delivery”. In: *Chemistry - a European Journal* 20 (2014), pp. 6019–6026. ISSN: 2050-084X (Electronic)2050-084X (Linking). DOI: 10.1002/chem.201304090. URL: https://www.ncbi.nlm.nih.gov/pubmed/26609808.

[168] Johannes Schindelin et al. “Fiji: an open-source platform for biological-image analysis”. In: *Nature Methods* 9 (2012), pp. 676–682. ISSN: 7. DOI: 10.1038/nmeth.2019. URL: https://doi.org/10.1038/nmeth.2019.

[169] Jean-Yves Tinevez et al. “TrackMate: An open and extensible platform for single-particle tracking”. In: *Methods* 115 (2017). Image Processing for Biologists, pp. 80–90. ISSN: 1046-2023. DOI: https://doi.org/10.1016/j.ymeth.2016.09.016. URL: https://www.sciencedirect.com/science/article/pii/S1046202316303346.

[170] G.E. Uhlenbeck and L.S. Ornstein. “On the theory of Brownian motion”. In: *Phys. Rev.* 36 (1930), pp. 823–841. ISSN: 2050-084X (Electronic)2050-084X (Linking). DOI: 10.1103/PhysRev.36.823. URL: https://www.ncbi.nlm.nih.gov/pubmed/26609808.

[171] Selmeczi D. et al. “Cell Motility as Persistent Random Motion: Theories from Experiments”. In: *Biophysical J.* 89.2 (2005), pp. 912–931. ISSN: 2050-084X (Electronic)2050-084X (Linking). DOI: 10.1529/biophysj.105.061150. URL: https://www.ncbi.nlm.nih.gov/pubmed/26609808.

[172] Matthew B. Kennel, Reggie Brown, and Henry D. I. Abarbanel. “Determining embedding dimension for phase-space reconstruction using a geometrical construction”. In: *Phys. Rev. A* 45 (6 Mar. 1992), pp. 3403–3411. DOI: 10.1103/PhysRevA.45.3403. URL: https://link.aps.org/doi/10.1103/PhysRevA.45.3403.

[173] E Hairer, S P Nørsett, and G Wanner. “Solving Ordinary Difference Equations 1 - Nonstiff problems”. In: *Springer Series in Computational Mathematics* (1993).

[174] Peter E. Kloeden and Eckhard Platen. “Numerical Solution of Stochastic Differential Equations”. In: *Numerical Solution of Stochastic Differential Equations* (1992). DOI: 10.1007/978-3-662-12616-5.

[175] Stephen R.D. Johnston and Alex Leary. “Lapatinib: a novel EGFR/HER2 tyrosine kinase inhibitor for cancer”. In: *Drugs of today (Barcelona, Spain : 1998)* 42 (7 July 2006), pp. 441–453. ISSN: 1699-3993. DOI: 10.1358/DOT.2006.42.7.985637. URL: https://pubmed.ncbi.nlm.nih.gov/16894399/.

[176] S. Hochreiter and J. Schmidhuber. “Long short-term memory”. In: *Neural Comp.* 9 (1997), pp. 1735–1780. DOI: https://doi:10.1162/neco.1997.9.8.1735.

[177] W. Maass, T. Natschlager, and H. Markram. “Real-time computing without stable states: a new framework for neural computation based on perturbations”. In: *Neural Comp.* 14 (2000), pp. 2531–2560. DOI: https://doi:10.1162/089976602760407955.

[178] Flora Bouchacourt and Timothy J. Buschman. “A Flexible Model of Working Memory”. In: *Neuron* 103 (1 July 2019), 147–160.e8. ISSN: 1097-4199. DOI: 10.1016/J.NEURON.2019.04.020. URL: https://pubmed.ncbi.nlm.nih.gov/31103359/.

[179] Omri Barak and Misha Tsodyks. "Working models of working memory". In: *Current Opinion in Neurobiology* 25 (Apr. 2014), pp. 20–24. ISSN: 0959-4388. DOI: 10.1016/J.CONB.2013.10.008.

[180] Xiao Jing Wang. "Synaptic reverberation underlying mnemonic persistent activity". In: *Trends in Neurosciences* 24 (8 Aug. 2001), pp. 455–463. ISSN: 01662236. DOI: 10.1016/S0166-2236(00)01868-3. URL: /record/2001-07690-003.

[181] Marta Miaczynska. "Effects of membrane trafficking on signaling by receptor tyrosine kinases". In: *Cold Spring Harbor perspectives in biology* 5 (11 Nov. 2013). ISSN: 1943-0264. DOI: 10.1101/CSHPERSPECT.A009035. URL: https://pubmed.ncbi.nlm.nih.gov/24186066/.

[182] Gilda2011 Da Cunha Santos, Frances A. Shepherd, and Ming Sound Tsao. "EGFR Mutations and Lung Cancer". In: *http://dx.doi.org/10.1146/annurev-pathol-011110-130206* 6 (Jan. 2011), pp. 49–69. ISSN: 15534006. DOI: 10.1146/ANNUREV-PATHOL-011110-130206. URL: https://www.annualreviews.org/doi/abs/10.1146/annurev-pathol-011110-130206.

[183] Yuan Qi and Hui Ge. "Modularity and Dynamics of Cellular Networks". In: *PLOS Computational Biology* 2 (12 Dec. 2006), e174. ISSN: 1553-7358. DOI: 10.1371/JOURNAL.PCBI.0020174. URL: https://journals.plos.org/ploscompbiol/article?id=10.1371/journal.pcbi.0020174.

[184] S. Wuchty, Z. Oltvai, and A. L. Barabási. "Evolutionary conservation of motif constituents in the yeast protein interaction network". In: *Nature Genetics 2003 35:2* 35 (2 Sept. 2003), pp. 176–179. ISSN: 1546-1718. DOI: 10.1038/ng1242. URL: https://www.nature.com/articles/ng1242.

[185] Roded Sharan et al. "Conserved patterns of protein interaction in multiple species". In: *Proceedings of the National Academy of Sciences* 102 (6 Feb. 2005), pp. 1974–1979. ISSN: 0027-8424. DOI: 10.1073/PNAS.0409522102. URL: https://www.pnas.org/content/102/6/1974%20https://www.pnas.org/content/102/6/1974.abstract.

[186] Tujin Shi et al. "Conservation of protein abundance patterns reveals the regulatory architecture of the EGFR-MAPK pathway". In: *Science signaling* 9 (436 July 2016), rs6. ISSN: 19379145. DOI: 10.1126/SCISIGNAL.AAF0891. URL: /pmc/articles/PMC5036860/%20/pmc/articles/PMC5036860/?report=abstract%20https://www.ncbi.nlm.nih.gov/pmc/articles/PMC5036860/.

[187] Eric K. Rowinsky. "The erbB family: targets for therapeutic development against cancer and therapeutic strategies using monoclonal antibodies and tyrosine kinase inhibitors". In: *Annual review of medicine* 55 (2004), pp. 433–457. ISSN:

0066-4219. DOI: 10.1146/ANNUREV.MED.55.091902.104433. URL: https://pubmed.ncbi.nlm.nih.gov/14746530/.

[188] Takafumi Watanabe et al. "Significance of the Grb2 and son of sevenless (SOS) proteins in human bladder cancer cell lines". In: *IUBMB Life* 49 (4 2000), pp. 317–320. ISSN: 15216543. DOI: 10.1080/15216540050033195.

[189] Ellen C. OShaughnessy et al. "Tunable Signal Processing in Synthetic MAP Kinase Cascades". In: *Cell* 144 (1 Jan. 2011), pp. 119–131. ISSN: 0092-8674. DOI: 10.1016/J.CELL.2010.12.014.

[190] Christina Kiel et al. "Integration of protein abundance and structure data reveals competition in the ErbB signaling network". In: *Science Signaling* 6 (306 Dec. 2013). ISSN: 19450877. DOI: 10.1126/SCISIGNAL.2004560/SUPPL_FILE/6_RA109_SM.PDF. URL: https://www.science.org/doi/abs/10.1126/scisignal.2004560.

[191] Martin H. Schaefer et al. "Protein Conservation and Variation Suggest Mechanisms of Cell Type-Specific Modulation of Signaling Pathways". In: *PLOS Computational Biology* 10 (6 2014), e1003659. ISSN: 1553-7358. DOI: 10.1371/JOURNAL.PCBI.1003659. URL: https://journals.plos.org/ploscompbiol/article?id=10.1371/journal.pcbi.1003659.

A

Formulare